NONDESTRUCTIVE EVALUATION AND ASSESSMENT OF CONCRETE BARRIERS FOR DEFECTS AND CORROSION

Final Report
November 15, 2013
WJE No. 2006.5773 (Iowa DOT, Project Number BARR-010)
WJE No. 2011.5553.2 (Illinois DOT)

Prepared for:
Mr. Michael Todsen, P.E.
Iowa Department of Transportation
Office of Bridges and Structures
800 Lincoln Way
Ames, Iowa 50010

Prepared for:
Mr. David Greifzu, P.E., S.E.
Illinois Department of Transportation
Bureau of Bridges and Structures
2300 S. Dirksen Parkway
Springfield, Illinois 62764

Prepared by:
Wiss, Janney, Elstner Associates, Inc.
330 Pfingsten Road
Northbrook, Illinois 60062
847.272.7400 tel | 847.291.9599 fax

Disclaimer Notice

The contents of this report reflect the views of the authors, who are responsible for the facts and the accuracy of the information presented herein. The opinions, findings, and conclusions expressed in this publication are those of the authors and not necessarily of the sponsors.

The sponsors assume no liability for the contents or use of the information contained in this document. This report does not constitute a standard, specification, or regulation.

The sponsors do not endorse products or manufacturers. Trademarks or manufacturer's names appear in this report only because they are considered essential to the objectives of the document.

Statement of Non-Discrimination

FEDERAL AND STATE LAWS PROHIBIT EMPLOYMENT AND/OR PUBLIC ACCOMMODATION DISCRIMINATION ON THE BASIS OF AGE, COLOR, CREED, DISABILITY, GENDER IDENTITY, NATIONAL ORIGIN, PREGNANCY, RACE, RELIGION, SEX, SEXUAL ORIENTATION OR VETERAN'S STATUS. IF YOU BELIEVE YOU HAVE BEEN DISCRIMINATED AGAINST, PLEASE CONTACT THE IOWA CIVIL RIGHTS COMMISSION AT 800-457-4416 OR IOWA DEPARTMENT OF TRANSPORTATION'S AFFIRMATIVE ACTION OFFICER. IF YOU NEED ACCOMMODATIONS BECAUSE OF A DISABILITY TO ACCESS THE IOWA DEPARTMENT OF TRANSPORTATION'S SERVICES, CONTACT THE AGENCY'S AFFIRMATIVE ACTION OFFICER AT 800-262-0003

1. Report No. BARR-010	**2. Government Accession No.** Optional	**3. Recipient Catalog No.** Optional
4 Title and Subtitle Nondestructive Evaluation and Assessment of Concrete Barriers for Defects and Corrosion		**5 Report Date** November 15, 2013 **6 Performing Organization Code** Optional
7. **Author(s)** McGormley, J.C.; Rende, N.S.; Krauss, P.D.		**8 Performing Organization Report No.** 2006.5773
9 Performing Organization Name and Address Wiss, Janney, Elstner Associates, Inc. 330 Pfingsten Road Northbrook, Illinois 60062		**10 Work Unit No. (TRAIS)** Not Required **11 Contract or Grant No.** 3330G
12 Sponsoring Organization Name and Address Iowa Department of Transportation 800 Lincoln Way Ames, Iowa 50010 Federal Highway Administration		**13 Type of Report and Period Covered** Final Report **14 Sponsoring Agency Code** **BARR-010**

15 Supplementary Notes
Optional

16 Abstract

Wiss, Janney, Elstner Associates, Inc. (WJE) evaluated potential nondestructive evaluation (NDE) methodologies that may be effective in 1) identifying internal defects within slip formed concrete barriers and 2) assessing the corrosion condition of barrier dowel bars. The evaluation was requested by the Bridge Maintenance and Inspection Unit of the Iowa Department of Transportation (IaDOT) and the Bureau of Bridges and Structures of the Illinois Department of Transportation (IDOT). The need arose due to instances in each Department's existing inventory of bridge barriers where internal voids and other defects associated with slip forming construction methods were attributed to poor barrier performance after completion of construction and where, in other barrier walls, unintentional exposure of the dowel bars revealed extensive corrosion-related section loss at previously uninspectable locations, reducing the capacity of the barriers to resist traffic impact loads. WJE trial tested potential NDE techniques on laboratory mock-up samples built with known defects, trial sections of cast-in-place barriers at in-service bridges in Iowa, and slip formed and cast-in-place barrier walls at in-service bridges in Illinois. The work included review of available studies performed by others, field trial testing to assess candidate test methods, verification of the test methods in identifying internal anomalies and dowel bar corrosion, and preparation of this report and nondestructive evaluation guidelines.

17 Key Words Nondestructive evaluation, NDE, concrete barriers, slip formed, dowel bars, corrosion		**18 Distribution Statement** No restrictions. This document is available to the public through the National Technical Information Service, Springfield, Virginia 22161	
19 Security Classification (of this report) Unclassified	**20 Security Classification (of this page)** Unclassified	**21 No. of pages** 118	**22 Price** N/A

Form DOT F 1700.7 (8-72)

NONDESTRUCTIVE EVALUATION AND ASSESSMENT OF CONCRETE BARRIERS FOR DEFECTS AND CORROSION

Nathaniel S. Rende, S.E.
Senior Associate

Jonathan C. McGormley, P.E., S.E.
Principal

Paul D. Krauss, P.E.
Principal

Final Report
November 15, 2013
WJE No. 2006.5773 (Iowa DOT, Project Number BARR-010)
WJE No. 2011.5553.2 (Illinois DOT)

Prepared for:
Mr. Michael Todsen, P.E.
Iowa Department of Transportation
Office of Bridges and Structures
800 Lincoln Way
Ames, Iowa 50010

Prepared for:
Mr. David Greifzu, P.E., S.E.
Illinois Department of Transportation
Bureau of Bridges and Structures
2300 S. Dirksen Parkway
Springfield, Illinois 62764

Prepared by:
Wiss, Janney, Elstner Associates, Inc.
330 Pfingsten Road
Northbrook, Illinois 60062
847.272.7400 tel | 847.291.9599 fax

WJE ENGINEERS ARCHITECTS MATERIALS SCIENTISTS

TABLE OF CONTENTS

TABLE OF FIGURES

TABLE OF TABLES

WJE ENGINEERS ARCHITECTS MATERIALS SCIENTISTS

NONDESTRUCTIVE EVALUATION AND ASSESSMENT OF CONCRETE BARRIERS FOR DEFECTS AND CORROSION

EXECUTIVE SUMMARY

Wiss, Janney, Elstner Associates, Inc. (WJE) evaluated potential nondestructive evaluation (NDE) methodologies that may be effective in 1) identifying internal defects within slip formed concrete barriers and 2) assessing the corrosion condition of barrier dowel bars. The evaluation was requested by the Bridge Maintenance and Inspection Unit of the Iowa Department of Transportation (IaDOT) and the Bureau of Bridges and Structures of the Illinois Department of Transportation (IDOT). The need arose due to instances in each Department's existing inventory of bridge barriers where internal voids and other defects associated with slip forming construction methods were attributed to poor barrier performance after completion of construction and where, in other barrier walls, unintentional exposure of the dowel bars revealed extensive corrosion-related section loss at previously uninspectable locations, reducing the capacity of the barriers to resist traffic impact loads. WJE trial tested potential NDE techniques on laboratory mock-up samples built with known defects, trial sections of cast-in-place barriers at in-service bridges in Iowa, and slip formed and cast-in-place barrier walls at in-service bridges in Illinois. The work included review of available studies performed by others, field trial testing to assess candidate test methods, verification of the test methods in identifying internal anomalies and dowel bar corrosion, and preparation of this report and nondestructive evaluation guidelines.

Testing

The nondestructive test methods tested to study their effectiveness in identifying slip formed production-related flaws were impact-echo, ultrasonic testing, shear wave ultrasonic testing (MIRA), ultrasonic pulse velocity testing, ground-penetrating radar (GPR), infrared thermography, and radiography. Nondestructive testing for corrosion-related distress was performed by half-cell potential surveying, corrosion rate measurement, impulse-response structural mobility testing, and concrete resistivity measurements. To evaluate the effectiveness of each NDE technique, WJE combined a laboratory study on the mock-up samples, testing of trail barrier segments commissioned by IDOT, and field testing of existing barrier walls within Iowa and Illinois.

Internal Flaw Detection

The ability of NDE testing to identify internal, production-related flaws in slip formed barriers depends on a number of variables, including ambient conditions, the type and severity of internal flaws present, the presence and severity of visible distress, and the specific advantages and limitations of each testing method. Of the NDE methods used during this assessment, GPR proved to be the most effective and versatile testing method. However, a combination of techniques may be best suited for barrier evaluation. Visual condition surveys can identify cracking or consolidation issues resulting from slip formed production problems or identify the extent of freeze-thaw or material deterioration present in existing barriers. Longitudinal GPR scans can be collected quickly on the lateral surfaces or top surface of a barrier and can provide useful information on reinforcing location and freeze-thaw and other degradation cracking. Additionally, GPR surveying was determined to be the most efficient and accurate approach for identifying a range of internal production-related flaws, including interconnected voids within the concrete, voiding around reinforcing resulting from consolidation issues or cage displacement during production, and wide internal cracking. Despite some limitations, MIRA tomography testing remains a

viable testing approach to investigate limited areas at suspect locations in order to better identify the extent and severity of voided areas. Regardless of the nondestructive testing approach used, exploratory coring remains the most effective method for classifying the specific internal defect present at suspect locations.

Dowel Bar Corrosion Detection

The study indicated that half-cell potential measurements provide the most accurate identification of corrosion-related distress. Identification of corroded dowel bars at barrier construction joints is practical using a rolling half-cell unit when the barrier is built using black reinforcing steel. A simple ground should be made to the barrier section and the rolling half-cell can be used to quickly traverse the bottom edge of the barrier. Corroding black bar dowels can be quickly identified through field analysis of the testing results. Field and laboratory tests of epoxy-coated dowels were inconclusive and further testing is required. Measuring the concrete electrical resistivity on the barrier surface in the black bar barriers showed a wide range of values and can provide useful information for locating areas of possible corrosion. Low resistivity measurements are indicative of water or deicer saturated areas that would be more prone to corrosive conditions. Visual inspection of the backside of the barrier can sometimes show corrosion staining at dowel locations, providing further evidence of corrosion related distress. None of the techniques were able to identify the amount of section loss of the reinforcing. However, impulse-response structural mobility testing may be able to identify sections of barrier having a series of multiple severed dowels. Visual inspection and rolling half-cell testing is a reasonable procedure for assessment of dowel bar corrosion in barriers with uncoated reinforcing steel.

Conclusions

An evaluation of available NDE techniques was carried out to assess each technique's capability to identify, characterize, and locate internal flaws and dowel bar corrosion in concrete barrier walls. Laboratory mock-ups were used to establish testing procedures and examine the effectiveness of the technology. Concrete barriers on three bridges identified by IaDOT were examined using a range of techniques. Additional field testing for the assessment of internal concrete flaws using the most promising NDE techniques was completed on four bridges identified by IDOT. Based on the laboratory and field testing, each NDE technique was judged on its capabilities with respect to internal flaw detection and dowel bar corrosion, respectively. Guidelines for preliminary assessment are given to assist IaDOT and IDOT in the selection of suitable NDE methods for detecting and evaluating specific conditions related to concrete distress and dowel bar corrosion distress of in-place barriers.

1. INTRODUCTION AND BACKGROUND

The Bridge Maintenance and Inspection Unit of the Iowa Department of Transportation (IaDOT) and the Bureau of Bridges and Structures of the Illinois Department of Transportation (IDOT) have identified a research need to determine cost-effective, nondestructive evaluation techniques to evaluate concrete barriers. Both Departments have experienced instances in their existing inventory of bridge barriers where internal voids and other defects associated with slip forming construction methods have manifested themselves after construction was complete. This has required both Departments to carry out corrective measures, typically at their own expense. In other barrier walls, unintentional exposure of the dowel bars has revealed extensive corrosion-related section loss at previously uninspectable locations. Such section loss reduces the capacity of the barriers to resist traffic impact loads.

This research report considers techniques that can nondestructively identify potential problem locations within concrete barriers associated with slip formed construction and corrosion of barrier dowel bars. These techniques may be implemented during acceptance and quality control processes to supplement visual condition inspection.

1.1. Slip Formed Construction Method

Slip formed concrete barriers have been routinely constructed on bridge decks in the states of Iowa and Illinois since the early 1980s. Compared with conventional form and cast-in-place construction methods for barrier walls, the slip formed method provided significant cost and time efficiencies and became the dominant approach to barrier construction. However, in early 2004, IDOT and the Federal Highway Administration (FHWA) completed the 2003 IDOT/FHWA Joint Process Review on Bridge Parapet Construction, aimed at evaluating the adequacy and long-term performance of concrete bridge barriers. The review identified widespread deterioration of slip formed barriers compared with barriers constructed using the conventional cast-in-place method. Similarly, IaDOT has identified serviceability-related performance issues of slip formed concrete barriers constructed as bridge rails and roadway dividers.

As a result of the IDOT/FHWA study, a moratorium on the use of the slip formed construction method in Illinois was established in July 2004 until improvements in the details, equipment, procedures and specifications related to the slip formed method could be implemented. After comprehensive design and specification changes and a series of trial tests performed from 2005 to 2007, the moratorium on slip formed barriers was effectively lifted. The role of NDE, however, in these processes has not been studied. Furthermore, changes in barrier shape have prompted questions as to the applicability of the current procedures. A spring 2006 conference hosted by the Midwest Concrete Consortium and attended by transportation representatives from Illinois, Wisconsin, Iowa, Michigan, Missouri, Minnesota, and others included extensive discussion and presentations on the common problems each entity has experienced with this style of barrier.

1.2. Slip Formed Concrete Distress

Numerous examples of premature deterioration, visible surface voiding, water leakage through barriers and joints, and other known internal consolidation-related anomalies have been reported in both Illinois and Iowa in recent years, resulting in greater maintenance expenditures and shortened service lives. States have tried to reduce the number of as-built defects by mandating reductions in slip form speeds, adjusting mix designs to include better total aggregate gradations and incorporating water reducers, requiring

stiffened/braced reinforcing cages, and incorporating full-thickness joints into continuously-slipped barriers. Examples of typical conditions identified included the following:

- Horizontal and vertical cracking
- Premature deterioration, most notably freeze-thaw damage
- Incomplete consolidation within slip form train
- Shadowing of internal reinforcing steel
- Tears, fissures, and other internal discontinuities associated with slip form speed
- Voids, bugholes, streaking, and other near-surface irregularities
- Infiltration of water and subsequent leaks at cracks and fissures, often with staining and efflorescence
- Water leakage through deck/barrier interfaces due to incomplete concrete consolidation and poor bond

1.3. Dowel Bar Corrosion Distress

Bridge barriers are cast after the bridge deck, resulting in a construction joint along the base of the barrier. Deicer-laden water can often penetrate this construction joint and cause corrosion of the vertical deformed reinforcing steel stirrups (dowel bars) at the interface and within the barrier. Corrosion-induced section loss of the dowel bars can eventually reduce the capacity of the barrier to transfer traffic impact forces into the deck. Since the construction joint is hidden and the joint allows potentially severe localized corrosion (pitting or knife-edging), it is difficult to assess the deterioration before bars are structurally compromised. Corrosion and bar section loss can occur without spalling concrete since the construction joint allows corrosion byproducts to move freely away from the bar without affecting the surrounding concrete.

Due to the hidden nature of the deterioration, determining an accurate condition assessment technique for concrete barrier dowel bars would be beneficial for routine maintenance and inspections of these elements.

1.4. Scope of Work

The objective of this work was to evaluate potential NDE methodologies that may be effective in 1) identifying internal defects within slip formed concrete barriers and 2) assessing the corrosion condition of the barrier dowel bars. Potential techniques were trial tested on laboratory mockup samples built with known defects, trial sections of cast-in-place barriers at in-service bridges in Iowa, and slip formed and cast-in-place barrier walls at in-service bridges in Illinois. This work included review of available studies performed by others, field trial testing to assess candidate test methods, verification of the test methods in identifying internal anomalies and dowel bar corrosion, and preparation of this report. The project scope included the following:

- Document Review
- Assessment of Candidate NDE Systems for Defect Identification
- Assessment of Candidate Methods for Identification of Dowel Bar Corrosion
- Laboratory Testing of Mockup Samples with Known Defects
- Field Testing of Barriers in Iowa (Phase A Field Testing)
- Draft Report Submittal (IaDOT)
- Field Testing of Barriers in Illinois (Phase B Field Testing)

- IDOT Report Submittal
- Final Report (Combined Study) and Development of *Guidelines for Preliminary Barrier Assessment*

Note that Phase B field testing of barrier walls in Illinois occurred subsequent to the initial study and draft report submittal for the IaDOT. Phase B field testing was focused on the detection of concrete defects within existing slip formed barrier walls using a refined testing approach based on the initial study results. Upon completion of the assessment performed for the IDOT, a separate report, entitled *Slip Formed Bridge Parapet Investigation: Work Oder No. 2* dated October 25, 2013, was prepared for IDOT. This report included several appendices containing the results of all Phase B testing, including optical and infrared images of the full barriers, selected results of ground penetrating radar (GPR) and shear wave ultrasonic testing, and documentation of all exploratory cores. The discussion and conclusions presented below include considerations of the field testing performed during both Phase A and Phase B.

1.5. Literature Review

A review of literature pertaining to the nondestructive evaluation of concrete for flaw detection and corrosion assessment was performed prior to this study. The American Concrete Institute provides resources for use in the inspection and testing of structural concrete. ACI 311-1R, *Manual of Concrete Inspection* provides guidelines of the post-construction inspection of concrete, including acceptance inspection, visual inspection, the use of nondestructive evaluation techniques, and destructive sampling and testing (ACI Commitee 311 2007). A comprehensive overview of selected nondestructive testing methods is provided in ACI 228-2R, *Nondestructive Test Methods for the Evaluation of Concrete in Structures* (ACI Committee 228 1998). For each of the nondestructive testing methods that are discussed, this document describes the principles and theory, a brief history of the development of the method for civil applications, guidelines for use in the evaluation of structural concrete, and discussion of the general capabilities and limitations.

Recent studies have investigated the usefulness of various nondestructive evaluation methods for the condition assessment of infrastructure and have provided some direct comparisons between various nondestructive methods. Pla-rucki and Eberhard summarized advances in imaging techniques for the evaluation of embedded reinforcing and for flaw detection in reinforced- and prestressed-concrete elements (Pla-rucki and Eberhard 1995). Although this study did not include direct testing, it provided a review of recognized imaging technologies, including ground-penetrating radar, radiography, and infrared thermography, and introduced several tomographic technologies, which were being employed in laboratory studies at that time. Of the tomographic imaging methods introduced, which included radiographic (gamma) tomography, microwave tomography, and acoustic tomography, only acoustic tomography based on shear wave ultrasonics has been made commercially available for routine concrete assessment applications. Several studies have focused on the evaluation and comparison of nondestructive methods for the assessment of corrosion and corrosion-related delamination in reinforced concrete bridge decks (Scott, et al. 2003) (Gucunski, et al. 2009).

A recent study at Iowa State University to evaluate methods to detect corrosion in highway barrier rails was funded by the Iowa Department of Transportation and the Federal Highway Administration (FHWA). (Jensen T April 2013). Their scope was similar to the goals of this project, but their research was limited to the evaluation of reinforcing section loss—produced by milling—using three techniques, x-ray radiation, GPR, and magnetic flux leakage (MFL). Radiographic (x-ray) techniques were evaluated in the laboratory and found to provide a visual image of the embedded bars if the proper radiation source is

selected and the source was positioned perpendicular to the bar. Bars with milled-reduced cross-section were examined in concrete; however corroded bars with rust pack that could make bar section determinations more difficult were not examined. Other complications included the barrier thickness and geometry. Field testing could not be done due to regulations regarding use of radiation sources, and further research was recommended to evaluate this technique in the field and using backscatter mode.

Iowa State also developed a custom MFL sensor and used it in the laboratory and field. Laboratory tests of single bar samples showed that MFL showed a monotonic decrease in signal response with material loss providing quantification of steel loss. Interference occurs when other reinforcing is in close proximity, so knowledge of the reinforcing steel locations is needed to interpret the response. Further research and verification of this method is needed to determine if it is practical for field use. GPR provided a technique to locate reinforcing, and differences were noted when bars had milled section loss in controlled laboratory tests. Field tests of the MEL and GPR both on the deck and raised 1.5 inch off the deck surface were performed to evaluate signal changes that might indicate bar corrosion and section loss. This testing indicated that the MFL and GPR were in general agreement and could be used complimentary; however, verification of the bar conditions in the field were not confirmed by coring or exploratory openings. Additional research is needed to evaluate the effects of field conditions such as concrete moisture, chloride content, barrier configurations, concrete cover, and reinforcing congestion.

Nondestructive evaluation methods considered as possible methods for the detection of corrosion-related distress or internal concrete flaw detection were selected based on our review of previous studies and our experience. Additional references specific to the methods selected for this study are presented in the technical discussion of each method provided below.

1.6. Nondestructive Test Methods: Internal Concrete Flaw Detection

The following nondestructive testing methods were included in this investigation to study their effectiveness in identifying slip formed production-related flaws.

1.6.1. Impact-Echo Ultrasonic Testing (IE)

1.6.1.1. Technical Background

Impact-echo (IE) testing is a nondestructive evaluation method based on the spectral analysis of reflected waves. IE testing of concrete elements can detect the presence and approximate depth of internal flaws, such as honeycombing, delamination, planar cracking and cold joints, or to measure overall member thickness (up to an approximate depth of 24 inches). The method involves introducing mechanical energy, in the form of a short pulse, on the surface of a structural element using a small steel impactor. Stress waves reflected from internal discontinuities or member boundaries are measured using a signal displacement transducer positioned near the impact. In general, as the transmitted energy travels through the material, changes in acoustic impedance in the material are encountered, and the energy is reflected back to the surface. The analysis of reflected waves is typically performed by assessing the amplitude and attenuation of the wave in the time domain. Additionally, dominant reflection frequencies can be identified in a frequency spectral plot obtained by performing a Fast Fourier Transform (FFT) analysis of the received waveforms. If the wave propagation velocity through the material is known, the frequency spectrum plot can be used to identify the depth to internal discontinuities or external boundaries. Figure 1 presents a schematic representation of the IE method and a typical frequency spectral plot resulting from analysis of the received signal. For unflawed plate-like structures, such as the vertical face of the barrier

wall, a majority of the compressive waves will reflect from the back surface of the wall, which can be identified on the frequency spectrum plot. Internal flaws or damage is indicated by response frequencies either higher or lower than the dominant frequency associated with the barrier wall thickness.

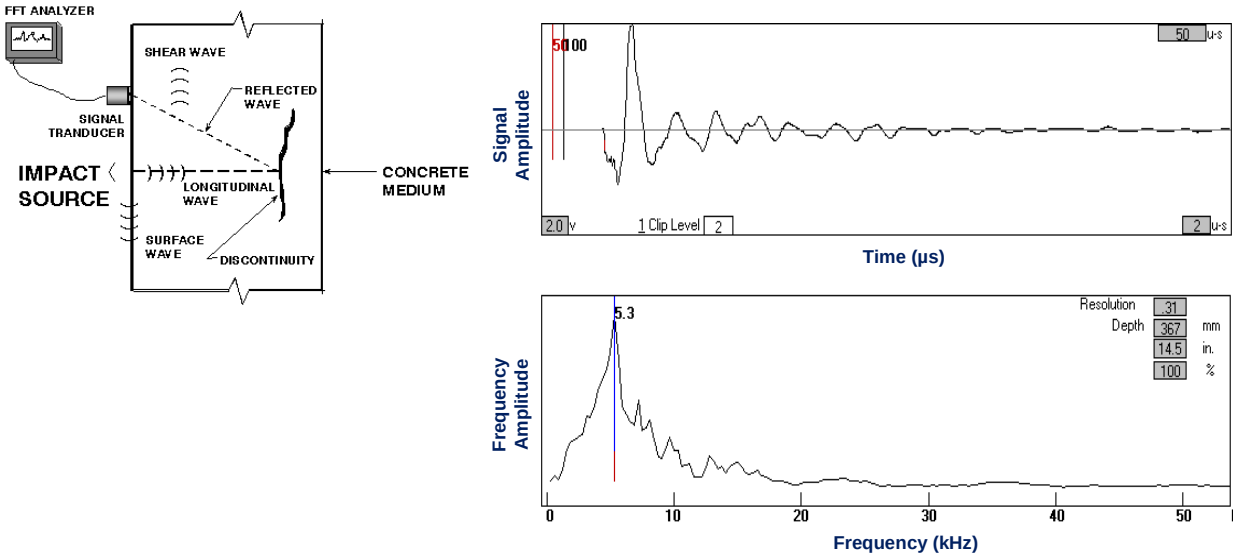

Figure 1. Representation of impact-echo testing (left). Typical output of IE testing showing time domain plot (right, top) and frequency spectrum FFT analysis (right, bottom).

Requirements for IE testing equipment and data acquisition system are standardized in American Society for Testing and Materials (ASTM) C1383-04 (2010), *Standard Test Method for Measuring the P-wave Speed and the Thickness of Concrete Plates Using the Impact-Echo Method*. The IE method was developed in the 1980s specifically for the testing of concrete structural members (Sansalone and Carino 1986). Applications have included determining the thickness of plate-like structural members and detecting flaws such as planar delamination, honeycombing, and ungrouted ducts within reinforced concrete elements (Sansalone and Carino 1988) (Sansalone and Streett 1997) (Gucunski, et al. 2009).

Based on the principles of the impact-echo method, scanning impact-echo (SIE) equipment has been developed that allows for automated collection of IE data at predefined test spacing along distinct scans. Automated systems were developed shortly after the development of the conventional IE method and have been used primarily for bridge deck and floor slab delamination detection (M. Sansalone 1993). Recent equipment includes a rolling hand cart assembly, which mechanically impacts the surface and simultaneously collects received waveforms using displacement transducers mounted to an internal wheel. The advantages and limitations of this testing method are congruent with conventional IE testing; however testing can be performed more quickly along individual scan lines, and the systems provide for more automated data analysis and processing.

1.6.1.2. Equipment Used

Trial testing of the IE method was performed using a conventional IE testing system consisting of a data acquisition unit and testing software supplied by Impact-Echo Instruments of Ithaca, New York and a Mach IV displacement transducer supplied by Germann Instruments of Evanston, Illinois (Figure 2). Use

of a scanning IE system was not included in this investigation; however it is anticipated that scanning IE equipment would provide analogous results while also providing higher speed data collection and increased testing resolution.

Figure 2. IE testing on the interior face of the mock-up barrier wall.

1.6.2. Shear Wave Ultrasonic Testing

1.6.2.1. Technical Background

Shear wave ultrasonic testing is a concrete flaw detection method capable of generating 3-D tomographic images of structural elements. Based on the principles of reflective ultrasonics, shear wave testing requires access to only one side of a structural element. The method is commonly used in concrete, stone, and masonry structures to detect internal flaws such as delamination, honeycombed concrete, and voids in grouted tendon ducts systems. Shear wave tomography involves introducing shear waves using an array of piezoelectric transducers at the testing surface. Shear waves reflected from changes in acoustic impedance in the material are measured by the transducer array. With knowledge of the propagation velocity through the material, the data can be analyzed to determine the depth to internal flaws or the back surface of the element. Experienced operators are required for data interpretation and analysis. Shear wave ultrasonic testing using the MIRA Tomographer system, described below, is a relatively new nondestructive testing method for the evaluation of reinforced concrete elements. Although research is limited, the ability of the method in element thickness determination and in detecting subsurface concrete flaws has been studied (Hoegh, Khazanovich and Yu 2011).

1.6.2.2. Equipment Used

Commercially-available shear wave systems include the Eyecon Monolith© and MIRA Tomographer© testing devices (Figure 3), both of which are supplied by Acoustic Control Systems, Inc. The Eyecon Monolith testing system is a smaller handheld device consisting of 24 transducers. The Eyecon unit can

be useful for localized testing and evaluation of the shear wave ultrasonic testing method; however, it has reduced imaging capabilities in comparison to the MIRA Tomographer.

The MIRA Tomographer system, the primary testing device for this investigation, consists of an antenna array with 40 ultrasonic transducers capable of transmitting and receiving ultrasonic shear waves. Figure 4 shows the MIRA Tomographer in use on a barrier wall. Each transducer is a spring-loaded, dry-point contact piezoelectric sensor capable of generating shear waves at variable frequencies. Each transducer is built with a wear-resistant ceramic tip, which allows testing on rough surfaces. Once the ultrasonic shear wave signal is emitted, the received signals are processed by the controlling console and then transferred to a laptop computer via Wi-Fi wireless technology for analysis. A synthetic aperture focusing technique (SAFT) data processing method is then performed to generate the 3-D images of the tested element. The reconstructed images are displayed as a plan view, cross-section, and isometric views.

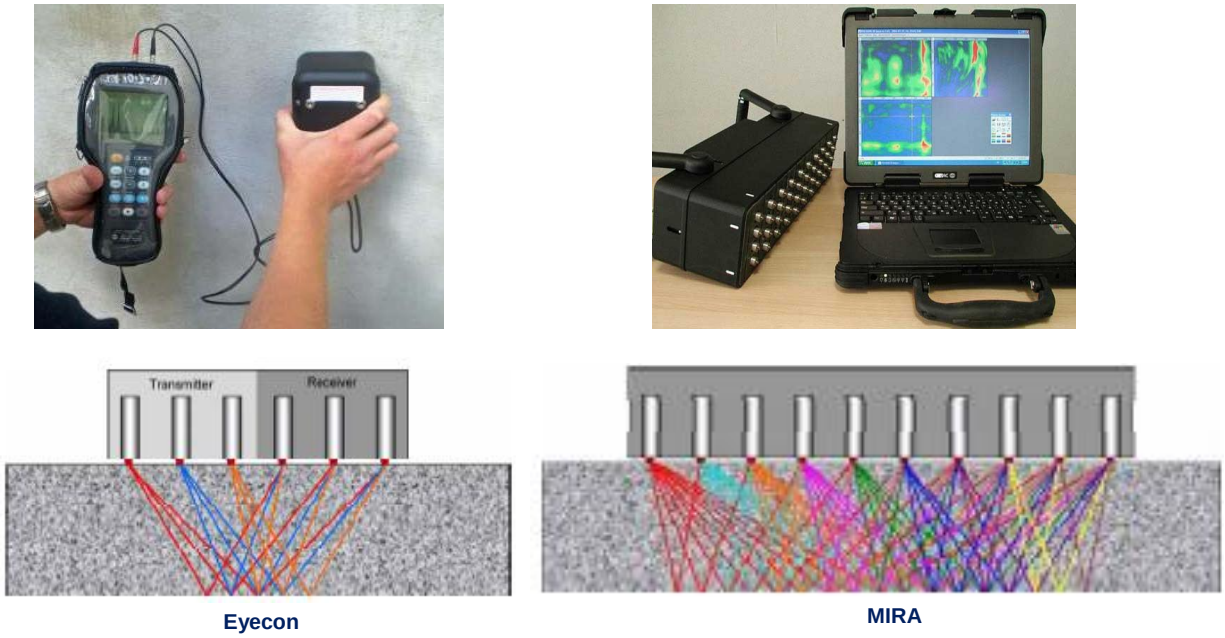

Figure 3. Representation of shear wave ultrasonic testing devices Eyecon Monolith (left) and MIRA Tomographer (right).

Figure 4. Shear wave ultrasonic testing (MIRA) using the MIRA Polygon testing device on the interior face of the south barrier wall of Westbound MRB.

1.6.3. Ultrasonic Pulse Velocity Testing (UPV)

1.6.3.1. Technical Background

Ultrasonic Pulse Velocity (UPV) is a nondestructive evaluation method for existing condition assessment, material property evaluation, and quality assurance testing. Based on the principles of through-transition ultrasonics, UPV testing of structural materials applies fundamental theories of vibrating elastic mediums to measure changes in material density and elastic modulus. Pulse velocity measurements on concrete members have been used to assess uniformity and relative quality of concrete, locate regions of internal cracking, and identify and assess the extent of internal voiding. Additionally, UPV has been used for quality control of concrete placement, and measurements have been used to assess compressive strength of cured concrete with proper correlation testing.

Ultrasonic pulse velocity testing involves the introduction of pulsed longitudinal stress waves at the surface and measurement of received signals on opposing or alternate faces of the test element (Figure 5). Stress pulses are transmitted and received using piezoelectric transducers that are acoustically coupled to the testing surfaces. Transit time and signal amplitude of a transmitted pulse are measured using a pulse velocity meter and a digital oscilloscope. Detected changes in arrival time, amplitude, and characteristics of the propagated waves can indicate corresponding differences in the internal condition of the element. Quantitative and qualitative assessments of measured signals are performed by experienced operators. For the testing of concrete, sound regions exhibit strong signal transmittance, with nominal signal attenuation normally associated with varying path lengths through the member. The presence of internal flaws or areas of deterioration effect stress wave propagation through the member. Poor surface conditions, such as delamination, laitance, or unsound surfaces, can also result in significant signal attenuation during testing. The testing method is based on procedures outlined in the ASTM C 597, *Standard Test Method for Pulse Velocity through Concrete.*

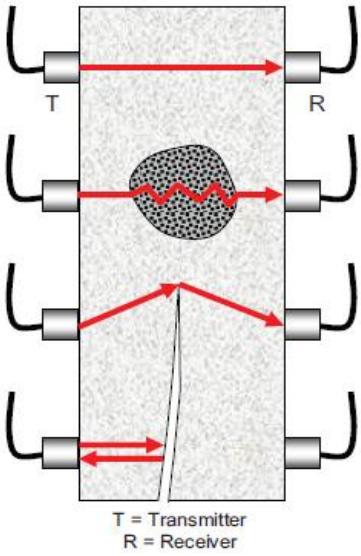

Figure 5. Representation of UPV ultrasonic testing of a concrete member with internal flaws.

1.6.3.2. Equipment Used

Evaluation of the UPV method was performed using a Proceq Pundit Lab© testing system in combination with two 54 kHz ultrasonic transducers (Figure 6). The Pundit Lab system allows for real-time evaluation of the received ultrasonic waveform using a software-based digital oscilloscope. A water-based ultrasonic gel was used to establish the necessary acoustic coupling with the test surface.

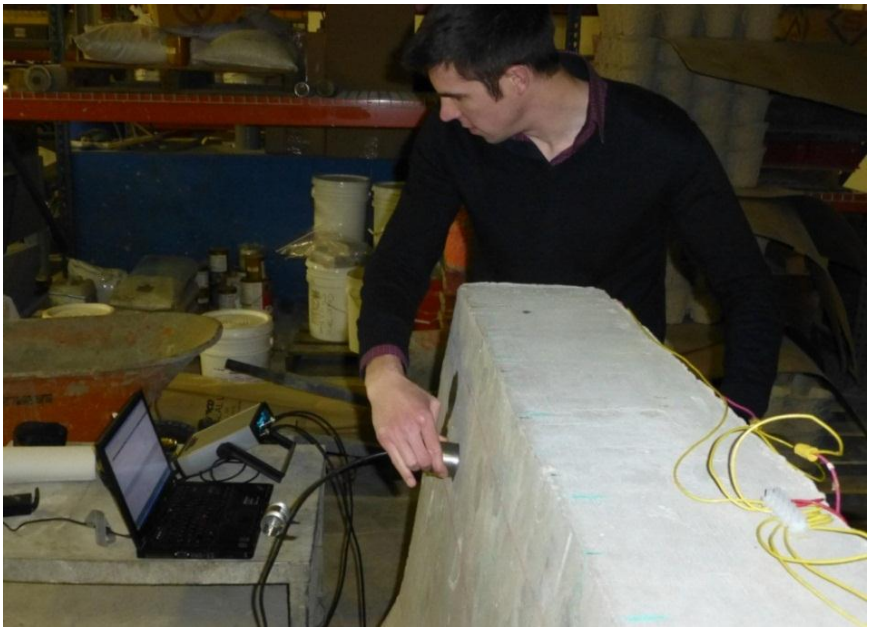

Figure 6. UPV testing on the mock-up barrier wall.

1.6.4. Ground-Penetrating Radar (GPR)

1.6.4.1. Technical Background

GPR is a geophysical nondestructive testing technique for the evaluation of structural elements and materials. The method involves using electromagnetic waves to assess the internal characteristics of the material. GPR surveys performed on structural concrete elements allow for the detection and location of embedded objects (such as mild steel reinforcement, prestressing/post-tensioning strand, metal and plastic conduit), assessment of member thickness and element geometry, identification of internal conditions (such as poor consolidation and flaws), and assessment of material interfaces (such as a slab-to-sub-base interface).

The technique involves the use of a high-frequency radar antenna that transmits electromagnetic radar pulses along a discrete longitudinal scan at the surface of a structural element or geological material. Electromagnetic signals are reflected from material interfaces of differing dielectric properties along the propagation path of the waves. Signals are collected by the antennas, amplified, and displayed for subsequent interpretation. GPR antennas with different operating frequencies provide for GPR surveying at various depths into the substrate. Additionally, post-processing software integrating signal filtering and visualization functions allows for subsequent analysis of the GPR scans collected.

The principles and general guidelines of GPR for the evaluation of structural concrete and subsurface assessment are provided in ACI 228.2R (ACI Committee 228 1998) and in ASTM D6432 *Standard Guide for Using the Surface Ground Penetrating Radar Method for Subsurface Investigation.* Early civil applications of GPR included the detection of voids beneath airfield pavements (Bertram, Morey and Sander 1974) and thickness measurement of concrete elements (Clemeña and Steele 1988). Study of the use of GPR for the detection of embedded reinforcing and the identification of delamination within reinforced concrete bridge decks has been widespread (Gucunski, et al. 2009) (Parrillo, Roberts and Haggan 2006) (Scott, et al. 2003). The effectiveness of GPR in identifying dry-cast production-related flaws such as voids around reinforcing bars and unconsolidated concrete is relatively unknown.

1.6.4.2. Equipment Used

Trial testing was completed using a Sir-3000© GPR control unit manufactured by Geophysical Survey Systems, Inc. (GSSI). Two types of antennas were used, 1) 2000 MHz frequency “palm” antenna with a signal penetration depth of 9-12 inches, and 2) 2600 MHz frequency “structure-scan” antenna with a signal penetration depth of 8-10 inches. Phase A field testing consisted of trial testing using both antennas. Phase B field testing consisted of more comprehensive testing of longer lengths of barrier wall using only the 2600 MHz frequency antenna. All data post-processing was completed using software manufactured by GSSI, commercially known as Radan. Figure 7 shows the “palm” and “structure-scan” antennas in use on the mock-up barrier wall in the laboratory.

Figure 7. GPR testing on the interior face of the mock-up barrier wall. Horizontal scans collected using 2.0 GHz Palm antenna (left) and vertical scans collected using 2.6 GHz antenna (right).

1.6.5. Infrared Thermography (IR)

1.6.5.1. Technical Background

Infrared (IR) thermography is a nondestructive testing method used for the evaluation of concrete, masonry, stone, and other building materials. Infrared thermography is based on the principle that subsurface anomalies affect heat flow through a material, and therefore affect the amount of emitted radiation at the surface. Specialized camera equipment measures emitted electromagnetic energy in the infrared spectrum, which can be correlated with the temperature of the object. IR data is commonly presented in the form of thermograms, which are color-coded photographs showing the temperature of the objects within the field of view. By analyzing IR thermograms and comparing the images relative to other areas of the element, detectable anomalies can be identified.

The technology behind IR thermography is well established, and the construction industry has made use of infrared technology as a NDE method for identifying variations in structural conditions for at least 20 years. Infrared thermography is used to detect near-surface internal conditions in concrete, such as delamination, voids, and cracks. The detectability of any internal anomaly depends on the physical properties (heat capacity, heat conductivity, density) of the materials within the test object, conditions at the surface of the test object, which may affect thermal emissivity, and ambient conditions affecting thermal variation around and within the test object. By studying differences in the surface temperature of a solid concrete slab and a slab with subsurface delamination, researchers have shown IR thermography can be used to quickly evaluate the presence of top surface delamination in bridge decks (Maser and Roddis 1990). The use of IR thermography in the evaluation of bridge decks is standardized as ASTM D4788-03 (2007) *Standard Test Method for Detecting Delaminations in Bridge Decks Using Infrared Thermography*. ASTM D4788-03 provides general guidelines for proper selection of equipment, data collection procedures and reporting applicable to the use of IR thermography for evaluating concrete elements other than bridge decks. Despite this standardization, interpretation of IR data relies on the subjective evaluation of the operator. Researchers have shown that even at low ambient temperatures, infrared thermography can be used to identify subsurface flaws in concrete bridges and to investigate the internal structure of masonry bridges (Clark, McCann and Forde 2003).

The IR method allows for the noncontact evaluation of concrete elements, but is typically limited to the detection of near-surface defects. Near-surface flaws and delamination in barriers are detectable as temperature differences because the thin layer of concrete in front of the flaw responds to changing environmental conditions at a different rate than the surrounding concrete. Detection can be difficult as temperature differences between intact and flawed areas are typically small (less than about 5ºF). Under ideal conditions, radiant heating by the sun or daily ambient temperature changes may be sufficient to produce the necessary thermal gradient. If ambient heating and cooling cycles are not sufficient, an additional external heating source can be used to produce a measurable heat flow. However, an active heating source must provide a uniform distribution of heat at the surface to provide a reliable IR result. Other interferences include moisture on the barrier surface, changes in surface color or texture, and shadows on portions of the barrier from adjacent structures, signs, and trees.

1.6.5.2. Equipment Used

Laboratory testing of infrared thermography was performed on the mockup barrier using a FLIR Model T620 infrared and optical image camera. The camera used is capable of producing images with an infrared resolution (pixel resolution) of 640x480 and a thermal sensitivity of 0.04°C. Phase A field testing was completed using a FLIR Model B20 ThermaCAM infrared and optical image camera. The camera used is capable of producing images with a thermal resolution (pixel resolution) of 320x240 and a thermal sensitivity of 0.08°C. Phase B field testing was completed using both camera types (Figure 8). Data analysis of the collected images was performed using FLIR Tools software commercially available from FLIR. The thermogram images collected contained embedded thermal data providing surface temperatures at each pixel within the image.

Figure 8. Infrared thermography (IR) trial testing on the interior face of the north barrier along westbound Mississippi River Bridge (MRB).

1.6.6. Radiography (X-ray)

1.6.6.1. Technical Background

Radiography (X-ray) is a nondestructive testing method used for the evaluation of internal characteristics of structural members. Methods of radiography include conventional film and digital radiographic testing. During radiographic testing, electromagnetic radiation is transmitted either in the form of X-rays or higher energy gamma rays. A radioactive source is typically placed on one side of the test object, and collection screens are placed on the opposite side. As the radiation passes through the member, it is attenuated depending on the density and thickness of the material that is traversed. Materials within the member that are higher density than the substrate block more of the transmitted radiation. The radiation that is emitted from the opposite face of the member is then measured using collection screens, producing an image of the interior of the member. Radiographic testing methods use radioactive materials, which require test personnel with specialized safety training and licensing. Additionally, areas that are exposed to radiation must be kept clear of the public for extended periods of time during the testing.

Conventional radiographic testing uses special photographic film as the collection screen. The film used is similar to standard photographic film as it is light sensitive, but it also reacts when exposed to radiation. At the completion of the radiation exposure, the image remains invisible as the radiation alone is not enough to reduce the film to a level where the image is visible. Further reduction is required through the developing process in a darkroom. Digital radiographic testing replaces the photographic film with panels of digital X-ray sensors. Results of digital radiographic testing can be post-processed and filtered and provide more accurate, enhanced images. Different techniques and equipment can be used in conjunction with digital radiography to produce real-time imaging. Other practices can create computed cross sections through the member in the direction of radiation.

For concrete member evaluation, radiography can be used to identify embedded metal elements (reinforcing steel, prestressing strand, conduit, etc.), air-filled or liquid-filled pipes, areas of internal voiding, and areas of low-density, or honeycombed concrete. Malhotra summarized early applications of film radiography in the assessment of reinforced concrete elements including determining the position and condition of reinforcing steel, identifying voids in concrete and in the grouting of post-tensioning ducts within concrete elements, and identifying areas of internal honeycomb (V. Malhotra 1976). The British Standards Institution adopted standards for gamma radiography, BS 1881-205, *Recommendations for radiography of concrete* (BS 1881: Part 205), which provides general guidelines and recommendations for those considering the use of radiography for the assessment of structural concrete. The BS 1881-205 standard specifically describes the use of radiography in identifying embedded steel and voids in concrete members.

1.6.6.2. Equipment Used

Traditional radiographic testing of the mock-up barrier wall was performed by Mistras Group, Inc. at WJE's laboratory in Northbrook. Figure 9 shows the radiation emitting device and the radiation collection screen, respectively, for imaging of the barrier wall mock-up. Film sheets measuring 1 foot-2 inch by 1 foot-5 inch were used to collect the radiographic images.

Figure 9. Radiographic testing in progress on the mock-up barrier wall sample. Radiographic source exposed to interior face of the barrier wall (left) and digital sensor panel installed on exterior face of the barrier wall (right).

1.7. Nondestructive Test Methods: Corrosion-Related Distress

1.7.1. Half-Cell Potential Surveying

1.7.1.1. Technical Background

Corrosion potentials, also known as half-cell potentials (HCP), are used to assess the thermodynamic corrosion tendency of reinforcing steel in concrete. As part of structural condition assessment, half-cell potential surveys may be used to identify the pattern and extent of corrosion. Survey data obtained can be used to infer corrosion of embedded reinforcing steel before visible damage to the concrete structure is evident. The method is applicable to concrete members regardless of their size or orientation and has been used in the assessment of bridge decks, piers and superstructure elements, retaining walls, concrete pipes and water-treatment structures.

Half-cell potential surveys were essentially performed according to the methods of ASTM C876, *Standard Test Methods for Half-Cell Potentials of Uncoated Reinforcing Steel in Concrete*. A copper-copper sulfate half-cell electrode (CSE) was used, which consists of a copper rod immersed into a saturated copper sulfate solution. An electrical connection is typically made between the copper rod and the reinforcing steel through a drilled hole in the concrete. The base of the reference cell has a porous plug that provides an ionic current path between the reinforcing steel and the copper rod when the electrode is placed on the surface of the concrete. A dampened sponge is used to provide contact between the porous plug and the surface.

By taking readings of half-cell potentials on the concrete surface over a uniformly-spaced grid, an evaluation of the corrosion risk of the embedded reinforcing steel over a large area can be made. In atmospherically exposed conditions in ordinary portland cement mixtures (such as typical bridge decks and barrier walls), interpretation of results relative to absolute values can be made. ASTM C876 provides general reference values for the interpretation of results in this manner. For buried structures, oxygen-deprived areas, and submerged areas, interpretation of half-cells using this method may not be applicable.

In these instances, contour plotting can provide additional information by graphically showing the relationship between anodic (more negative) and cathodic (more positive) areas.

Due to the nature of the measurements, half-cell potentials do not directly locate spalls, delamination, repair areas, or other damage sites. However, these regions are often anodic and corroding, and thus coincide with more negative potential readings. Additionally, anodic regions that have not yet caused delaminations or spalls are also measured by this technique, and thus can be used as a leading indicator of regions likely to become damaged by corrosion in the near future.

Epoxy-coated bars present some difficulties for corrosion potential surveys. An intact epoxy coating electrically isolates the steel in each bar, preventing measurements of corrosion potential. However, if the epoxy coating is degraded or has a sufficient number of holidays (holes), electrical conductivity may be sufficient for some indication of corrosion tendency.

1.7.1.2. Equipment Used

Two types of equipment were used for trial testing. The first piece of equipment was a single, hand-held CSE reference cell used with a digital multimeter to record potentials in a grid pattern (Figure 10). Second, an automated data collection device with an integrated rolling wheel CSE reference cell (Canin+ by Proceq USA) was used (Figure 11). The rolling wheel equipment is capable of taking readings at measured intervals along the rolling path. For this evaluation, the equipment was set to use measure intervals in the range of 2 inches to 6 inches.

Figure 10. Half-cell potential data collection with a single point reference cell.

Figure 11. Rolling wheel reference cell for half-cell potential measurements.

1.7.2. Corrosion Rate Measurements

1.7.2.1. Technical Background

Corrosion rate measurement involves the assessment of the extent and severity of reinforcing steel corrosion within existing concrete structures in corrosive environments. Corrosion rate is measured using the linear polarization technique and provides a direct, quantitative measurement of the rate of oxidation of embedded steel reinforcing. The corrosion rate measurements are instantaneous measurements of the rate of corrosion at the time of testing. The technique requires sophisticated equipment but is the most conducive method for in-situ corrosion rate assessment.

Linear polarization testing is a recognized corrosion rate assessment technique based on the linear relationship between corrosion current and polarization resistance. During linear polarization testing, an anodic current pulse is induced in embedded reinforcing from a counter electrode placed on the surface of the concrete element. The current is confined to a defined area of the reinforcement. A built-in electrode is used to record the change in potential due to the applied current. From this, the polarization resistance is determined, and the corrosion current is calculated. The corrosion rate measured in terms of mils of section loss per year can be estimated from this current.

1.7.2.2. Equipment Used

Two units are commonly used to measure corrosion rate of reinforced concrete structures. James Instruments Gecor© uses a guard ring to confine the applied current for the steel reinforcing bar corrosion rate determination. Embedded microprocessor systems analyze the data automatically and provide a corrosion rate value. Utilizing the information obtained by the two reference electrodes in a feed-back network, the unit automatically adapts the electrical field produced by the guard ring to the conditions of the concrete. This allows the instrument to reach a quasi steady-state condition for the 30 to 100 seconds

required for determining the polarization resistance through a galvanostatic pulse. The sensor diameter is 7 inches, which makes it impractical for measuring the corrosion rate of dowel bars imbedded at barrier bases.

The GalvaPulse© unit from Germann Instruments evaluates the corrosion rate of reinforcement by measuring polarization resistance using the galvanostatic pulse technique. The applied current is usually in the range of 5 to 400 microamps and the typical pulse duration is 5 to 10 seconds. The reinforcement is polarized in the anodic direction compared to its free corrosion potential. Readings can usually be taken more quickly than with the Gecor unit, and the probe diameter is smaller.

The two different units measure corrosion rates slightly differently and will give different results. However, each unit should provide relative corrosion rate values between bars within a certain barrier. For our study the GalvaPulse unit was used due to its smaller probe size and shorter scanning period.

1.7.3. Impulse-Response Structural Mobility Testing

1.7.3.1. Technical Background

Impulse-response testing is a nondestructive evaluation method based on the mobility response of a structure to a dynamic energy pulse. An impact imparted on the surface of an element produces a dynamic excitation, which is measured to determine the mobility of the element. Impulse-response testing is typically used to assess the internal, support, or bonded conditions of structural elements. This method will not measure corrosion of dowel bars directly but may be useful for determining when a series of dowels have corroded completely through, affecting structural impact (tip-over) capacity.

Impulse-response testing consists of exciting a structural element with a low-strain impact and measuring the modal response at the surface of the element. The impact is imparted and measured using an instrumented hammer capable of generating response frequencies of up to 1000 Hz. The modal response of the structural element is measured using a velocity transducer positioned adjacent to the impact point. Output from the hammer load cell and the velocity transducer are collected and the mobility (velocity per unit force) of the test element as a function of frequency is analyzed at distinct testing points. Evaluation of the data includes assessment of the dynamic stiffness, average mobility, mobility slope, and voids ratio. Testing results indicating a relatively high mobility response compared to surrounding points are indicative of a potentially anomalous internal or support condition that could be present due to failed dowel bars. Data can be combined to create contour plotting of the data collected throughout a testing grid.

1.7.3.2. Equipment Used

Impulse-response field testing was performed using a Germann Instruments s'MASH© impulse-response testing system. For each measurement, an impact was imparted along the base of the lateral face of the barrier wall using a rubber-tipped modal hammer, and the response was measured using a surface mounted velocity transducer. Data was exported from the integrated propriety software into a tabular format for subsequent plotting.

1.7.4. Concrete Resistivity Measurements

1.7.4.1. Technical Background

Concrete resistivity provides an indication of the corrosiveness of the concrete environment. Areas of high moisture or deicer salt concentrations will have lower electrical resistivity than drier areas or areas with less chloride. Resistivity probes are based on 4-point Wenner probe design. A current is applied to the two outer probes, and the potential difference is measured between the two inner probes. The current is carried by ions in the pore liquid. The calculated resistivity depends on the spacing of the probes. Resistivity $\rho = 2\pi a V/I$ [kΩcm], where *a* is the spacing between each probe, V is the measured potential, and I is the applied current.

Surface resistivity measurement can provide useful information about the state of the concrete at the time of the measurement. Resistivity is linked to the likelihood of corrosion and the corrosion rate. It also provides indications of variations in chloride diffusion rate. It is completely nondestructive test that can be rapidly performed. Equipment is only moderately expensive.

1.7.4.2. Equipment Used

A Proceq Resipod© resistivity meter (38 mm, 1.5 inch) was used for this work.

2. MOCK-UP AND FIELD TEST LOCATION DETAILS

In order to evaluate the effectiveness of each NDE technique to detect internal voids or dowel bar corrosion, WJE combined a laboratory study on two mock-up samples, testing of trail barrier segments commissioned by IDOT, and field testing of existing barrier walls within Iowa and Illinois. The two laboratory mock-up samples consisted of a flat slab sample and a barrier wall segment cast on a slab with a construction joint, both of which were constructed and evaluated in our structural laboratory in Northbrook, Illinois. The trail barrier segment commissioned by IDOT consisted of approximately 40 feet of slip formed barrier constructed by Killian Construction Company. Following construction and testing of the laboratory mock-ups, field testing of selected areas of the barrier walls on three bridges in Iowa using selected NDE techniques was performed (Phase A field testing). Furthermore, at the request of IDOT, field testing was performed on slip formed and cast-in-place barriers on several in-service bridges in Illinois (Phase B field testing). Phase B field testing consisted of the evaluation of larger lengths of barrier wall using GPR, infrared, shear wave ultrasonic testing (MIRA) and exploratory coring. Construction details for the mock-ups, exposure and distress conditions for the mockups, and details of the field test locations for both Phase A and Phase B field testing are discussed in the following sections.

2.1. Laboratory Mock-up: Flat Slab

A flat slab mock-up sample was created to represent the construction joint between the concrete deck slab and the barrier wall. The purpose of this sample was to evaluate corrosion detection methods without the confounding influence of the barrier geometry.

2.1.1. Flat Slab Mock-up Construction

The overall measurements of the flat slab were 10 feet long by 2 feet-6 inches wide and 5-1/2 inches thick. The concrete slab sample was cast in two pours in order to create a construction joint at the center of the slab along the entire length. The construction joint was formed with smooth edges to allow water to pass through the joint. An overall view of the flat slab sample is shown in Figure 12.

Figure 12. View of flat slab mock-up with heated box enclosure.

The flat slab contained ten No. 5 transverse reinforcing steel bars equally spaced across the length of the construction joint in the slab. Each reinforcing bar represented a dowel across the construction joint between the deck and the barrier wall in typical bridge construction. To reflect the range of conditions that may exist at this interface, the reinforcing bars were prepared in multiple ways including removal of the epoxy coating, artificial section loss of one-half the bar area, and section loss of one-half of the bar diameter.

2.1.2. Chloride Exposure

Prior to placement in the slab sample, corrosion was introduced into various reinforcing bars by exposure to wetting and drying cycles with salt solution. Each cycle consisted of wetting the bar in a salt-water solution and then placing the bar in a heat chamber to dry. This process was performed approximately ten times per week for a total of six to eight weeks. An example of a corroded reinforcing bar prior to placement in the slab sample is shown in Figure 13. After the pre-corrosion process was completed, surface chlorides were removed, and the reinforcing bars were cast into the slab sample with the corroded portion of the bar located directly in-line with the construction joint. The placement of the pre-conditioned reinforcing bars is shown schematically in Figure 14.

After the flat slab sample was cast, corrosion of the embedded reinforcing bars was accelerated by additional ponding and cycling of saltwater over the construction joint. A salt-water solution was ponded on the surface of the slab sample and was allowed to soak into the concrete and joint for approximately six to eight hours. At the end of this soaking period, the water was removed and the flat slab sample was covered with an insulated box and exposed to heat lamps to allow the slab to dry. Approximately five cycles of wetting and drying were performed per week for a total of 12 weeks. The ponded salt-water solution at the construction joint and the insulated cover can be seen in Figure 12.

Figure 13. Pre-corroded reinforcing bar prior to placement in flat slab mock-up.

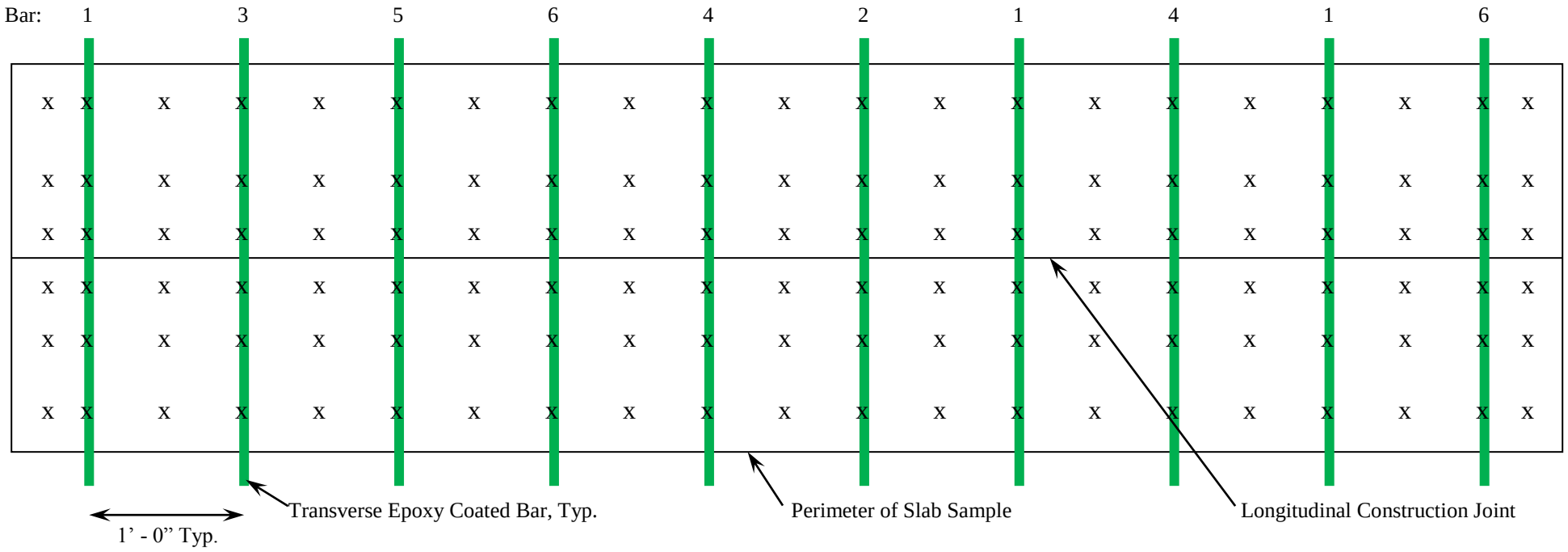

Bar Legend:

1 – Epoxy not removed, no initial corrosion
2 – Epoxy removed, no initial corrosion
3 – Epoxy removed, initial corrosion = 6 weeks
4 – Epoxy removed, initial corrosion = 8 weeks
5 – Epoxy removed, milled to ½ area, initial corrosion = 8 weeks
6 – Epoxy removed, milled to ½ diameter, initial corrosion = 8 weeks

X – Location of half-cell potential testing

Figure 14. Schematic of flat slab construction.

2.2. Laboratory Mock-up: Barrier Wall

The barrier wall mock-up sample consisted of an initially constructed reinforced concrete 'deck' slab and a subsequently constructed vertical barrier wall section, resulting in a doweled joint. The vertical portion of the wall segment was reinforced based on IaDOT barrier wall standard drawings. The wall design included internally embedded voids and flaws to represent those found in slip forming and physically altered reinforcing dowels to simulate corrosion-related distress.

2.2.1. Barrier Wall Mock-up Construction

The barrier wall was constructed based on the standard dimensions of an IaDOT slip formed barrier wall, as shown in Figure 15. Epoxy coated reinforcing bars were used exclusively in the construction of the sample. The sample was created by initially constructing a portion of a bridge deck approximately six feet long and 7-1/2 inches thick. The size and spacing of the longitudinal and transverse bars in the bridge deck portion matched typical construction used by IaDOT. In addition, the 5c2 dowel bars detailed in the standard drawing were cast into the deck portion and hooped around the longitudinal bars at the edge of the deck. The deck reinforcing steel prior to concrete placement can be seen in Figure 16.

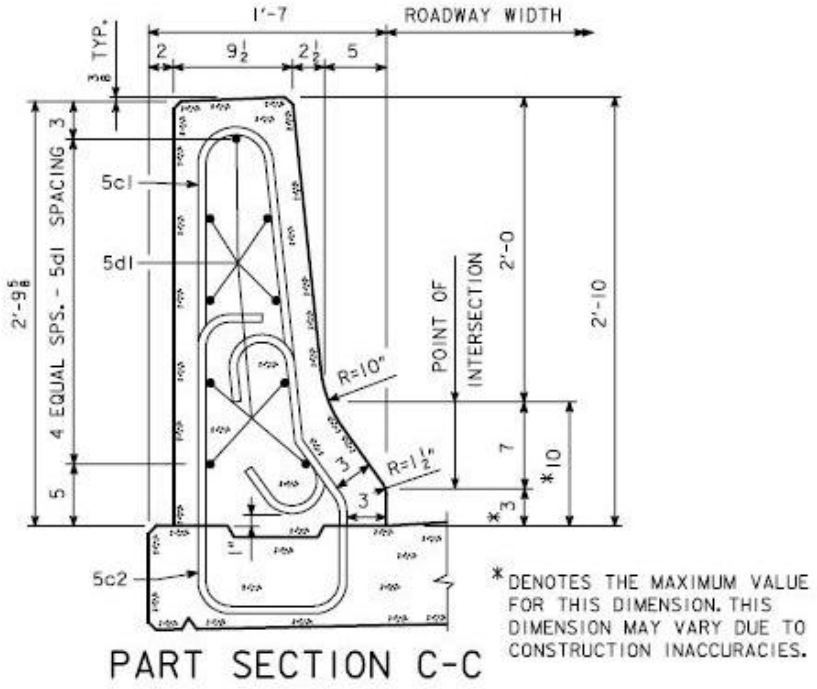

Figure 15. Standard detail for Iowa DOT slip formed barrier wall used for the laboratory mock-up construction.5c2 bars are the embedded dowel bars crossing the construction joint and attach the barrier to the bridge deck.

Figure 16. Deck reinforcing and 5c2 bars (dowels) prior to concrete placement. The six 5c2 bent dowel bars are labeled from left to right in this view 1L, 4S, 1C, 4NS, 4B, AND 1R.

Similar to the flat slab laboratory mock-up, the (5c2) bars crossing the deck/wall construction joint were prepared to represent varying levels of corrosion-induced deterioration. The artificial deterioration introduced into these bars ranged from breaches in the epoxy coating to a severed bar representing full section loss. From left to right when standing on the deck portion, the bar deterioration types (and labels) were:

- Breaches in epoxy coating only (1L), Figure 17
- Epoxy coating removed, necking and severing of bar (4S), Figure 18
- Breaches in epoxy coating only (1C) , Figure 19
- Epoxy coating removed, necking of bar to near-severed condition (4NS) , Figure 20
- Epoxy coating removed, no section loss (4B), Figure 21
- Breaches in epoxy coating only (1R), Figure 22

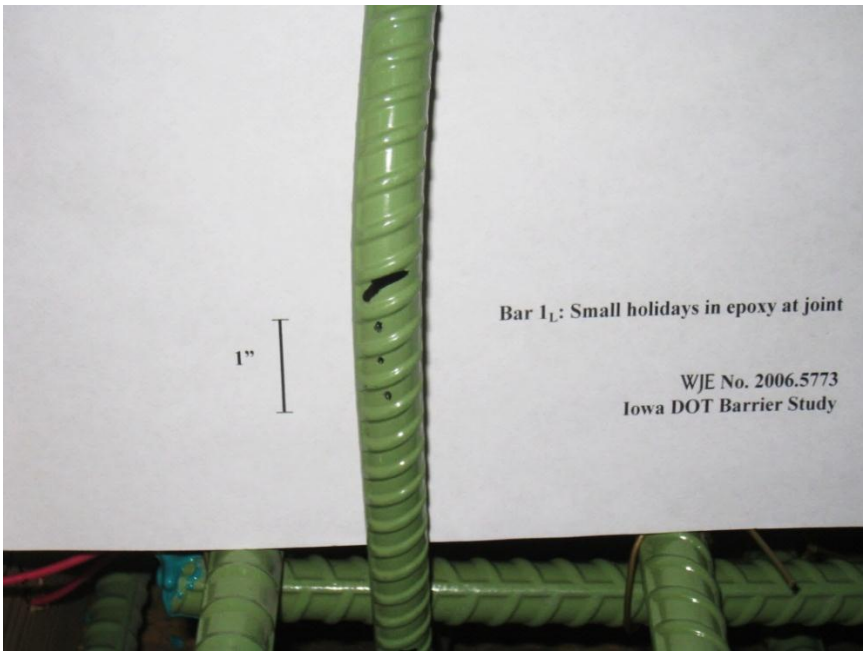

Figure 17. Defect in bar 1L - Small holidays in epoxy at construction joint.

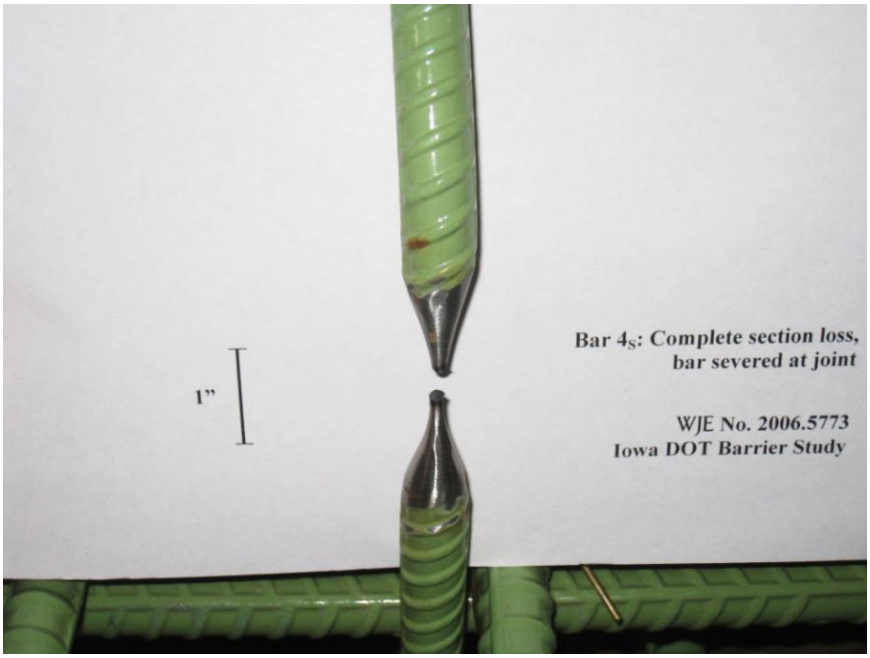

Figure 18. Defect in bar 4S - Complete section loss, bar severed at construction joint.

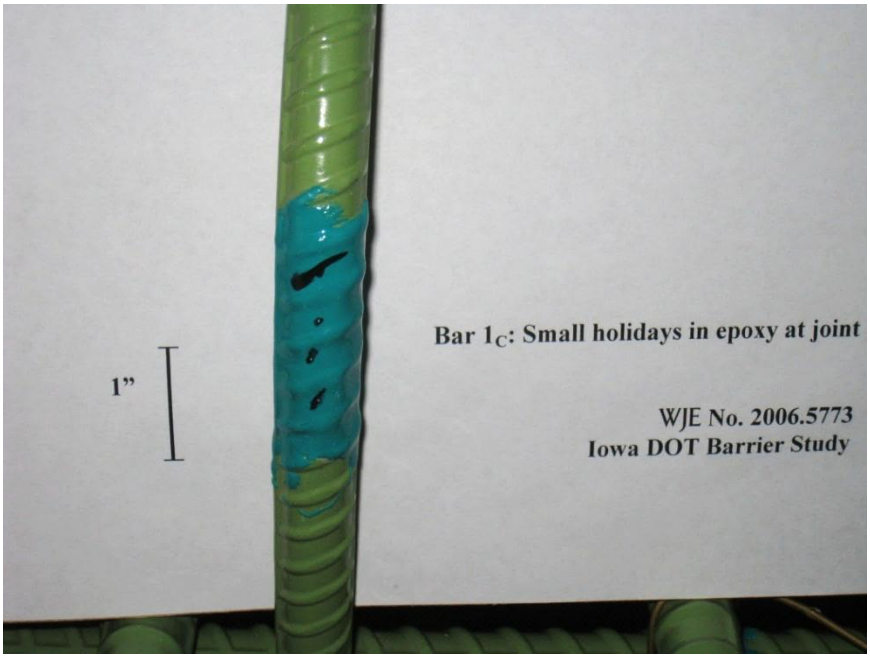

Figure 19. Defect in bar 1C - Small holidays in epoxy at construction joint.

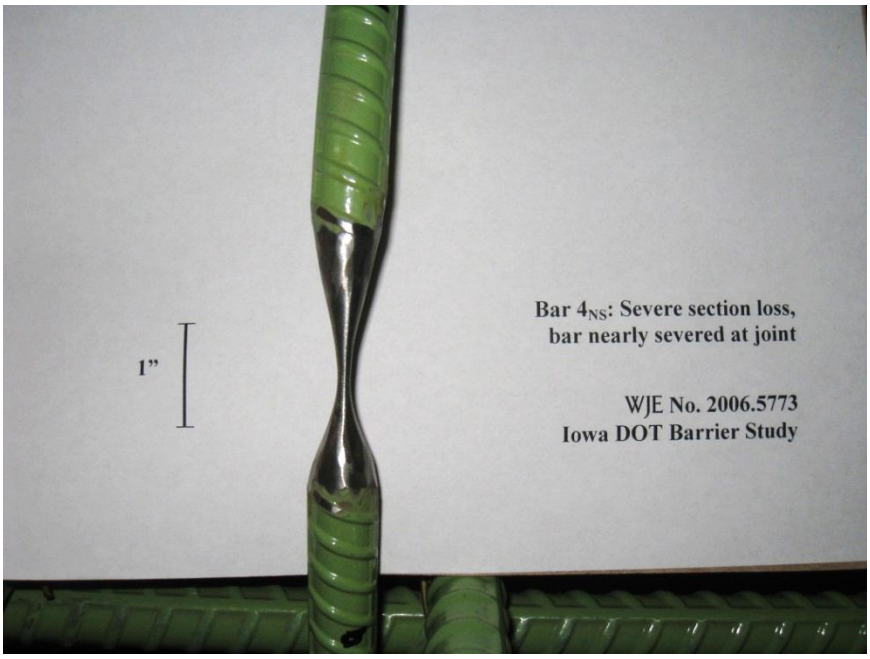

Figure 20. Defect in bar 4NS - Severe section loss, bar nearly severed at construction joint.

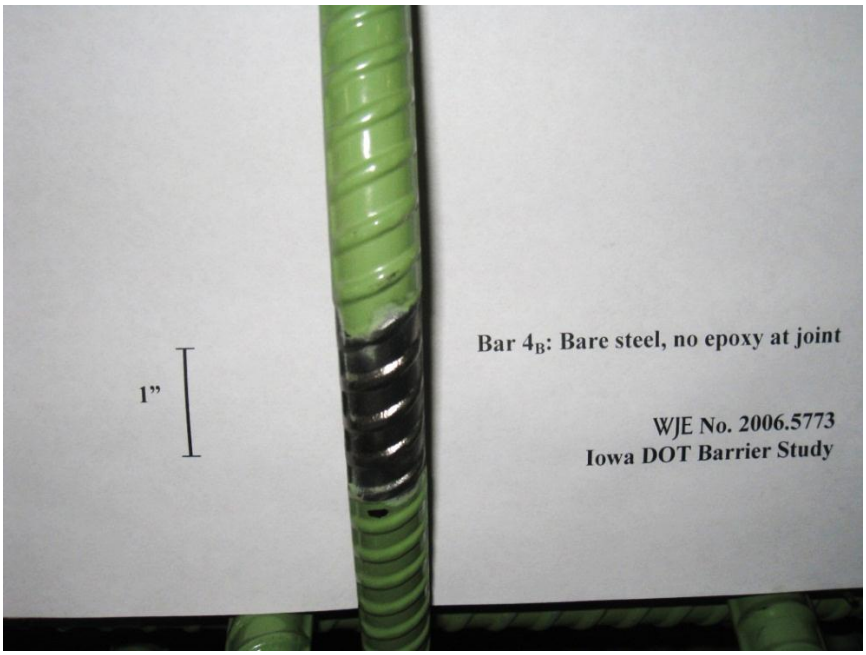

Figure 21. Defect in bar 4B - Bare steel, no epoxy at construction joint.

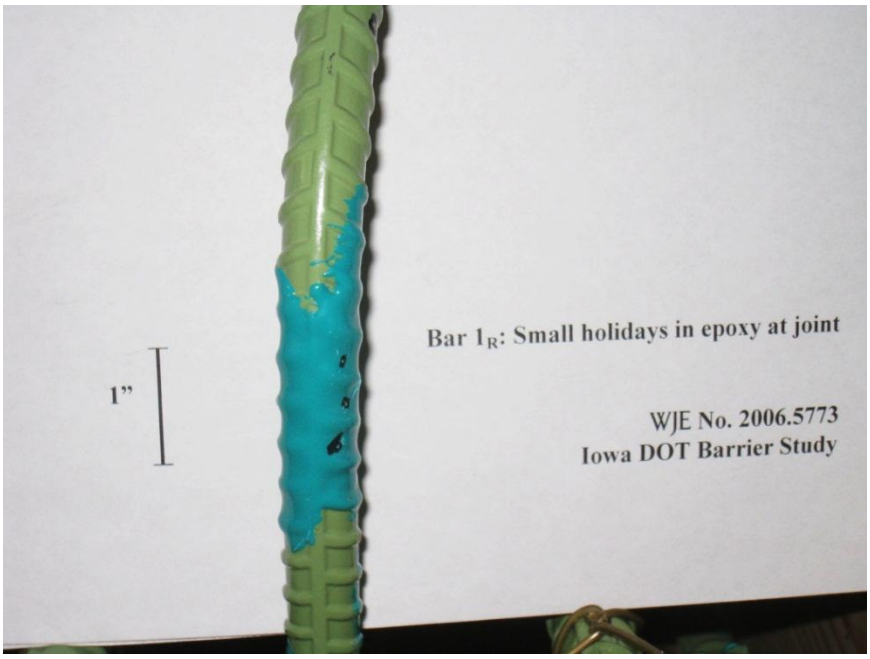

Figure 22. Defect in bar 1R - Small holidays in epoxy at construction joint.

When the hooped 5c2 dowel bars were machined to represent section loss, the removed steel shavings were saved and confined with gauze around the bar prior to placement of the concrete. The steel shavings

were placed to create a partial void in the area around the deteriorated bar as well as to mimic corrosion product produced after application of the salt water solution. For each of the 5c2 bars, the center of the artificial deterioration was located at the construction joint between the deck and the barrier wall.

The longitudinal reinforcement was attached to the hooped 5c2 bars and the 5c1 hoop extensions using zip-ties and padded tape to prevent undocumented abrasion of the epoxy coating and to isolate each bar electrically. Eight internal defects were then placed throughout the reinforcement grid to mimic internal consolidation anomalies, as shown in Figure 23 and Figure 24. Defects were represented by embedded foam insulation, honeycombed concrete defects, and a thin metal plate. The embedded foam insulation panels, labeled V1, V2, and V3, were designed to simulate moderate air-filled voids within the barrier wall, and consisted of three 1 inch thick by 3-1/4 inch square panels positioned at multiple depths from the interior face of the wall segment. The void panel depth (cover) measurements, as measured from the front face of the barrier wall, were 1-1/8, 4, and 6-3/16 inches for V1, V2 and V3, respectively. The embedded honeycomb defects, labeled D1 to D5, were designed to replicate local regions of paste-voided concrete and consisted of pre-made circular pucks and panels of poorly-consolidated aggregate and cement paste. Defects D1 and D2 were circular pucks measuring 6 inches in diameter and 2 inches thick. Defect D1 was positioned with a depth (cover) measurement of 2-1/4 inches from the front face of the wall. Defect D2 was positioned with a depth (cover) measurement of 1-3/4 inches from the rear face of the wall. Defects D3 to D5 were rectangular-shaped defects measuring approximately 8 inches long by 5 inches high by 2 inches thick. Defect D3 was positioned in a skewed configuration with a depth (cover) measurement of 2-3/8 inches from the front face of the wall. Defects D4 and D5 were positioned perpendicular to the longitudinal axis of the barrier wall with a depth (cover) measurement of 2-1/4 and 2-3/4 inches from the front face of the wall, respectively. The remainder of the wall was constructed with no voids to provide for control areas to allow for comparison of flawed and unflawed internal conditions.

Figure 23. Barrier wall reinforcing bars and concrete internal consolidation voids and defects (view of rear face of barrier wall).

Figure 24. Barrier wall reinforcing bars and concrete internal consolidation voids and defects (angled view of rear face of barrier wall).

To allow for corrosion potential studies, wiring was attached by taping to the longitudinal bars of the deck and barrier wall, as well as the 5c1 bent bars. The deck reinforcement and 5c2 bent dowel bars were placed in forms and supported to maintain proper position. The base deck slab was cast first and allowed to cure. A shallow, salt-laden mix of concrete consisting of 15 percent by weight of sodium chloride was placed by hand at the bottom of the barrier to simulate salt infiltration at the joint and to accelerate corrosion of the dowel bars. The remaining barrier wall concrete was placed taking care not to disturb the pre-placed artificial defects.

2.2.2. Chloride Exposure

A saltwater solution pond was created on the traffic side of the construction joint between the barrier and the deck after the forms were removed. The ponding allowed saltwater to flow through the construction joint to promote corrosion of the embedded dowels. Cycles of ponding and drying were carried out.

2.3. Trial Slip Formed Barrier Wall Segment

Killian Construction Company constructed a trial parapet segment within a storage and staging yard outside Edwardsville, Illinois (Figure 25) as part of the project-specific slip forming prequalification process required by IDOT. The trial parapet was intended to demonstrate construction practices for the production of 42-inch high barriers using the slip formed construction method per IDOT standards.

As part of the trial, portions of the parapet were destructively evaluated. Within 24 hours of the barrier wall construction, the wall segment was saw cut into seven segments, each of which measured approximately 5 feet long. The saw cut sections of wall allowed for assessment of the internal conditions within the barrier segment. Additionally, a four inch diameter core was taken from one of the segments.

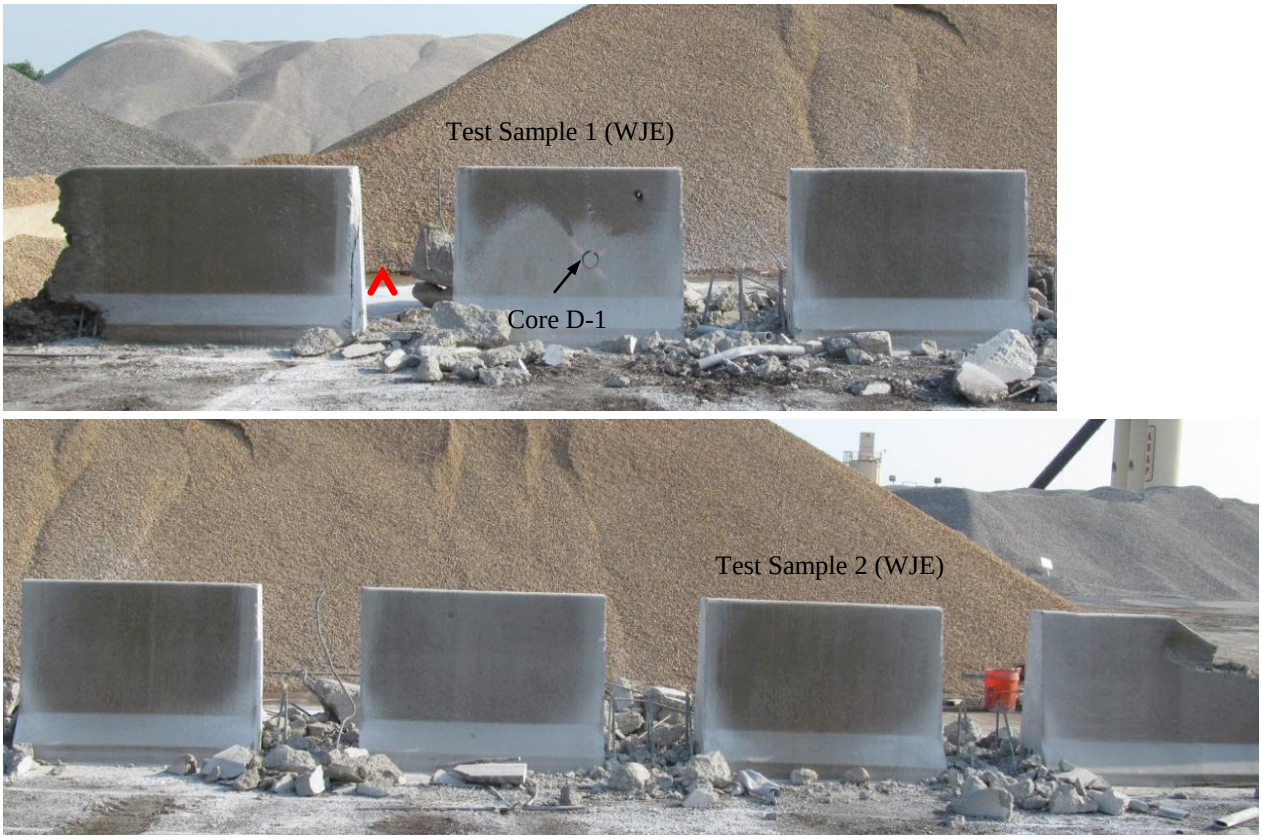

Figure 25. View of trial parapet segment within storage yard. Portions of barrier wall trial tested by WJE are identified as Test Sample 1 and Test Sample 2.

During the Phase B field testing program described below, WJE conducted trial testing of selected NDE methods on two parts of the Killian wall segment. Trial testing was performed primarily to evaluate the feasibility of performing testing of barrier walls shortly after construction. The testing was performed approximately 48 hours after slip forming.

2.4. Phase A Field Testing: Iowa Barrier Walls

Field testing of the selected nondestructive testing techniques was performed on limited sections of barrier wall at three bridges selected by IaDOT. Descriptions and relevant features of the three bridges, identified for this report as US 30, Iowa 150, and US 218, are provided in Table 2. Field testing at each bridge comprised of general visual assessment of the barrier walls, selection of a representative portion of barrier wall for in-depth study, condition documentation of the in-depth study area, NDE testing data collection using various selected testing methods, and subsequent data analysis. IaDOT personnel were on site during a majority of the field testing activities at each location.

2.4.1. US Route 30 over Missouri River [IaDOT No. 4300.0S030]

Iowa 4300.0S030 (Blair Bridge) carries US Route 30 over the Missouri River in Harrison County, Iowa, and straddles the border between Iowa and Nebraska. This structure is a seventeen span bridge with an overall length of 1,983 feet, measured to the outside faces of the abutment back walls. IaDOT inspection reports indicate that the bridge was built in 1991. The roadway is 40 feet-0 inches wide and carries one lane each of eastbound and westbound traffic. The two main spans over the river are constructed of a set of four welded steel plate girders, while the approach spans on the east and west are supported by a series of six precast, prestressed concrete, I-shaped, Iowa Type D beams. The barrier is a Jersey-type barrier with dimensions as shown in Figure 26.

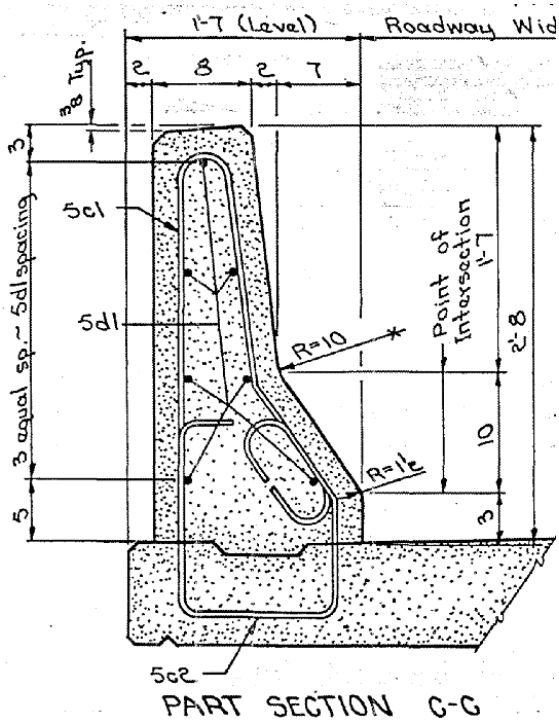

Figure 26. Barrier wall construction details for US Route 30 and IA 150.

A 40-foot long detailed test area was selected at both the north and south barriers as shown in Figure 27. The test areas were selected in the main span near the peak of the vertical curve where the profile slope was lower. In addition, corrosion staining was observed along the construction joint between the concrete deck and the exterior face (back side) of the barrier wall as shown in Figure 28. In general, the barrier contained regularly spaced vertical shrinkage-type cracks with some moisture staining. Random horizontal cracks and fine map cracks were also observed at selected locations. Hammer tapping did not identify any delaminations within the barrier.

Figure 27. Overview of test barrier on US Route 30 bridge.

Figure 28. Indications of dowel bar corrosion on backside of barrier wall.

2.4.2. US Route 218 over Hinkle Creek [IaDOT No. 0648.4S218]

Iowa 0648.4S218 in Benton County on Route 218, is a 130 foot by 30 foot pretensioned prestressed concrete beam bridge over Hinkle creek in Vinton, Iowa. The cast-in-place barrier is reportedly typical of many older structures in Iowa. After the deck was cast, a curb was cast onto the deck creating a horizontal construction joint. However, the exposed deck was then overlaid up to the curb face so the horizontal construction joint is buried from view, as shown in the deck cross section in Figure 29.

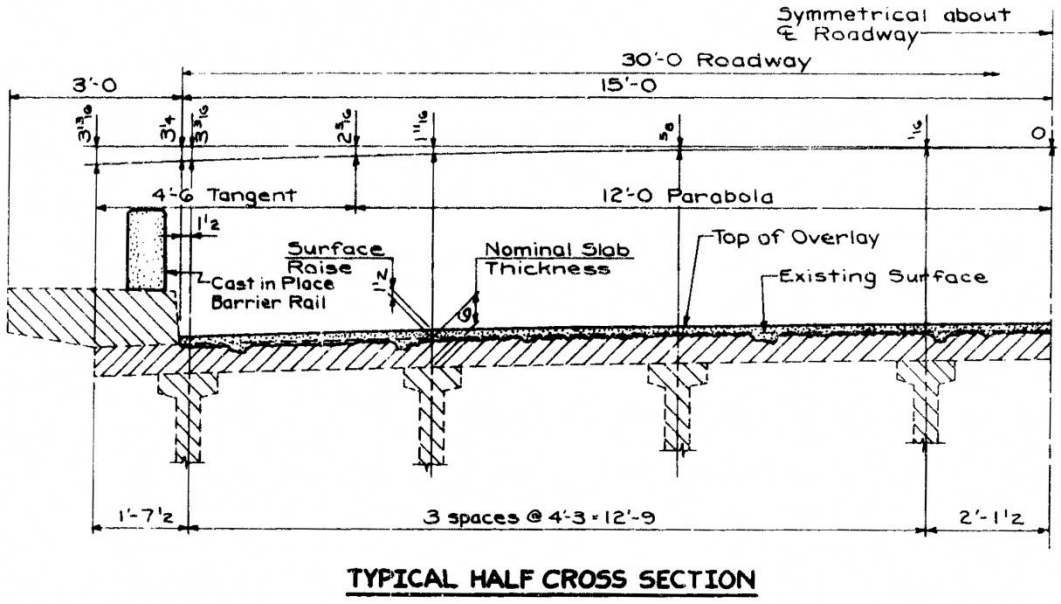

Figure 29. Barrier wall with overlay construction details for US Route 218.

Lane protection was provided for examination of the southbound (west) barrier wall. The entire barrier length of approximately 130 feet was examined. Figure 30 shows the tested barrier wall. Generally, the barrier was in good condition. Fine vertical cracks were present on the barrier faces with many cracks having efflorescence staining. Cracking was more prevalent along the top and bottom edges of the barrier. Corrosion stains were noted as several local areas along the front face at the bottom edge of the barrier. Hammer tapping did not identify any delaminations or spalling. Examination of the underside of the bridge deck did not show any evidence of water leakage through the construction joint.

Figure 30. Test barrier for US Route 218.

2.4.3. Iowa Route 150 [IaDOT No. 0601.5S150]

Iowa 0601.5S150 in Benton County on IA150 on the north side of Vinton, Iowa is a mainline multi-span, prestressed concrete girder bridge. Lane protection was provided in the northbound lane for inspection of the east barrier wall. The barrier wall separates the roadway from a sidewalk, therefore full access to both the interior and exterior faces of the wall were possible. The barrier is more typical of a Jersey-type barrier as shown in Figure 26. The detailed test area selected was 140 feet to 260 feet from the south end of the bridge as shown in Figure 31. The barrier contained regularly spaced vertical shrinkage-type cracks with some efflorescence or water staining. Some barrier patches were present. Some fine and random horizontal cracking was present with evidence of moisture intrusion. Corrosion stains were not noted on the barrier face. Hammer tapping did not identify any delaminations within the barrier.

Figure 31. Test barrier for Iowa 150.

2.5. Phase B Field Testing: Illinois Barrier Walls

Based on the results of the mock-up sample testing and testing performed during Phase A field testing, WJE developed refined testing procedures for the detection of slip formed production-related concrete flaws and performed additional field testing of barrier walls in Illinois. This subsequent phase of field testing, Phase B, was performed on slip formed and cast-in-place barriers on several in-service bridges in southern Illinois during the weeks of July 15 and July 22, 2013. Testing included visual assessment, infrared thermography, GPR testing, shear wave ultrasonic tomography testing, and selected exploratory coring. IDOT personnel were on site during a majority of the field testing activities at each location. The barrier walls included in this testing program, as described in Table 3, were the following:

1. Armington Spur over Middle Fork Sugar Creek [IDOT Str. No. 054-0503]
2. Emden Road over I-155 [IDOT Str. No. 054-0078]
3. Old 121 over Kickapoo Creek [IDOT Str. No. 054-0505]
4. I-70 Mississippi River Bridge (MRB): Illinois Approach

Standard details for cast-in-place and slip formed barrier walls per current IDOT standards are shown in Figure 32 and Figure 33. Note that the Emden Road barriers were constructed prior to the release of the current IDOT standard details. Therefore, reinforcing details and barrier dimensions between test bridges vary.

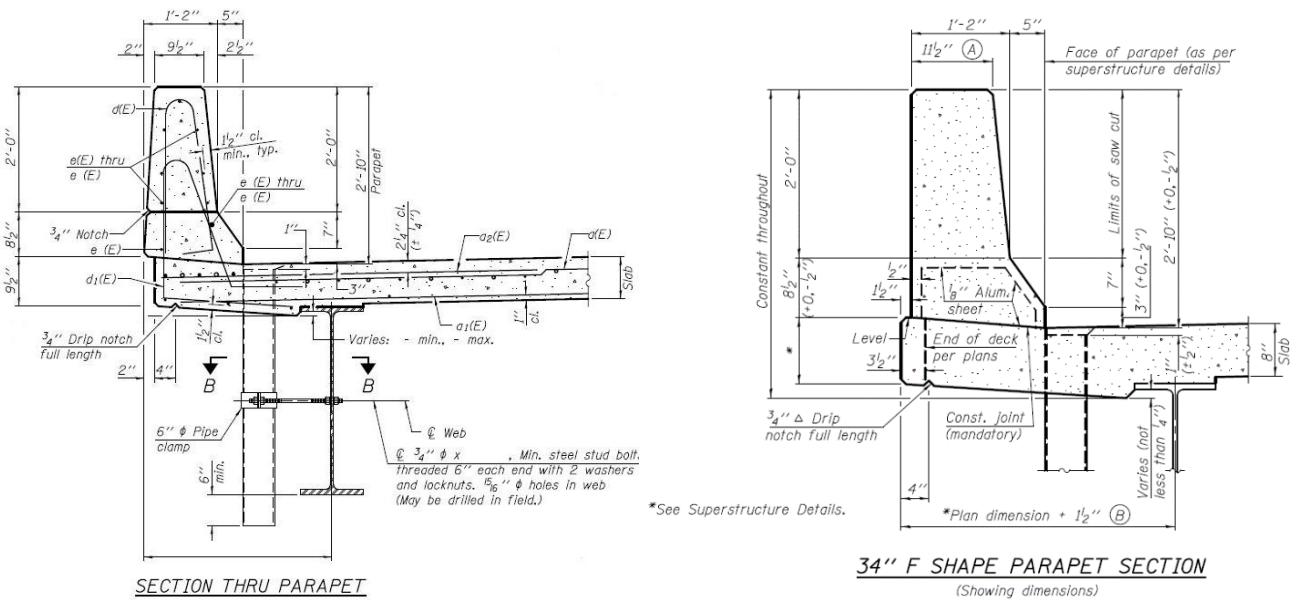

Figure 32. Standard details for 34 inch barrier wall per IDOT standards. Reinforcing detail (left) from Sheet S-D1, IDOT Superstructure Details (08-31-12). Slip formed barrier detail (right) from Sheet SFP 34-42, IDOT Concrete Parapet Slipforming Option (08-16-12).

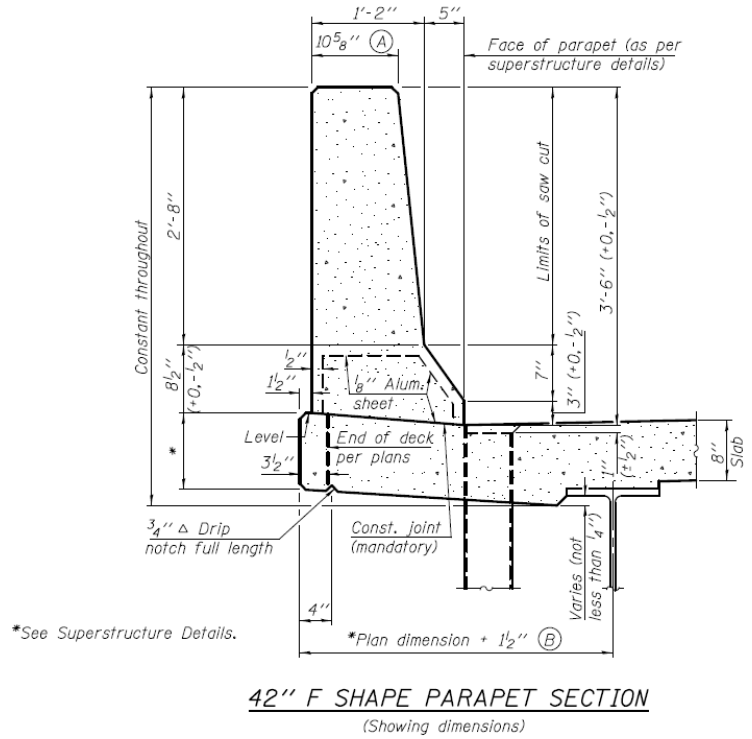

Figure 33. Standard details for 42 inch barrier wall per IDOT standards. Slip formed barrier detail from Sheet SFP 34-42, IDOT Concrete Parapet Slip Forming Option.

2.5.1. Armington Spur over Middle Fork Sugar Creek [IDOT Str. No. 054-0503]

Armington Spur over Middle Fork Sugar Creek [IDOT Str. No. 054-0503] is a two-lane bridge along Armington Road (1575th Avenue) located north of Lincoln, Illinois in Logan County. The Armington Spur runs north-south from US Route 136 to Armington Road. The bridge is a three-span steel structure with an overall length of 222 feet. It was built in 2004. The bridge deck width is 32.2 feet and carries one lane each of northbound and southbound traffic. The east barrier is a 34-inch tall cast-in-place Jersey-type barrier. The west barrier is a 34-inch tall slip formed barrier constructed per IDOT requirements in effect at the time.

Figure 34. View (north) of Armington Spur over Middle Fork Sugar Creek.

Lane protection was provided for examination and testing of the full lengths (approximately 217 feet) of the east and west barrier walls. Regularly spaced vertical shrinkage cracks were present along the length of the east barrier wall (cast-in-place barrier). Minor staining indicating moisture ingress at the cracks was apparent. Similar vertical cracks were also present at a regular spacing along the length of the west barrier wall (slip formed barrier); however, the cracks were tighter (generally <0.005-inch width) and did not show signs of water ingress. Minor slumping of the top of the barrier resulted in horizontal cracking at some locations along the length.

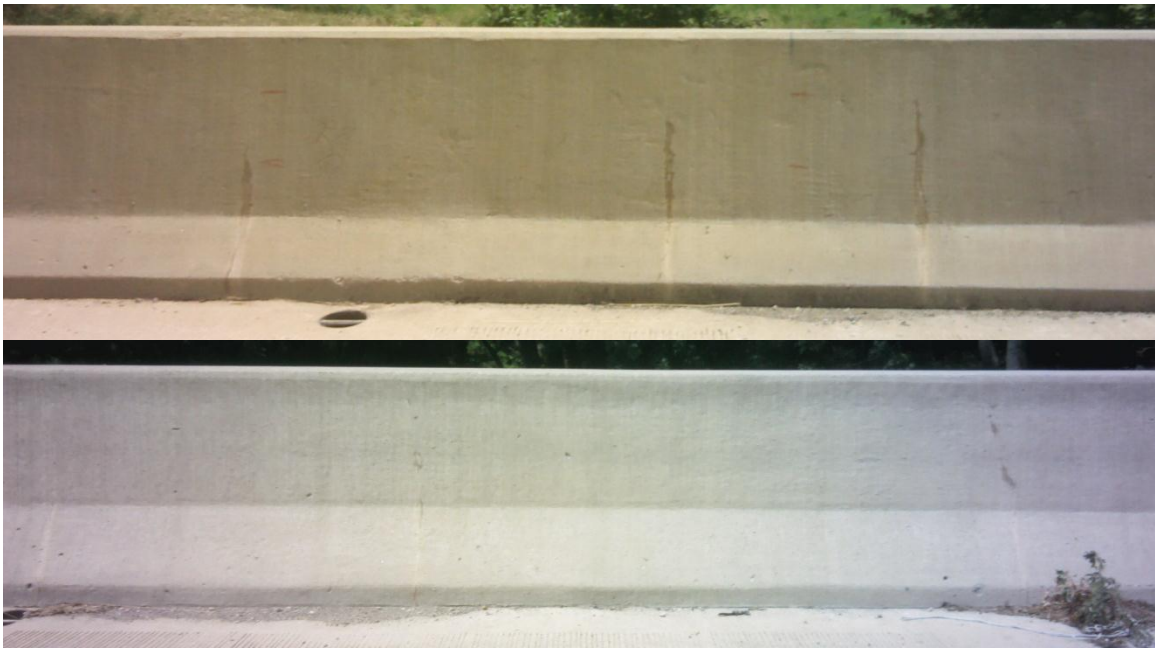

Figure 35. Representative portions of the east barrier (top) and west barrier (bottom) of Armington Spur over Middle Fork Sugar Creek.

2.5.2. Emden Road over I-155 [IDOT Str. No. 054-0078]

Emden Road over I-155 [IDOT Str. No. 054-0078] is a two-lane bridge along Emden Road (2600th Street) located east of Emden, Illinois in Logan County. The bridge is a steel structure consisting of three main spans and two approach spans with an overall length of 324 feet. The structure was built in 1991. The bridge deck width is 37.2 feet and carries one lane each of eastbound and westbound traffic. The north and south barriers are 34 inch tall slip formed barriers (Figure 36).

Figure 36. Views of Emden Road over I-155.

Lane protection was provided for examination and testing of the full lengths (approximately 291 feet) of the north and south barrier walls. The condition of the north barrier wall showed signs of material deterioration and moisture ingress at several locations typically measuring 10-20 feet in length. Pattern cracking with some mineral efflorescence was present on the side faces typically near the top of the barrier (Figure 37). The condition of the south barrier wall was considerably worse than the north barrier. Vertical cracks were typical along the length of the barrier. At several locations along the length, pattern cracking was severe and extended the full height of the wall (Figure 38). At these locations, mineral efflorescence was severe and wide longitudinal cracks were present near the middle of the top surface of the barrier.

Figure 37. Representative section of the north barrier wall of Emden Road over I-155.

Figure 38. Representative section of the south barrier wall of Emden Road over I-155.

2.5.3. Old 121 over Kickapoo Creek [IDOT Str. No. 054-0505]

Old 121 over Kickapoo Creek [IDOT Str. No. 054-0505] is a two-lane bridge along Old Route 121 located northwest of Lincoln, Illinois in Logan County. The bridge is a steel structure consisting of 4 main spans with an overall length of 227 feet. The structure was built in 2006. The bridge deck width is 37.2 feet and carries one lane each of northbound and southbound traffic. The east and west barriers are 34 inch tall slip formed barriers (Figure 39).

Figure 39. Views of Old 121 over Kickapoo Creek.

Lane protection was provided for examination and testing of the full lengths (approximately 223 feet) of the east and west barrier walls. The condition of the east and west barrier walls was similar. No visible distress was observed on the sides or top faces of the barriers.

2.5.4. I-70 Mississippi River Bridge (MRB): Illinois Approach

The new I-70 Mississippi River Bridge (MRB) is currently being constructed over the Mississippi River at East Saint Louis, Illinois. The Illinois approach to the MRB consists of two independent bridge approaches, eastbound and westbound, each of which will carry several lanes of traffic (Figure 40).

IDOT selected limited areas of the north and south barriers of the westbound approach and the south barrier of the eastbound approach to be included in this study. Approximately 244 feet of the westbound approach were studied; from Sta. 127+44 to Sta. 125+00. Both the north and south barriers on the westbound approach were 42-inch high Jersey-style barriers. However, the north barrier was slip formed and the south barrier was cast-in-place. Additionally, a 10-foot portion of the south barrier on the eastbound approach was studied; from Sta. 105+21 to Sta. 105+14. The south barrier of the eastbound approach was a 42-inch high slip formed barrier (Figure 33). The barriers had been recently constructed and no visible distress was observed on the sides or top faces of any of the barriers. IDOT had performed quality control core sampling of each of the barriers in accordance with the project specifications.

Figure 40. View of the westbound Illinois approach of the new Mississippi River Bridge (MRB).

3. TESTING PROCEDURES AND TEST RESULTS

Testing of the laboratory mock-ups was performed over several months and in different exposure conditions. The NDE methods evaluated in the mock-up testing program were selected based on review of common concrete flaws inherent in dry-cast barrier walls and the known capabilities and limitations of each candidate nondestructive testing method. Testing of the mock-up barrier wall using each test method aided in defining optimal testing procedures and in the evaluation of the test method to detect specific embedded flaw types. Specific conclusions related to processing and analysis procedures, the ability to accurately detect specific flaws of various types and sizes, and recommendations for additional trial testing are provided below for each of the selected testing methods.

Phase A field testing aided in evaluating data collection procedures and collection rates as well as evaluating each test method to detect flaws and dowel bar corrosion, which were either visible on the surface or found via exploratory coring of the barrier. Phase B field testing provided for the evaluation of the most promising NDE methods specifically for concrete flaw detection on longer lengths of the barrier walls and allowed for correlation to internal flaw types located via exploratory coring. Sample testing results and specific conclusions obtained during the mock-up and field testing programs have been compiled below for each of the selected testing methods.

The different methods used for the mock-ups and field evaluation trials are identified in Table 4. For each selected method, trial testing generally consisted of the following multi-step approach for data collection and analysis:

1. Determine the optimal testing procedures and data collection settings.
2. Determine optimal data post-processing and analysis procedures.
3. Identify capabilities and limitations of each method for specific flaw detection.
4. Identify additional testing necessary on the in-situ barrier walls to evaluate methodology.

3.1. Internal Flaw Detection

3.1.1. Impact-Echo Ultrasonic Testing (IE)

3.1.1.1. Mock-up Testing Procedures

Testing of the mock-up barrier wall comprised the initial layout of a testing grid, IE testing at each grid location, and subsequent data analysis and interpretation. A 6-inch by 6-inch testing grid was laid out on the interior face of the mock-up wall. IE testing at each grid location consisted of impacting the surface with selected steel ball impactors and measuring the stress wave reflection using the displacement transducer positioned adjacent to the impact. Selection of the most appropriate impactor was based on impact contact time, the barrier wall thickness, and anticipated flaw depths. Several individual tests were performed at each grid location to assess repeatability and ensure that a representative test result was retained. Additional testing was performed at each flaw location as necessary to evaluate the test method. Individual test results were analyzed to determine the effectiveness of the test method in identifying the embedded flaws and to determine the optimum data collection and analysis procedures.

3.1.1.2. Phase A Field Testing Procedures

Field testing of the IE method was performed during Phase A field testing on the westbound and eastbound barrier walls of the US 30 bridge. Testing was completed using the conventional IE testing system described above.

Trial testing was performed as described at the following locations:

US 30, Eastbound Barrier.

5 by 30 testing grid with 6-inch vertical spacing and 12-inch horizontal spacing.

US 30, Westbound Barrier.

6 by 25 testing grid with 6-inch vertical spacing and 12-inch horizontal spacing.

3.1.1.3. Testing and Analysis Results: Laboratory Mock-up

Analysis of IE data involves examination of the time domain plot of displacement measured directly by the transducer and of the spectral frequency plots produced through use of an FFT analysis. Figure 41 through Figure 44 provide examples of the IE results for testing performed on the mock-up barrier wall sample. An elevation view of the interior face of the mock-up barrier wall indicating the locations of the IE testing grid and embedded flaws is provided in Figure 41. Subsequent figures provide individual test results at selected grid locations coinciding with an unflawed location on the barrier wall (Figure 42), embedded void V2 (Figure 43) and an embedded honeycomb panel D3 (Figure 44).

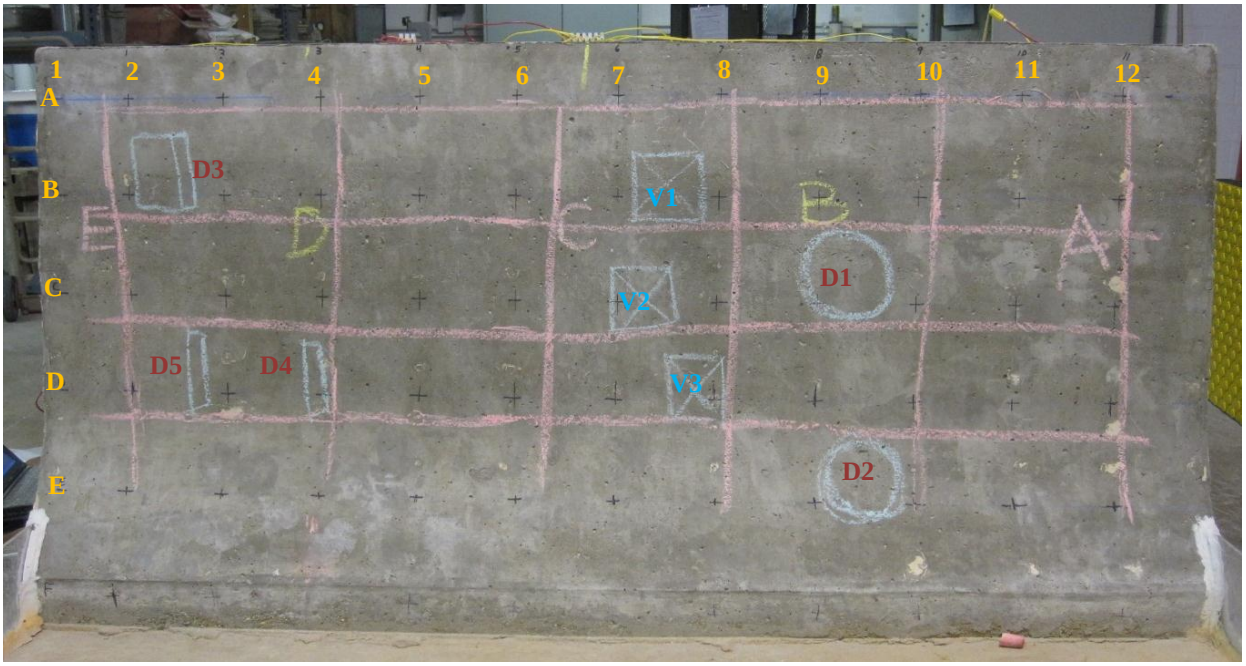

Figure 41. View of interior face of the mock-up barrier wall indicting locations of embedded voids (V1-V3) and honeycomb defects (D1-D5) and IE testing grid labels.

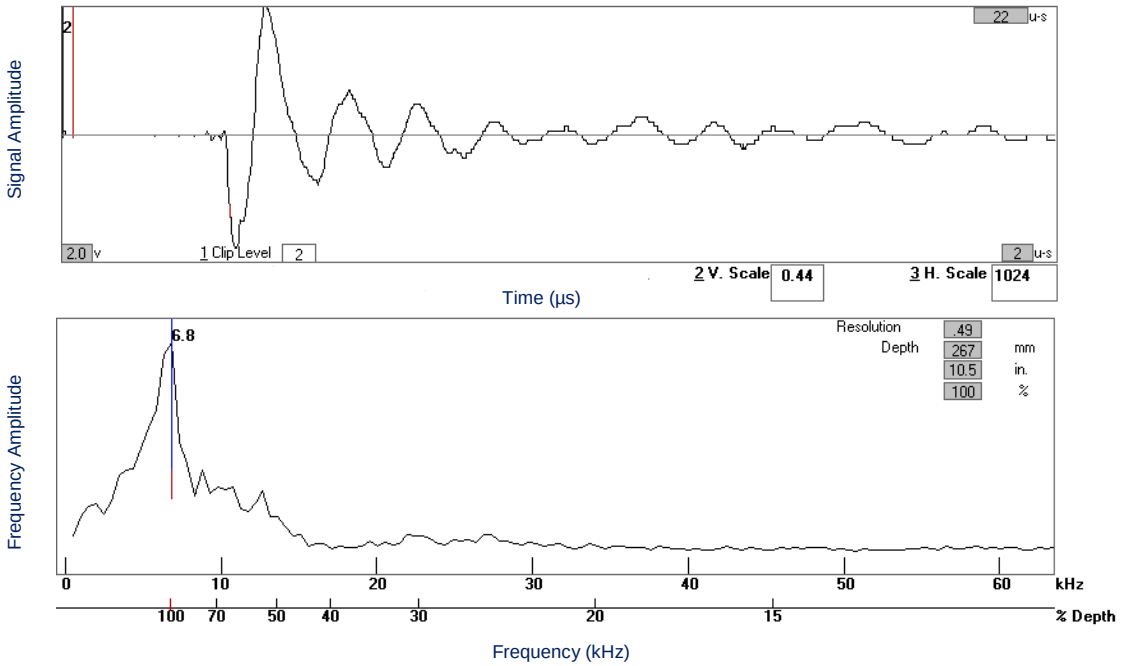

Figure 42. IE test result showing a reflection from the exterior surface of the barrier wall at a depth of 10.5 inches (IE Test Location A-7).

Figure 42 provides the test result at a location on the interior face of the mock-up wall at which no internal flaws were present (IE Test Location A-7). The upper plot in Figure 42 shows the time domain for the longitudinal stress wave received by the displacement transducer. The time domain plot, which displays the signal amplitude on the y-axis and time along the x-axis, represents the sinusoidal waveform received after reflection from any internal interfaces, in this case from the back surface of the mock-up wall. The lower portion of the figure displays the spectral plot, which displays the occurrence of each frequency at which the received waveform occurs. Each dominant frequency peak corresponds to a thickness at which a possible internal interface occurs. At this test location, the only dominant frequency occurs at 6.8 kHz; indicative of the nominal 10.5-inch thick concrete wall using a calibrated ultrasonic velocity of 11,900 feet per second.

Testing at areas of potentially unsound concrete, internal cracking, or planar delamination results in variations in the time signal and frequency spectrum. Shallow delamination, for instance, typically results in erratic, high amplitude time signals and low frequency peaks in the spectral plot. Deeper internal cracks and planar delamination typically results in irregular time signals, which may identify several dominant frequencies coinciding with the approximate flaw depths. Figure 43 shows an IE test result at void panel location V2. At this test location, the received time-domain waveform consists of higher frequency content and the spectral plot displays high-frequency peaks. Note that a dominant frequency peak occurs at 17.6 kHz, a frequency corresponding to an approximate void depth of 3.7 inches from the exterior surface. Figure 44 shows an IE test result at honeycomb panel location D3. At this test location, the received time-domain waveform consists of higher frequency content and the spectral plot displays high-frequency peaks. Note that several high-frequency peaks occur, including one at 23.4 kHz, a frequency corresponding to an approximate flaw depth of 2.8 inches from the exterior surface.

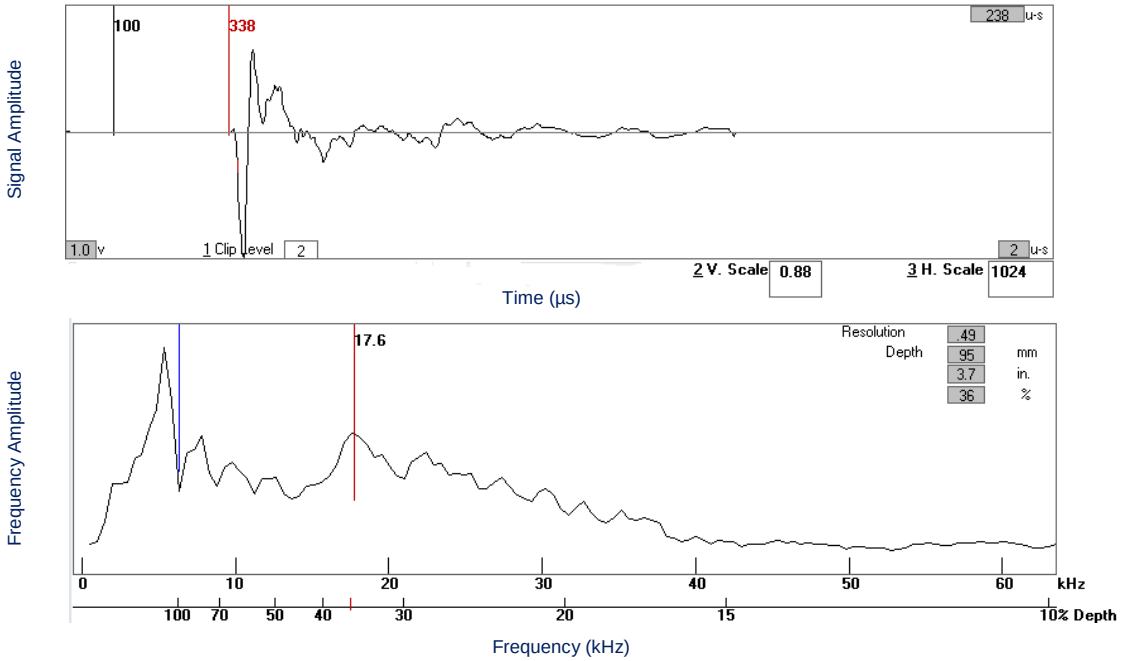

Figure 43. IE test result at embedded void location V2 (IE Test Location C-7.2).

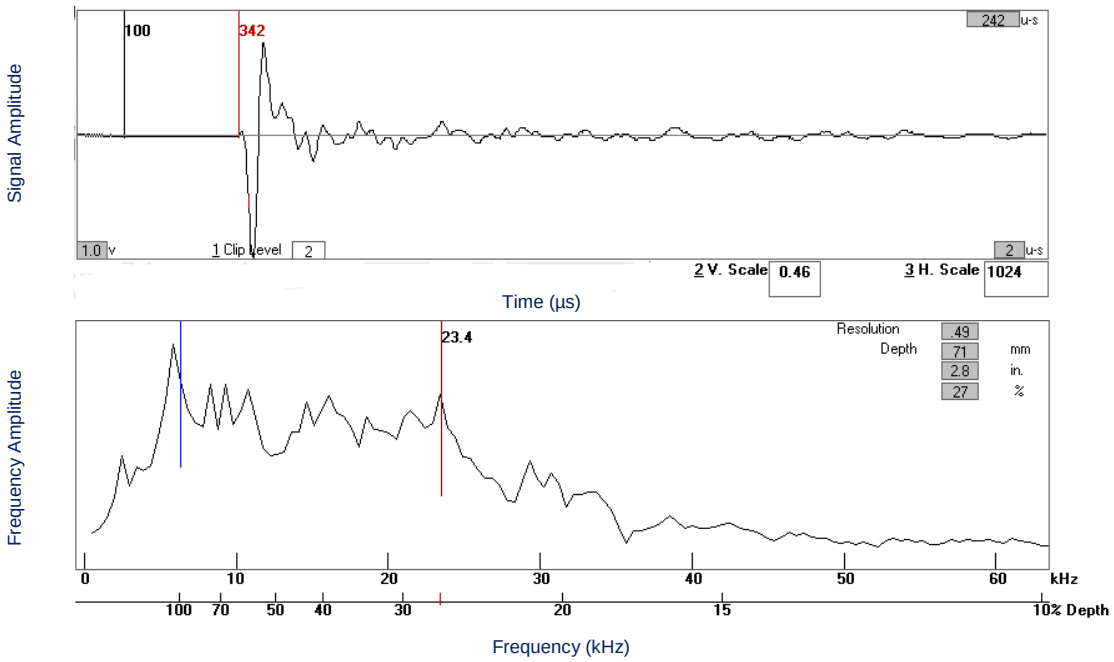

Figure 44. IE test result at embedded flaw location D3 (IE Test Location B-2.5).

3.1.1.4. Testing and Analysis Results: Phase A Field Testing

Field testing of the impact-echo test method was performed at several hundred test locations on two testing grids on the eastbound and westbound barriers of the US-30 Blair Bridge. In general, IE testing

identified clear reflections from the back of the barrier at a majority of the test locations. Note that the variable barrier wall thickness must be accounted for during analysis of the testing results. Ultrasonic waves propagate in all directions from the impact location and reflect from all available surfaces or flaws. Therefore, testing on or adjacent to visible cracking resulted in erratic time domain plots, making signal interpretation difficult at these locations. In general, no clear internal flaws or delaminations were identified using the IE test method within the test areas.

3.1.1.5. Advantages and Limitations of Test Method

The following summarizes the results and conclusions of trial-testing of the IE ultrasonic test method for concrete flaw detection:

Capabilities and Advantages:

- Accurate thickness measurement of barrier wall thickness at unflawed test locations.
- Identification of the presence and approximate depth of embedded voids measuring 3-inch wide and greater, positioned within 6 inches of tested surface, and coincident with test location. Detection of deeper voids possible with increased flaw size.
- Identification of the presence and approximate depth to internal planar cracking or delamination and disbonding of patch repairs coincident with test location.
- Detection of internal honeycombing coincident with test location; however, signal interpretation is complicated and depth determination is not possible.
- Data collection requires access to one side of the barrier wall.
- Multiple tests performed at each test location can ensure repeatability of data.

Limitations:

- Testing is performed at individual test locations, requiring setup of test grids on an accessible face of the barrier wall.
- Data collection requires testing at individual grid locations, which is time-consuming. Defects must be in-line with sensor requiring a closely spaced grid to identify small defects.
- Complex geometry of barrier wall design complicates data interpretation and may hinder flaw detection along the thickened base and construction joint of the barrier wall.
- Depth to internal honeycombing (as measured from the lateral surface of the barrier) and overall depth of honeycomb cannot be determined.
- Small voids (less than 2 inches in diameter), thin voids around reinforcing bars, and minor consolidation issues cannot be detected. IE may not be suitable for detecting typical slip formed production-related concrete flaws.
- Corrosion of reinforcing steel and dowels cannot be directly detected. Not a candidate test method for corrosion and corrosion-related section loss assessment.

3.1.2. Scanning Impact-Echo Ultrasonic Testing (SIE)

3.1.2.1. Advantages and Limitations of Test Method

The use of recently developed scanning IE testing equipment may provide the following:

Capabilities and Advantages:

- Testing can be performed more efficiently along continuous scan lines. Layout of testing grids is not necessary. Typical test spacing along scan line of 6 inches or less would identify most large barrier defects.

Limitations:

- Individual tests are performed at each location during data collection and repeatability is not routinely assessed.
- Available systems are optimized for delamination detection. System hardware and firmware and analysis software may need to be modified to detect production-related internal voids.
- Equipment is expensive to purchase and may be difficult to rent.
- Use of equipment and data analysis requires significant training and experience.

3.1.3. Shear Wave Ultrasonic Testing (MIRA)

3.1.3.1. Mock-up Testing Procedures

Trial testing of the shear wave ultrasonic testing method was performed using the MIRA Tomographer system. Laboratory testing of the mock-up barrier wall comprised of initial layout of a testing grid, MIRA testing at each grid location to collect a "map" of the tested surface, and subsequent data analysis and interpretation. Test settings, specifically the selection of an appropriate test frequency and gain settings, were initially established through trial testing and review of collected scans. A 12-inch by 4-inch testing grid was laid out on the interior face of the mock-up wall. MIRA testing at each grid location consisted of orienting the antenna array horizontally on the surface and collecting the resultant data. Testing using the established testing grid resulted in coverage of the entire vertical face of the barrier wall. Trial testing of the Killian barrier wall segment was performed using the testing procedures described in the Phase B field testing section below.

3.1.3.2. Phase A Field Testing Procedures

Phase A field testing of the shear wave ultrasonic testing method was performed using the Eyecon Monolith testing device on the eastbound barrier of the Blair Bridge (US30 over the Missouri River) and using the MIRA Tomographer on the northbound barrier of Iowa 150 over Cedar River.

The following trial testing was performed at each field testing location:

US 30, Eastbound Barrier.

Equipment used: Eyecon Monolith.

Individual location testing, trial testing of 10-foot x 3-foot testing grid.

Iowa 150, Northbound Barrier.

Equipment used: MIRA Tomographer.

Testing of 10-foot x 3-foot testing grid (including surface cracking and material degradation zones) on west (interior) face, 50 kHz test frequency.

Testing of 10-foot x 3-foot testing grid (including surface cracking and material degradation zones) on west (interior) face, 75 kHz test frequency.

Testing of 5-foot x 3-foot testing grid on east (exterior) face, encompassing core holes drilled to various depths, 75 kHz test frequency.

3.1.3.3. Phase B Field Testing Procedures

Shear wave ultrasonic testing using the MIRA Tomographer was performed at selected grid locations on each barrier wall. MIRA grid locations were selected based on the preliminary results of GPR testing, observations made at previously collected core locations (as reported by IDOT), or at representative locations in areas of visible distress. A summary of the Phase B MIRA ultrasonic testing detailing the

testing location and approximate test grid size is provided in Table 5. Exploratory coring during Phase B field testing allowed for direct correlation of the test results with known defects.

Testing was typically performed with the antenna array oriented horizontally at each gird location; however, several grids were also tested with the antenna array positioned vertically. The typical horizontal testing grid consisted of individual test locations measuring 10 inches wide by 4 inches high providing coverage to the vertical portion of the interior face of the barrier wall. The typical vertical testing grid consisted of individual test locations measuring 4 inches wide by 10 inches high. Note that the tomographic images resulting from MIRA shear wave ultrasonic testing typically include reflections from embedded reinforcing positioned nearest the test surface. For the horizontal test grids, MIRA test results typically include signal reflections from vertical reinforcing elements, such as the vertical legs of the stirrups. Conversely, the resultant tomographic images from vertically-oriented test grids typically include signal reflections from horizontal reinforcing bars. Processing of the MIRA data consisted of a series of signal gain adjustments. Analysis of the resultant 3-D tomographic data included review of 3-D isometric views and planar section views to identify potential internal reflections from internal cracking, voids, or other distress.

3.1.3.4. Testing and Analysis Results: Laboratory and Field Mock-ups

Analysis of MIRA shear wave ultrasonic testing data collected during the laboratory mock-up testing involved signal filtering and interpretation of 2-D “B”-scans and 3-D tomographic images. Post-processing software provided by ACS allowed for selection and filtering of data and adjustment of signal gain settings. Figure 45 through Figure 47 provide examples of the MIRA trial testing performed on the mock-up barrier wall sample using a dominant testing frequency of 50 KHz. An elevation view of the interior face of the mock-up barrier wall indicating the locations of selected testing areas in relation to the embedded flaws is provided in Figure 45. Selected individual test results, displayed as B-scan section views of the barrier wall, are shown in Figure 46. The B-scans show high amplitude reflections from embedded reinforcing, internal defects (specifically honeycomb defect D1) and the back surface of the barrier wall. A composite tomographic image of the internal reflections resulting from testing of a full grid of MIRA testing, referred to as a testing 'map', is provided in Figure 47. The filtered tomographic image shows the capability of the MIRA testing method to identify embedded reinforcing, embedded internal void panels at various depths, and larger embedded defect panels. Note that trial testing of the mock-up barrier wall at frequencies higher than 50 kHz resulted in significant near-surface reflections, which interfered with signal penetration. At 50 kHz, near-surface reflections could be effectively filtered out of the image. In doing so, signal reflections from the shallow void panel V1 were also filtered out of the image. Rough surface conditions, the presence of moderate surface bug holes, or near-surface micro cracking may be the cause of the observed near-surface signal disruption on the mock-up barrier wall. This issue could also be a factor during testing of in-service barriers having rough surface conditions.

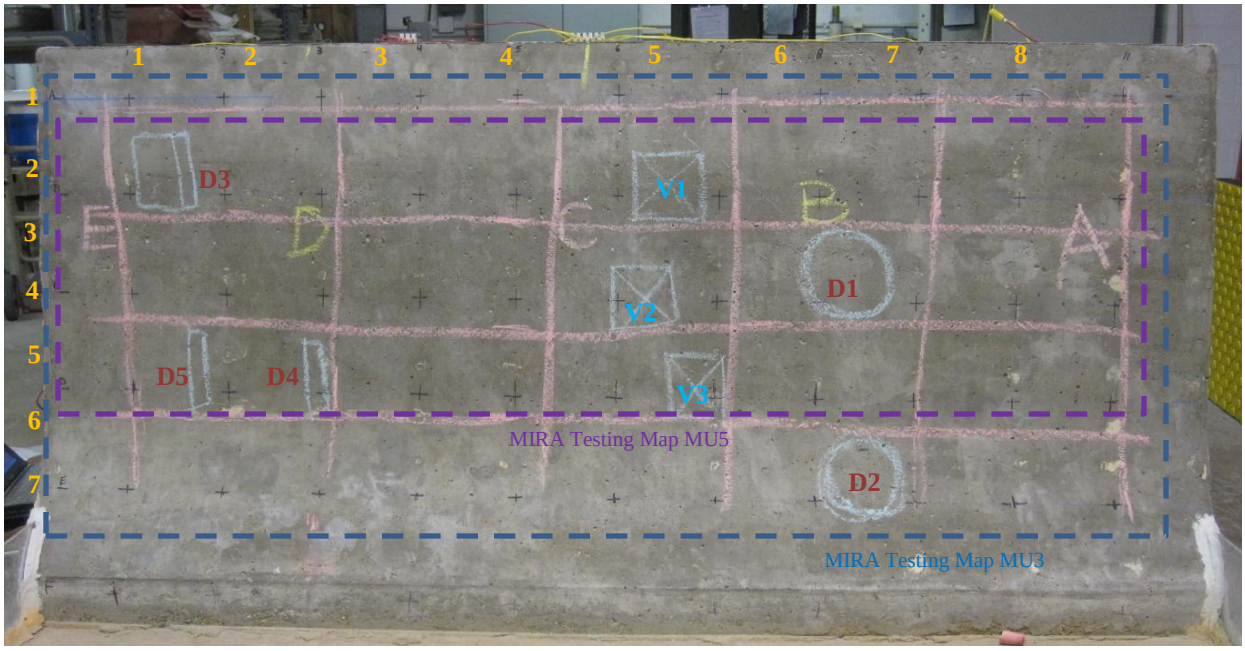

Figure 45. View of interior face of the mock-up barrier wall indicting locations of embedded voids (V1-V3) and honeycomb defects (D1-D5) and shear wave ultrasonic (MIRA) testing grids.

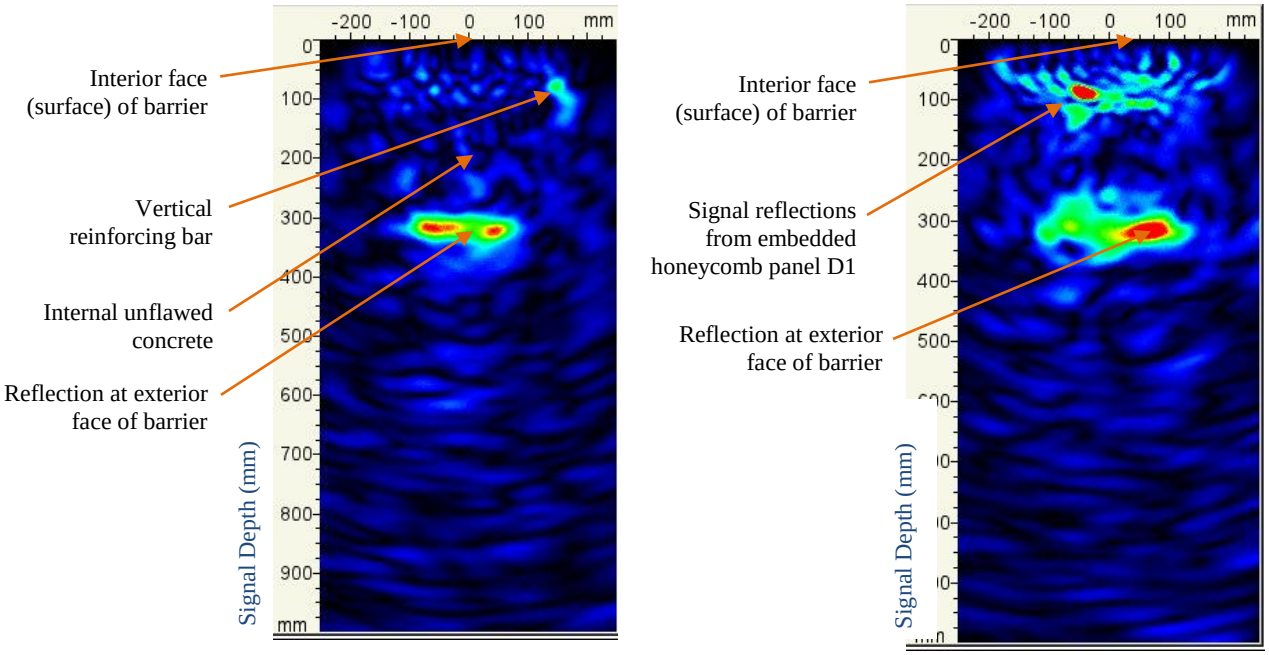

Figure 46. MIRA test results (B-scan) at two test locations on the mockup barrier wall. Left: Test result at unflawed location showing reflection from the exterior face of the wall and vertical reinforcing. Right: Test result at flawed location showing internal reflections resulting from embedded honeycomb panel D1.

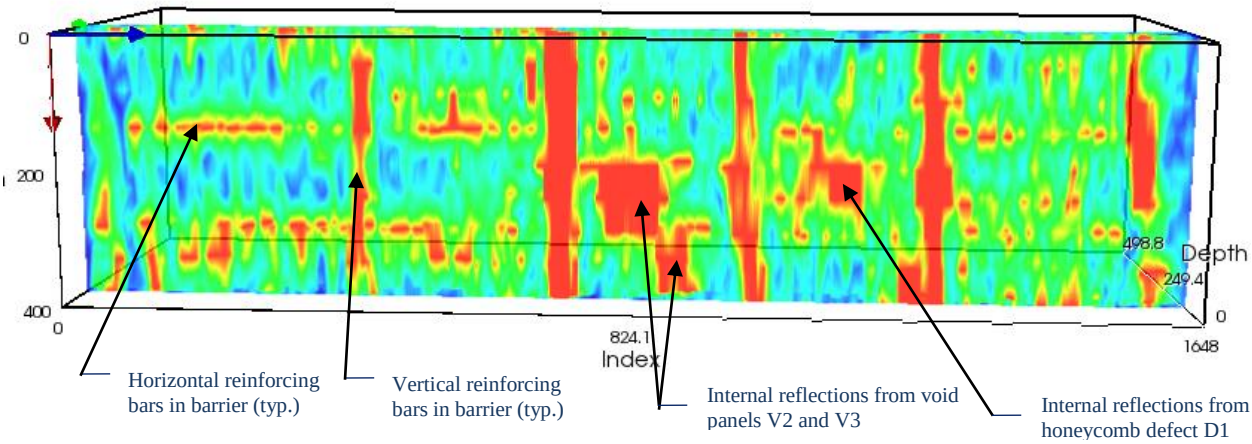

Figure 47. Internal tomographic image (filtered) of a portion of the mockup barrier wall resulting from MIRA testing at testing grid MU5 (indicated in Figure 45). Filtered image includes data from depth of 3 to 8 inches.

In additional to the laboratory mock-up testing, MIRA testing was performed on the Killian trial barrier segments. Results of the testing indicated that shear wave ultrasonic testing of early-age slip formed barrier walls (48 hour after construction) was feasible and could provide relatively high resolution tomographic imaging for internal flaw detection (Figure 48). Furthermore, MIRA testing performed along the bottom of the Killian barrier wall segments was able to identify the presence of embedded 2-inch diameter conduit (Figure 49 and Figure 50).

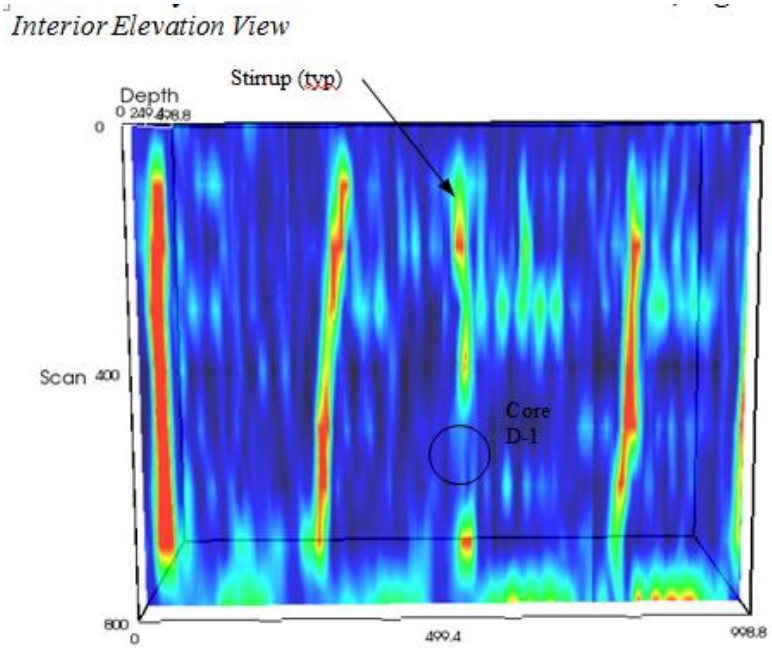

Figure 48. MIRA Result: Elevation view, Killian Test Sample 1, Interior Face. MIRA Analysis Results: No anomalies identified, high resolution through full thickness of barrier.

Figure 49. View of saw cut end of Killian barrier Test Sample 2.

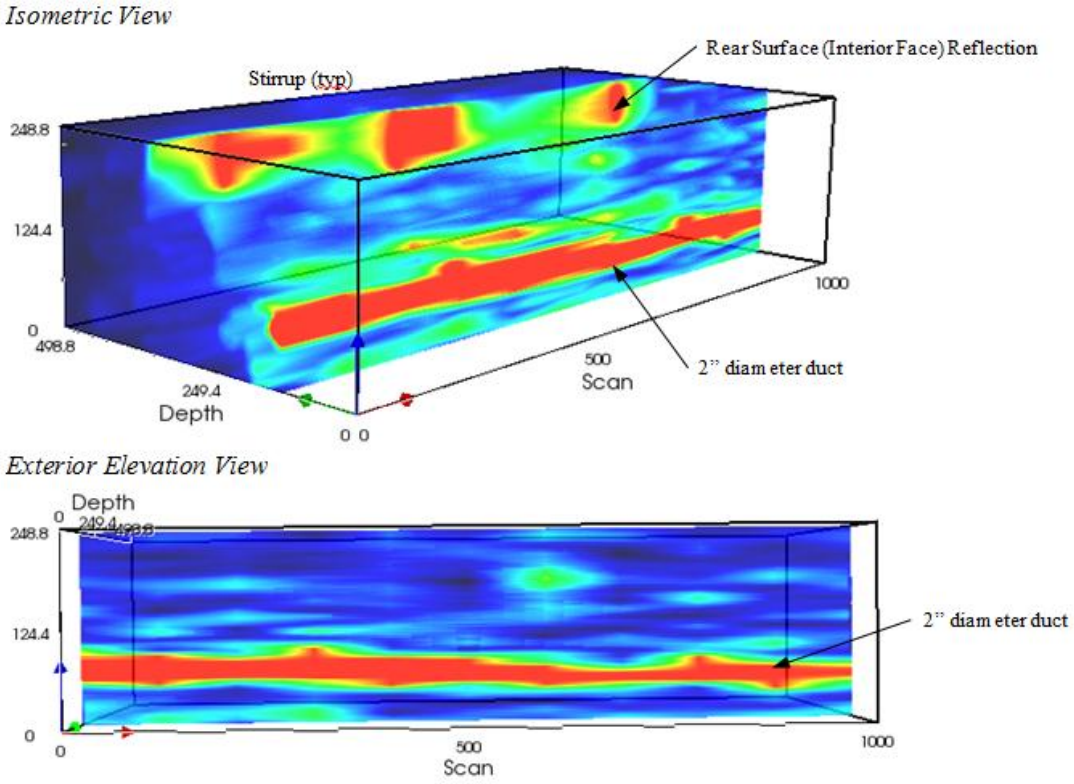

Figure 50. MIRA Result: Isometric view, exterior elevation view. Killian Test Sample 2, Exterior face. MIRA Analysis Results: 2" diameter cable duct (nearest tested surface) clearly identified.

3.1.3.5. Testing and Analysis Results: Phase A Field Testing

Trial testing of the Eyecon Monolith testing device on the eastbound barrier of US 30 consisted of data collection, preliminary interpretation of received reflections on the device, and subsequent review of 2-D "B"-scans. Although no internal flaws were identified within the testing grid, results indicated that shear wave ultrasonics could provide accurate thickness measurement of the barrier wall. Trial testing of the Eyecon unit confirmed that multiple-sensor shear wave devices could provide for faster data collection and analysis compared with alternative ultrasonic testing methods.

Testing of the selected portions of the northbound barrier wall at Iowa 150 over Cedar River using the MIRA system yielded similar testing results compared with the mock-up barrier wall assessment. Figure 51 through Figure 54 provide examples from several MIRA testing maps collected on the northbound barrier wall using a dominant testing frequency of 75 KHz. Testing at the higher frequency provided better resolution and did not result in near-surface signal reflections during field testing compared with the mock-up barrier wall testing. An elevation view of the interior face (west elevation) of the northbound barrier wall indicating the locations of selected testing maps is provided in Figure 51. Selected individual test results, displayed as B-scan section views of the barrier wall, are shown in Figure 52. The B-scans show high amplitude reflections from embedded reinforcing and the back surface of the barrier wall at an unflawed testing location (Figure 52, left) and internal reflections resulting from freeze-thaw cracking visible at the surface of the barrier (Figure 52, right). A composite tomographic image of the internal reflections resulting from testing of a full testing map is provided in Figure 53 and Figure 54. The unfiltered tomographic image provided in Figure 53 shows the capability of the MIRA testing method to identify embedded reinforcing, the exterior surface of the barrier, and the extent of internal and surface cracking and material degradation. A filter isometric image provided in Figure 54 further highlights the deterioration.

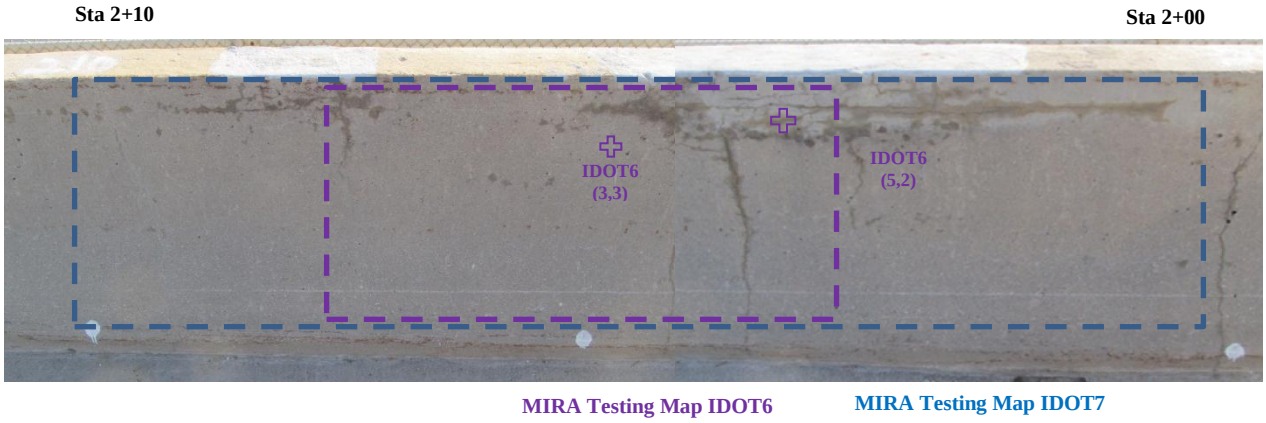

Figure 51. Photograph of interior face of the northbound barrier wall of Iowa 150 over Cedar River showing condition of barrier and indicating locations of MIRA testing grids and individual test points referenced in the following figures.

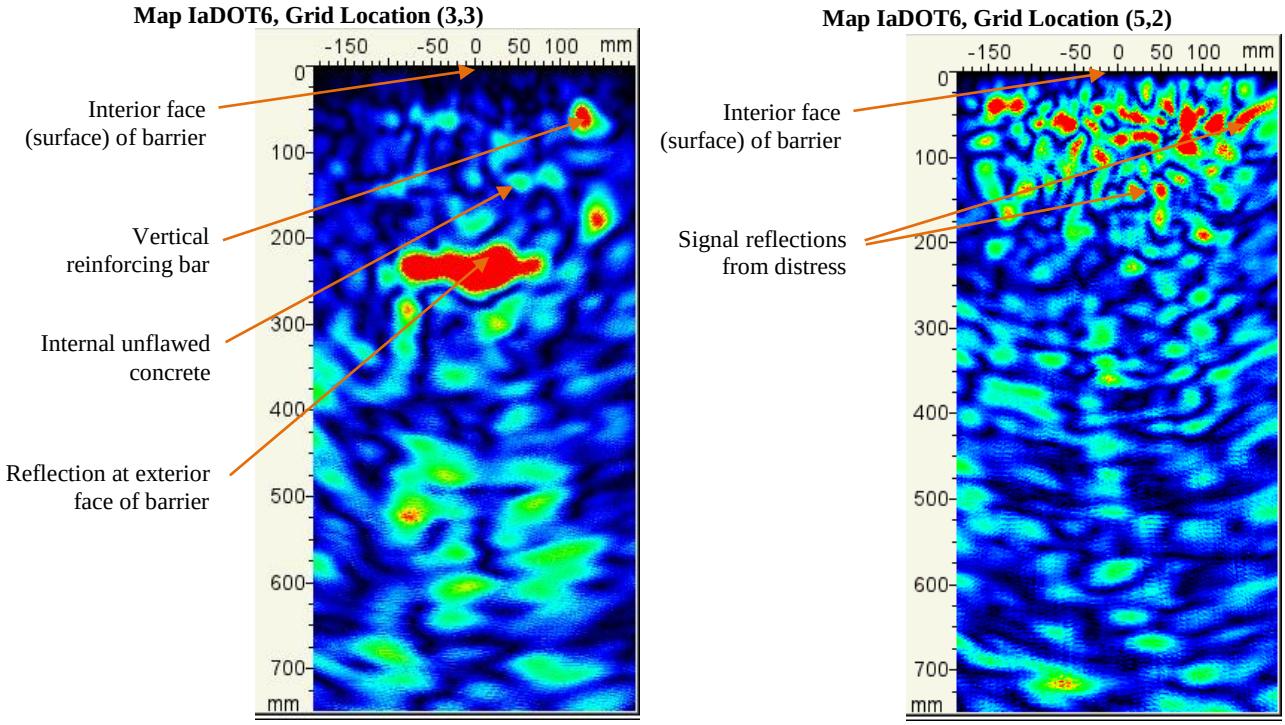

Figure 52. MIRA interior B-scan of the northbound Iowa 150 barrier wall. Left: Test result at unflawed location showing reflection from the exterior surface and embedded reinforcing Right: Test result at flawed location showing reflections resulting from cracking within barrier wall.

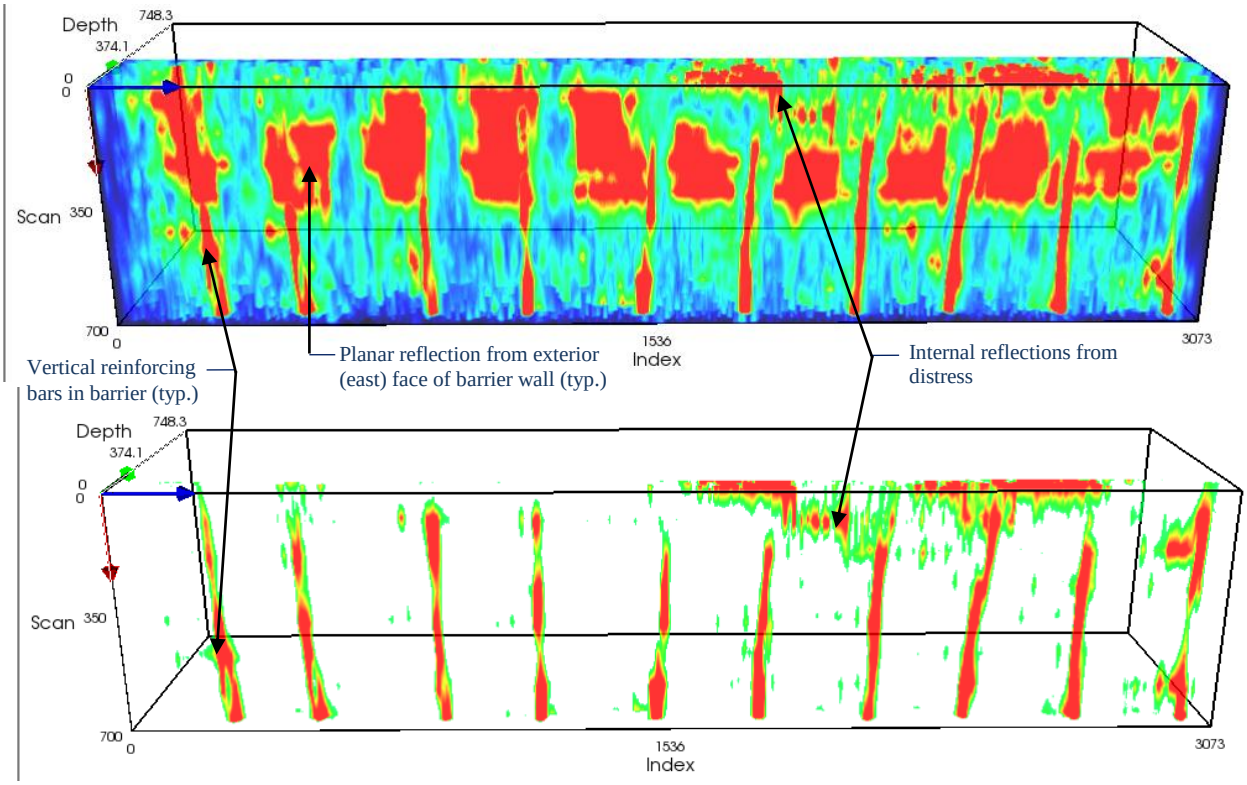

Figure 53. Internal image of the northbound Iowa 150 barrier wall resulting from MIRA testing at Map IaDOT7. Views of interior (west) face of wall showing composite image to depth of approximately 10 inches (top) and filtered image to depth of approximately 6 inches (bottom).

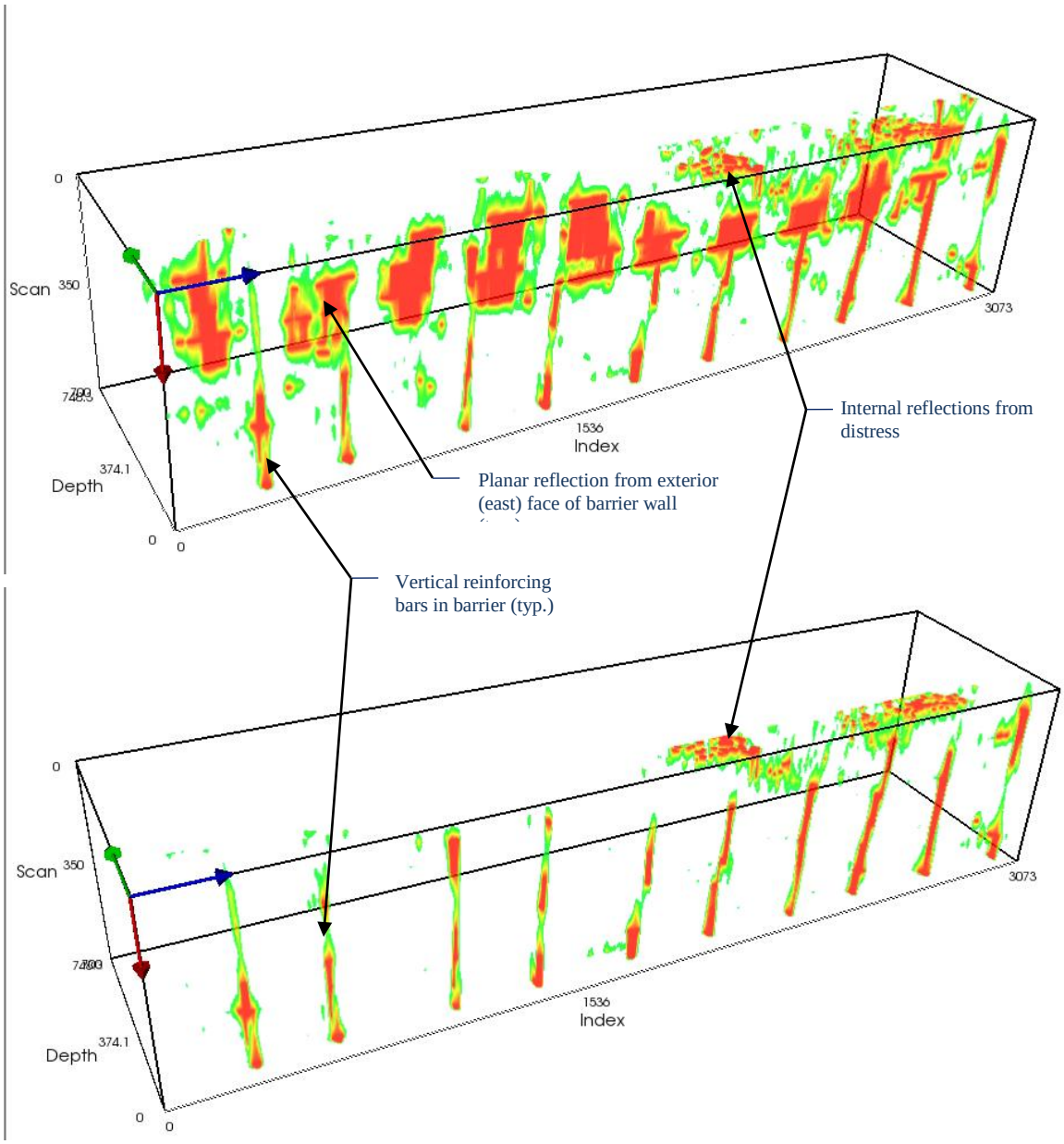

Figure 54. Isometric internal image of the northbound barrier wall of Iowa 150 over Cedar River resulting from MIRA testing at Map IaDOT7. Filtered image to depth of approximately 10 inches (top) and filtered image to depth of approximately 6 inches (bottom).

3.1.3.6. Testing and Analysis Results: Phase B Field Testing

Shear wave ultrasonic testing (MIRA) and subsequent exploratory coring during Phase B field testing provided specific conclusions about the method's ability to detect production-related concrete flaws within both slip formed and cast-in-place barriers. Selected results are provided in Figure 55 through Figure 65.

Figure 55 shows MIRA testing grid H-1/H-2 on the interior surface of the east barrier of the Kickapoo Creek Bridge [IDOT Str. No. 054-0505]. Results of the MIRA testing are provided in a selection of views of the tomographic data shown in Figure 56. The interior elevation views provided for Grid H-1 (horizontal test grid) and H-2 (vertical test grid) show that the reinforcing can be clearly identified. Signal reflection from the exterior face of the barrier is visible in the B-scan (horizontal section) from Grid H-1 and the isometric view and D-scan (vertical section) from Grid H-2. Signal resolution was relatively good at this location, indicating unflawed internal conditions. Core H-2, shown in Figure 57, indicated well-consolidated concrete and one isolated void (~1/2 inch diameter) near the exterior face. This void was not identified in the MIRA data and is likely too small to be detected from the interior face.

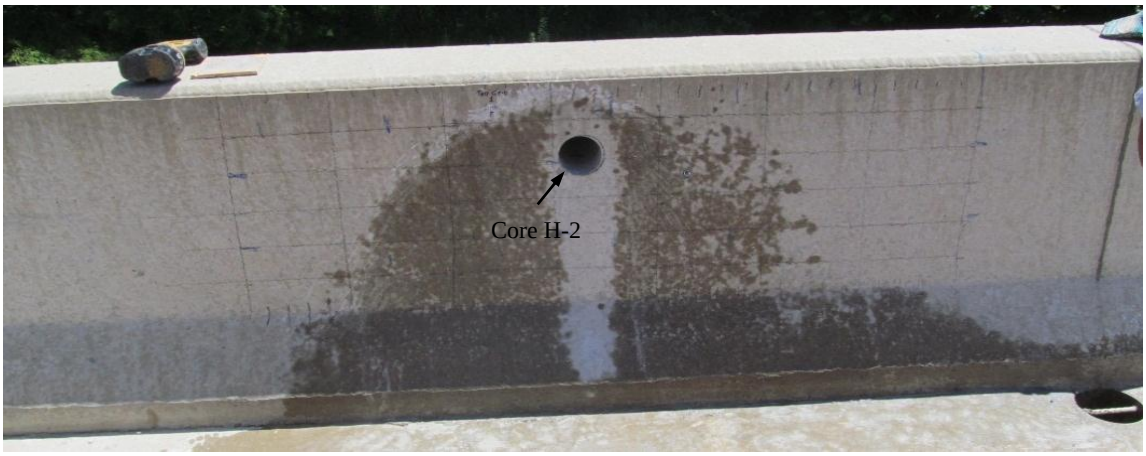

Figure 55. Photograph of Grid H-1/H-2. Grid Location: Kickapoo Creek, east barrier, 74'-2" - 80'-0" from N end.

Grid H-1; Interior Elevation View

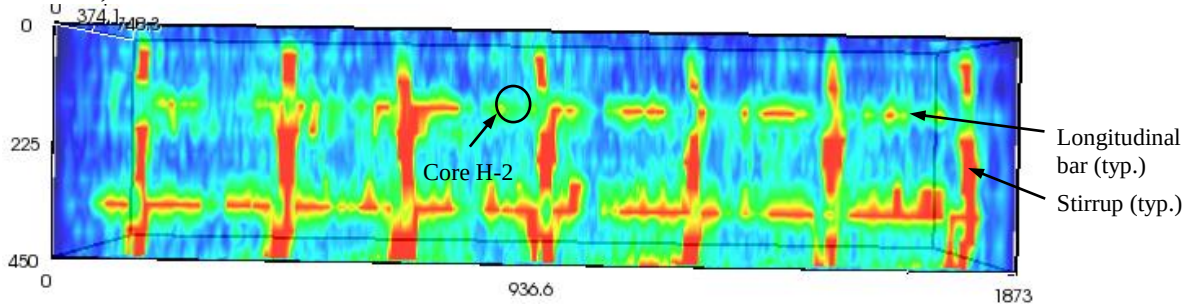

Grid H-1; B-scan

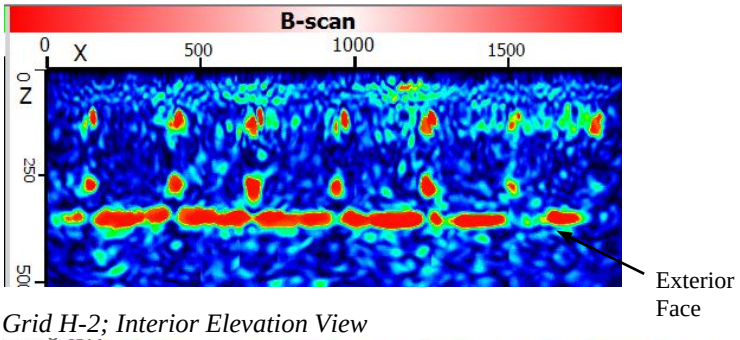

Grid H-2; Interior Elevation View

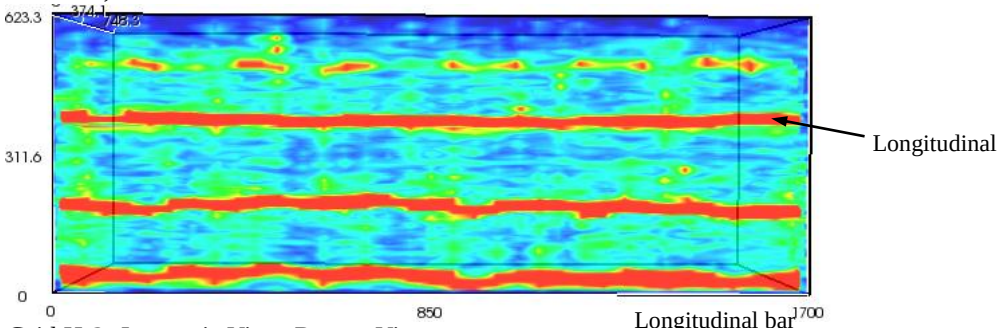

Grid H-2; Isometric View, D scan View

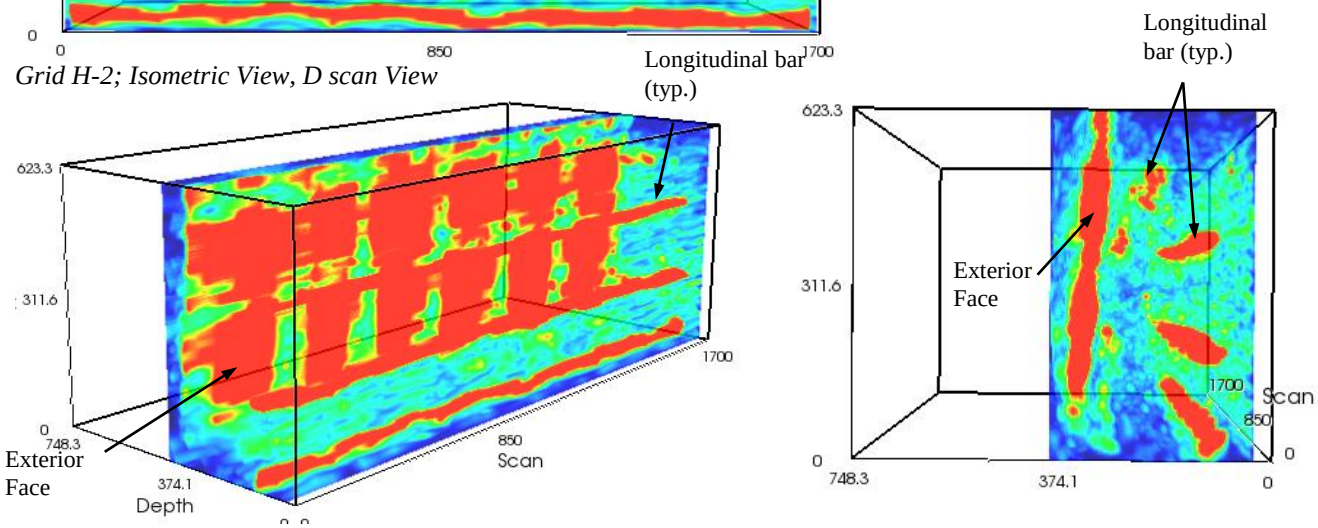

Figure 56. Grid G-2 MIRA Result:Elevation, B-scan, and sliced isometric images. Grid Location: Kickapoo Creek, east barrier, 74'-2" - 80'-0" from N end. MIRA Analysis Results: Interior and exterior reinforcing identifiable, good reflection from back surface, no internal voids observed.

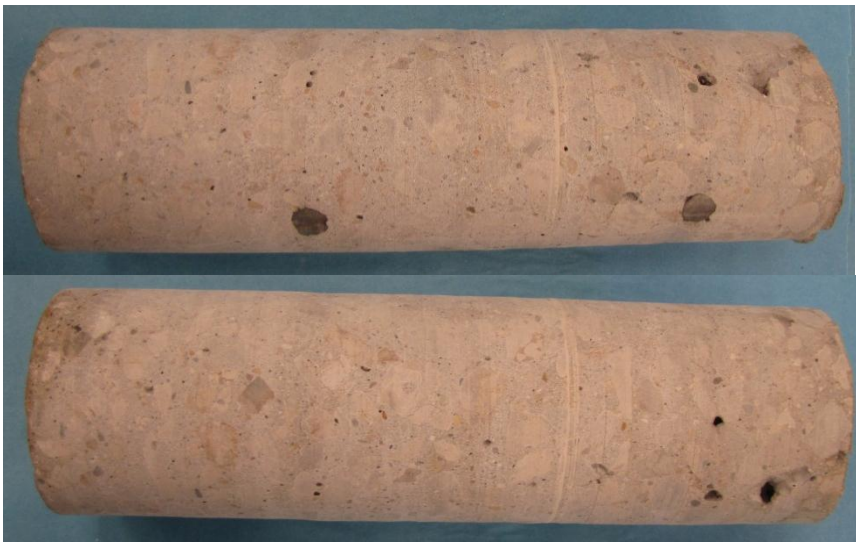

Figure 57. Core H-2. Core Location: Kickapoo Creek, east barrier, 76'-11", 8.5" from top of barrier. Observations: Well-consolidated through core, (1) isolated void (~1/2 inch diameter) near ext. face.

Figure 58 shows MIRA testing grid G-2 collected on the interior surface of the south barrier of the Emden Road Bridge [IDOT Str. No. 054-0078]. Results of the MIRA testing, shown in Figure 59, show the inability of the test method to penetrate beyond areas that are visibly deteriorated on the surface (surface cracking, evidence of freeze-thaw deterioration). Note that MIRA testing did identify additional internal distress extending beyond those areas that were visibly deteriorated on the surface. Embedded reinforcing and the exterior surface of the barrier can be identified at the right side of the testing grid, within tested areas in which no internal or exterior cracking is present. Core G-3, shown in Figure 60, indicated moderate voiding (3/8 to 1/2-inch diameter) behind reinforcing and around aggregate. Given the typical reflections from reinforcing, MIRA was not capable of identifying these voids.

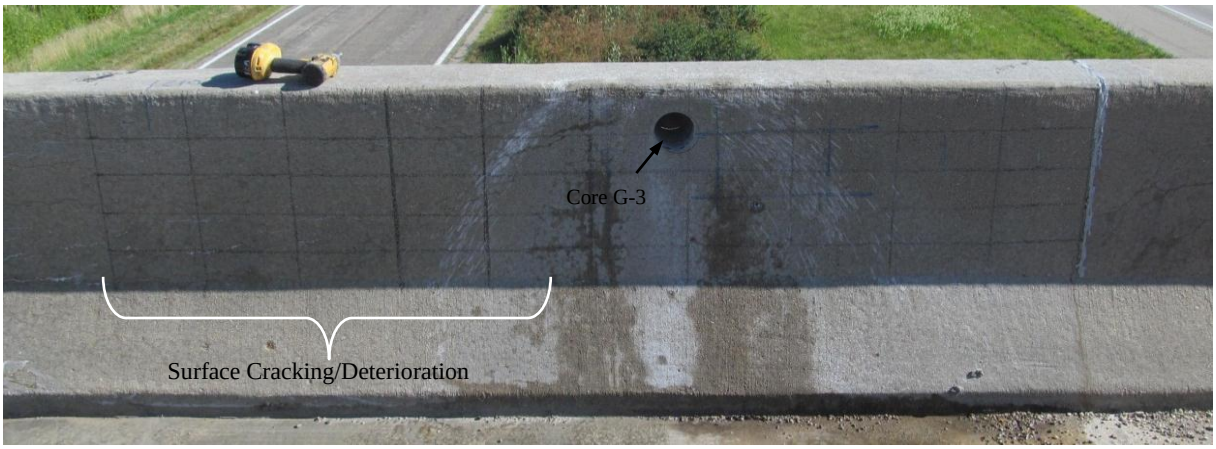

Figure 58. Grid G-2. Grid Location: Emden Road, south barrier, 203'-0" - 210'-6" from W end.

Grid G-2; Interior Elevation View

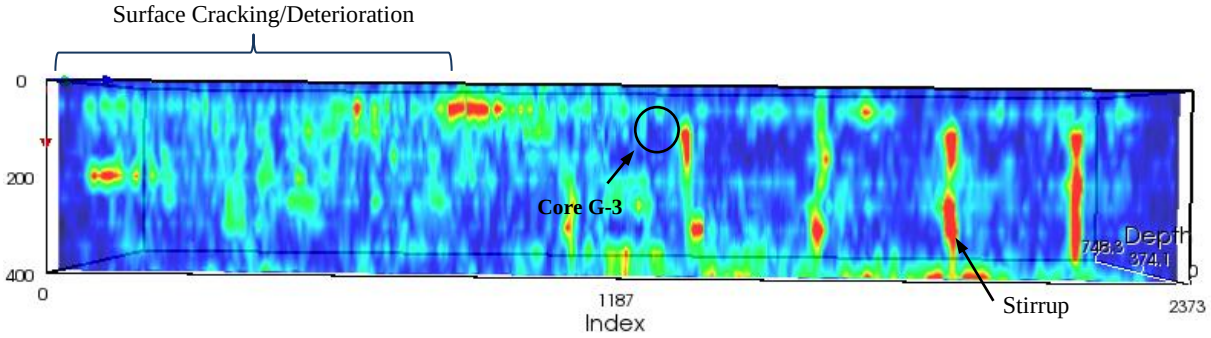

Grid G-2; B-scan & Isometric (Planar Section) Views

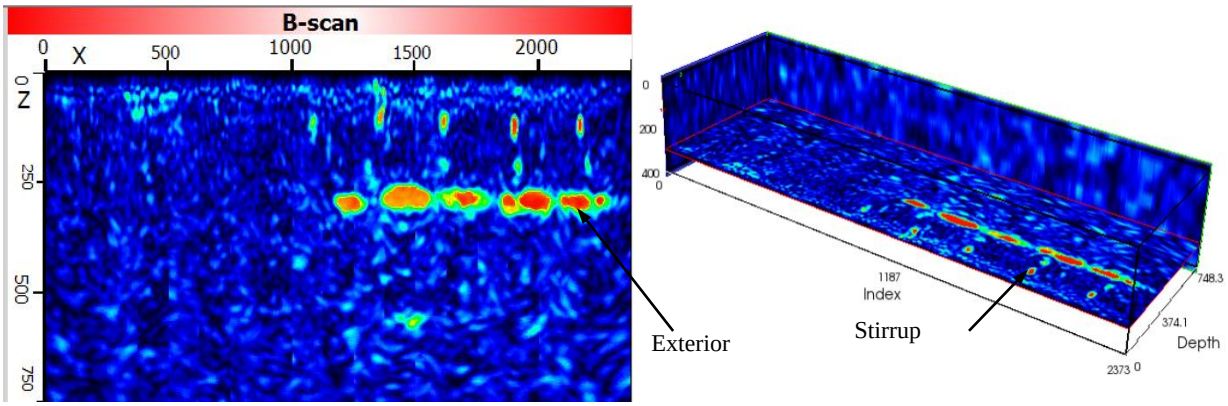

Figure 59. Grid G-2 MIRA Result:Elevation, B-scan, and sliced isometric images. Grid Location: Emden Road, south barrier, 203'-0" - 210'-6" from W end. MIRA Analysis Results: Stirrups and exterior face not identifiable on left side of grid (adjacent to areas that are visibly deteriorated). Extent of deterioration (surface and possible internal cracking) can be seen in MIRA result. MIRA result does not confirm presence of voiding around longitudinal bars.

Figure 60. Core G-3. Core Location: Emden Road, south barrier, 206'-6", 5 inches from top of barrier. Observations: Moderate voiding (3/8-to1/2-inch diameter) behind reinforcing and around aggregate

Figure 61 shows MIRA testing grid C-1 on the interior surface of the south barrier of MRB Eastbound. The resultant interior elevation view provided in Figure 62 shows several areas of internal reflections adjacent to the construction joint on the right side of the testing grid. These internal reflections were present near the interior layer of reinforcing stirrups. IDOT Core No 16, inspected by WJE after completion of the field testing, showed interconnected voids near the interior reinforcing typical of consolidation problems during slip forming (Figure 63).

Figure 61. Photograph of Grid C-1. Grid Location: MRB Eastbound, south barrier, Sta. 105+21 - 105+14.

Interior Elevation View

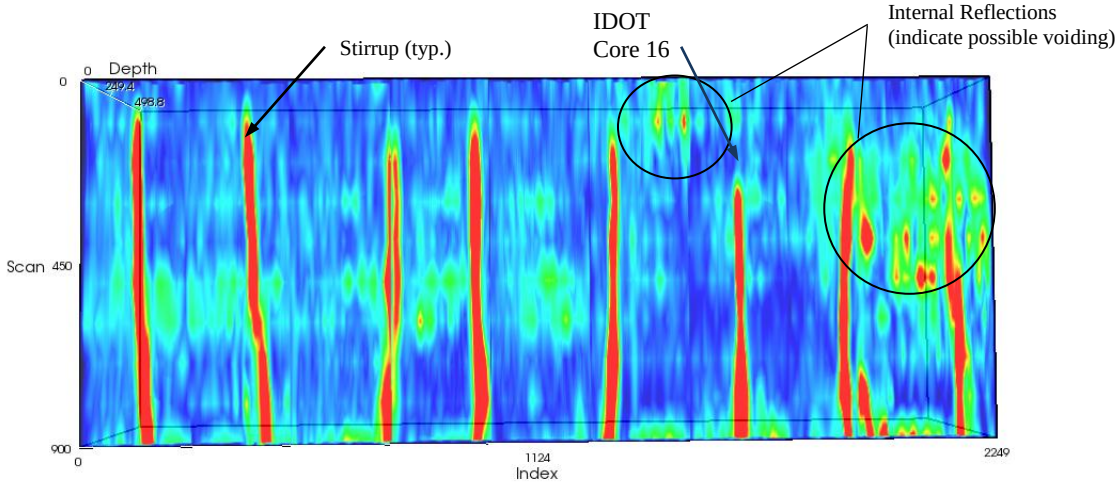

Figure 62. Grid C-1 MIRA Result:Interior elevation image. Grid Location: MRB Eastbound, south barrier, Sta. 105+21 - 105+14. MIRA Analysis Results: Internal reflections near IDOT Core No. 16 and east of joint. Probable internal voiding.

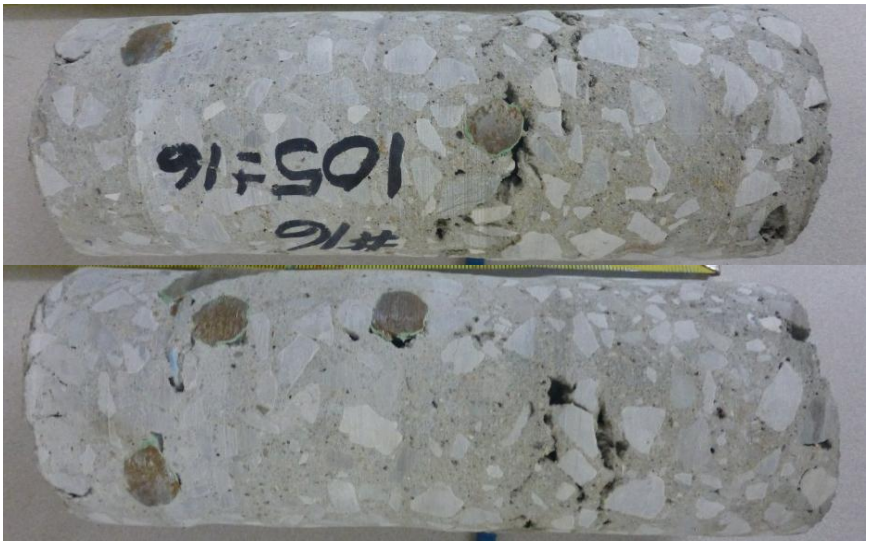

Figure 63. Core IDOT 16. Core Location: MRB Eastbound, south barrier, Sta. 105+16, 8" from top of barrier. Observations: Moderate voiding at interior reinforcing and in surrounding concrete.

Figure 64 shows the top of the barrier at MIRA testing grid H-3 on the east barrier of the Kickapoo Creek Bridge [IDOT Str. No. 054-0505]. A horizontal crack measuring approximately 10 inches long was observed near the middle of the top surface of the wall. MIRA testing at this location identified signal reflections from the planar separation extending from the top of the wall to the top layer of longitudinal bars (Figure 65). The planar separation did not appear to extend beneath the reinforcing at this location.

Figure 64. Photograph of longitudinal cracking at top of barrier at Grid H-3. Grid Location: Kickapoo Creek, east barrier, 214' - 220' from N end.

Grid H-3; Interior Elevation View

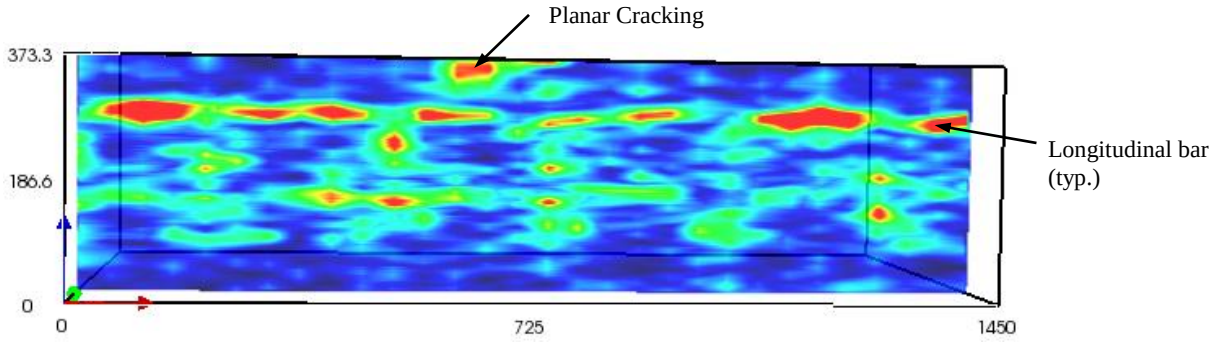

Grid H-3; Isometric View

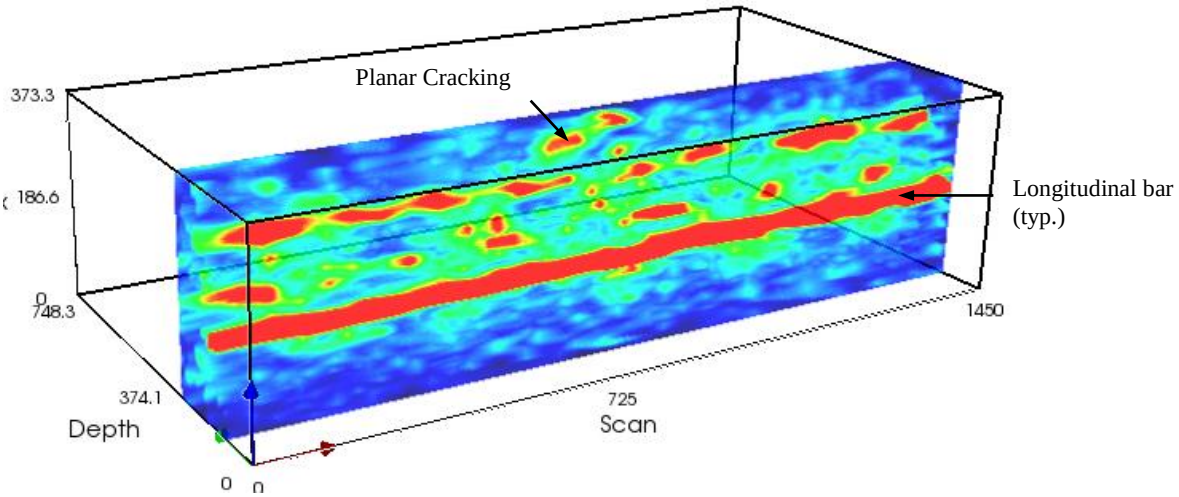

Figure 65. Grid H-3 MIRA Result: interior elevation, isometric images. Grid Location: Kickapoo Creek, east barrier, 214' - 220' from N end. MIRA Analysis Results: Interior and exterior reinforcing identifiable, good reflection from back surface, planar separations above longitudinal bars at top of barrier.

3.1.3.7. Advantages and Limitations of Test Method

The following summarizes the results and conclusions of trial-testing of the shear wave ultrasonic test method for concrete flaw detection:

Capabilities and Advantages:

- Although testing is performed at individual test locations, the size of the MIRA device provides for testing of a relatively large area (approximately 10-inches wide by 4-inches high) at each location. Additionally, data collection of a full 'map' of testing points can be collected relatively quickly using the device.
- Identification of the presence and approximate depth of individual internal voids measuring 3-inches wide and greater, positioned at any depth within the barrier wall, and coincident with test location.

- Identification of interconnected voids in concrete measuring ≥1/4-inch thick if these voids are situated near near-surface reinforcing or shallower. Larger internal flaws and voids positioned deeper within the barrier may be detectable depending on flaw type and severity.
- Identification of the presence and approximate depth to internal planar cracking coincident with test location.
- Identification of disbonding of patch repairs.
- Identification of the presence and approximate depth of internal honeycombing depending on size and position of the honeycombing.
- Accurate thickness measurement of barrier wall at unflawed test locations.
- Data collection requires access to only one side of the barrier wall.

Limitations:
- Testing is performed at individual test locations, requiring setup of testing grids on the interior face of the barrier wall.
- Complex geometry of barrier wall design complicates data interpretation and may hinder flaw detection along the thickened base of the barrier wall.
- High amplitude signal reflections from embedded reinforcing cannot be distinguished from embedded voids or flaws and must be accounted for during data analysis.
- Surface deterioration such as surface scaling, microcracking, and freeze-thaw deterioration prevents ultrasonic wave propagation and internal flaw detection.
- Small or thin voids or production-related flaws present near and behind reinforcing bars cannot be detected.
- Detection of internal honeycomb defects is limited to larger (3-inch square) embedded defects positioned within 5 inches of the tested face of the barrier wall.
- Equipment is expensive to purchase and may be difficult to rent.
- Use of equipment and software and data analysis requires significant training and experience.

3.1.4. Ultrasonic Pulse Velocity Testing (UPV)

3.1.4.1. Mock-up Testing Procedures

Testing of the mock-up barrier wall comprised of initial layout of a testing grid, UPV testing at each grid location, and subsequent data analysis and interpretation. UPV testing was performed on the 6-inch by 6-inch testing grid laid out on the interior and exterior faces of the mock-up wall. UPV testing at each grid location consisted of coupling the transducers to each face of the wall using a water-based ultrasonic coupling gel and measuring the time and relative signal amplitude of ultrasonic wave propagation through the wall. Several individual tests were performed at each grid location to assess repeatability and ensure that a representative test result was retained. Additional testing was performed at each flaw location as necessary to evaluate the test method. Individual test results were analyzed to determine the effectiveness of the test method in identifying the embedded flaws and to determine the optimum data collection and analysis procedures.

3.1.4.2. Field Testing Procedures

Field testing of the UPV testing method was not performed.

3.1.4.3. Testing and Analysis Results: Laboratory Mock-up

Analysis of UPV data includes examination of the received waveform in the time domain using a digital oscilloscope, measurement of signal amplitude, and calculation of pulse velocity based on the time of

signal propagation through the tested element. Changes in the time of signal propagation can indicate either changes in the pulse velocity due to the presence of material degradation or embedded honeycombing, or a difference in path length due to the presence of internal voiding or cracking. Figure 66 through Figure 70 provide examples of the results of UPV testing performed on the mock-up barrier wall sample. An elevation view of the interior face of the mock-up barrier wall indicating the locations of the UPV testing grid and embedded flaws is provided in Figure 66. Subsequent figures provide individual test results at selected grid locations coinciding with an unflawed location on the barrier wall (Figure 67), embedded void V2 (Figure 68), embedded honeycomb panel D1 (Figure 69), and embedded honeycomb panel D3 (Figure 70).

Figure 67 provides the UPV test result at a location on the mock-up barrier at which no internal flaws were present through the thickness of the wall (UPV Test Location B-3). The plot displays the time domain waveform of the stress wave collected at the receiving transducer. The test result shows a time delay of 63.0 µs, corresponding to a measured ultrasonic pulse velocity of 14,206 feet per second, at which time an unimpeded, high amplitude signal is received. Figure 68 provides the UPV test result at embedded void V2. The embedded void results in an increase in the transit time of the stress wave and reduction in the measured ultrasonic pulse velocity to 12,590 feet per second. The amplitude of the received waveform is also severely affected by the presence of the flaw. The difference between the acoustic impedance of the embedded foam and the concrete at this location results in reflection of a majority of the propagating stress wave at the surface of the void. Therefore, the stress wave collected at the receiving transducer likely represents waves which have traveled around the embedded void panel, resulting in an increased path length. Similarly, testing at the embedded honeycomb panels D1 and D3, as shown in Figure 69 and Figure 70, respectively, resulted in a reduction in the measured pulse velocity and a notable effect on the amplitude of the received signal. The stress waves at these test locations, however, likely propagate directly through the honeycomb concrete, directly reducing the pulse velocity.

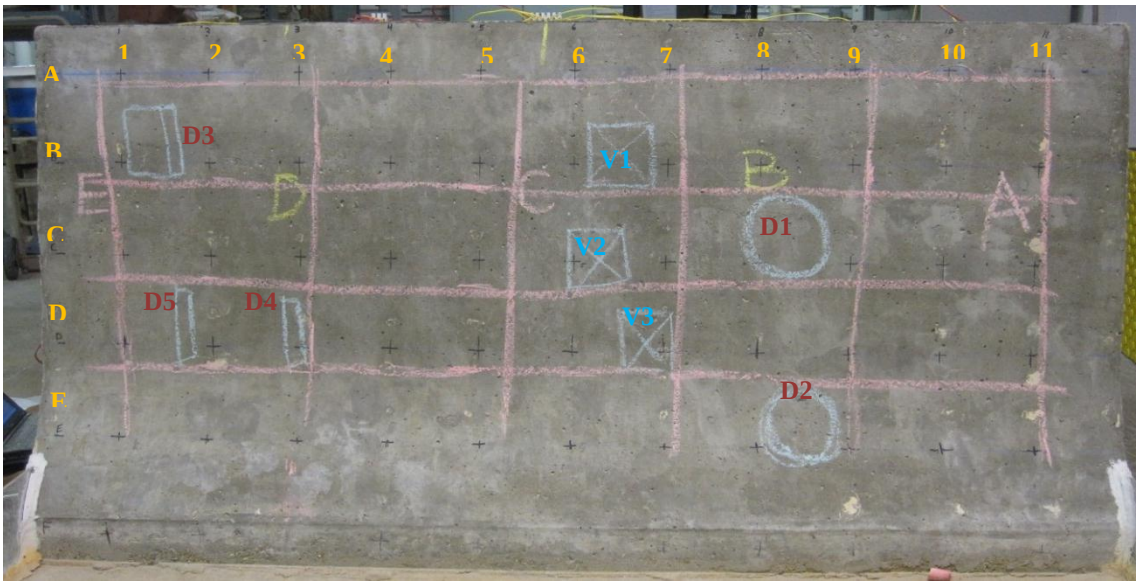

Figure 66. View of interior face of the mock-up barrier wall indicting locations of embedded voids (V1-V3) and honeycomb defects (D1-D5) and UPV testing grid labels (corresponding grid on opposite face).

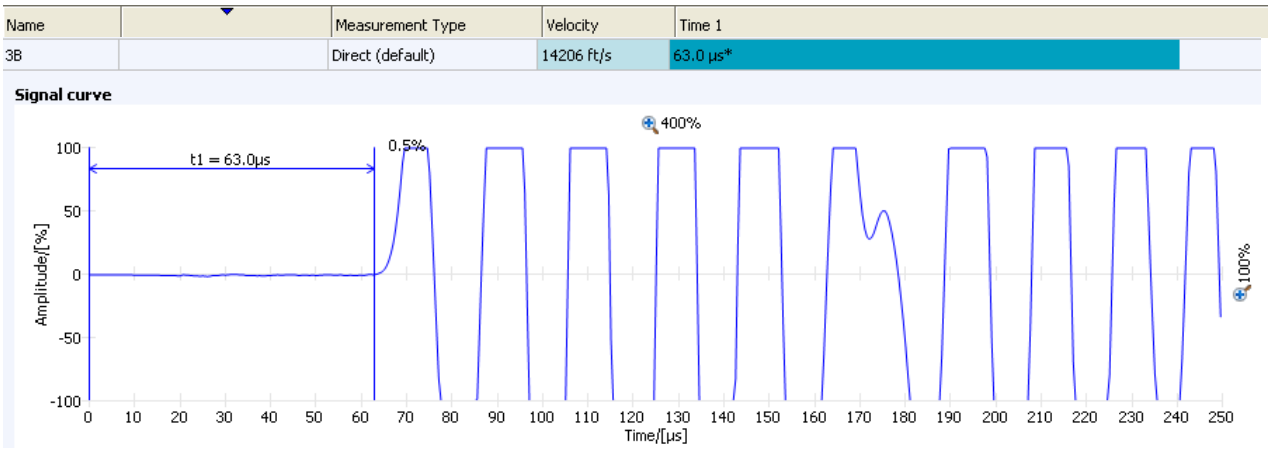

Figure 67. UPV test result at Test Location B-3; no flaw. Measured UPV velocity of 14206 ft/s.

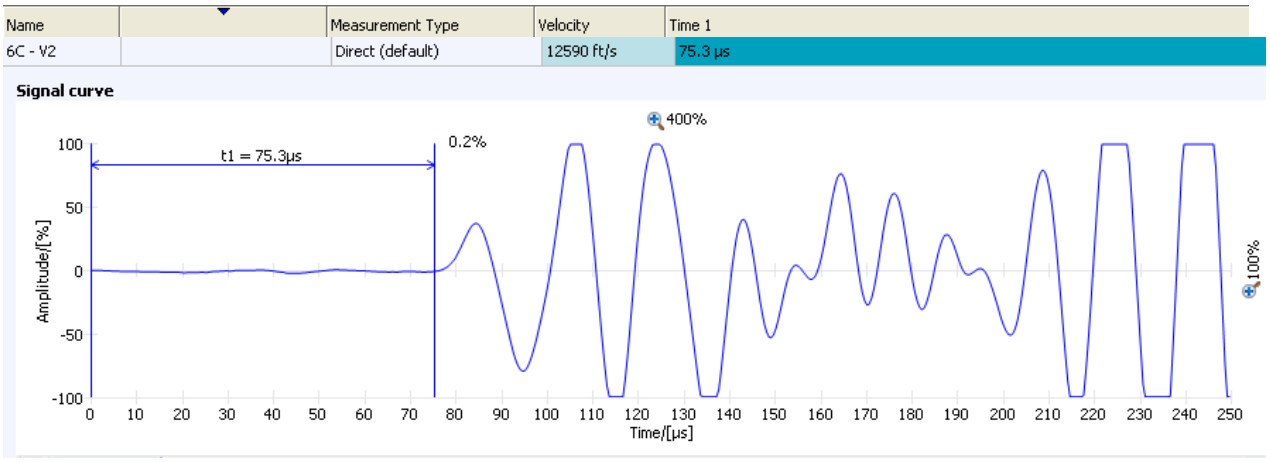

Figure 68. UPV test result at Test Location C-6; embedded void panel V2. Measured UPV velocity of 12590 ft/s.

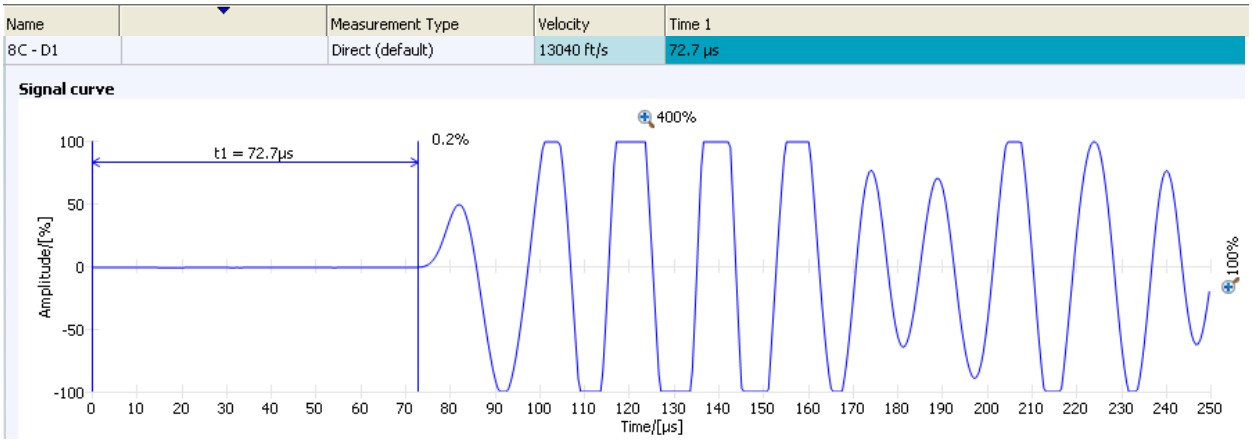

Figure 69. UPV test result at Test Location C-8; embedded honeycomb panel D1. Measured UPV velocity of 13040 ft/s.

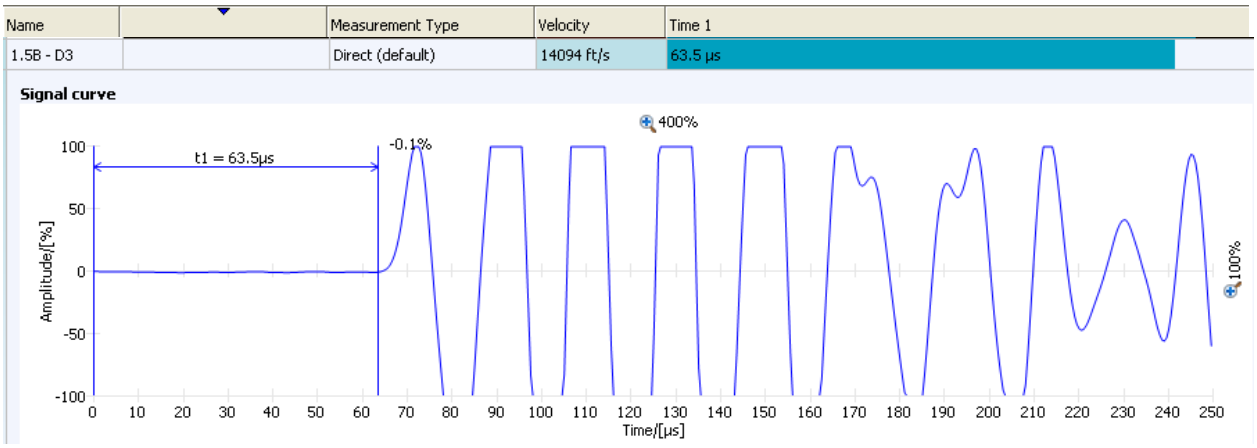

Figure 70. UPV test result at Test Location B-1.5; embedded honeycomb panel D3. Measured UPV velocity of 14094 ft/s.

3.1.4.4. Advantages and Limitations of Test Method

The following summarizes the results and conclusions of trial-testing of the UPV ultrasonic test method for concrete flaw detection:

Capabilities and Advantages:

- Measurement of pulse velocity at unflawed test locations can provide a relative indication of concrete quality. Research has shown that UPV measurements of unflawed concrete can be correlated to compressive strength with proper correlation testing.
- Identification of the presence of embedded voids measuring 3-inches wide and greater and coincident with test location, regardless of void depth within the barrier wall.
- Identification of internal planar cracking or delamination and disbonding of patch repairs coincident with test location.
- Detection of presence and relative severity of internal honeycombing coincident with test location.
- Multiple tests performed at each test location can ensure repeatability of data.

- Testing devices are commercially available from a number of suppliers and are relatively inexpensive.

Limitations:

- Through-transmission UPV testing requires access to both sides of the barrier wall at each test location.
- Testing is performed at individual test locations, requiring setup of testing grids on both the interior and the exterior face of the barrier wall. Careful alignment of the transducers is necessary for accurate measurements.
- Data collection requires testing at individual grid locations, which is time-consuming. The amount of data collection is limited.
- Testing requires accurate measurement of barrier wall thickness at each test location.
- Complex geometry of barrier wall design may hinder flaw detection along the thickened base of the barrier wall.
- Depth to any internal flaws detected by UPV testing cannot be determined.
- Small voids (less than 2-inches in diameter), thin voids around reinforcing bars, and minor consolidation issues cannot be detected.

3.1.5. Ground-Penetrating Radar (GPR)

3.1.5.1. Mock-up Testing Procedures

Testing of the laboratory mock-up barrier wall comprised the initial layout of embedded reinforcing and the subsequent collection of continuous longitudinal and vertical scans on the sides of the barrier wall segment. Scans were positioned to intersect known locations of embedded defects. Individual scans were analyzed to determine the effectiveness of the test method in identifying the embedded flaws and to determine the optimum data collection and post-processing procedures. Trial testing of the Killian barrier wall segment was performed using the testing procedures described in the Phase B field testing section below.

3.1.5.2. Phase A Field Testing Procedures

Phase A field testing of GPR was performed on the eastbound and westbound barrier walls of the Blair Bridge (US30 over Missouri River) and the northbound barrier wall of Iowa 150 over the Cedar River. Testing comprised of collection of continuous longitudinal scans on the interior and exterior sides of the selected lengths of barrier walls at various heights. For each tested barrier, individual GPR scans were analyzed to determine correlation of testing results with the surface conditions observed and results of core sampling at selected locations.

The following trial testing was performed at each field testing location:

US 30, Eastbound Barrier.

2.6 GHz Antenna: Longitudinal scans at 6 inches from top of barrier, 12 inches from top of barrier, middle of diagonal, top of vertical face (bottom of barrier); 40-foot scan lengths.

US 30, Westbound Barrier.

2.0 GHz Antenna: Longitudinal scan at 6 inches from top of barrier; 36-foot scan length.

2.6 GHz Antenna: Longitudinal scans at 6 inches from top of barrier, 12 inches from top of barrier, middle of diagonal; 40-foot scan lengths.

Iowa 150, Northbound Barrier:

2.6 GHz Antenna: East (exterior) face; Longitudinal scans at 8-inch, 20-inch, 26-inch and 32-inch heights (as measured on non-vertical face); 115-foot scan lengths, Sta. 145 to Sta. 260.
2.6 GHz Antenna: Top surface; Longitudinal scan; 115-foot scan length, Sta. 145 to Sta. 260.
2.6 GHz Antenna: West (interior) face; Longitudinal scans at 6-inch, 18-inch, and 28-inch heights, 115-foot scan lengths, Sta. 145 to Sta. 260.

Additionally, several core samples were removed from the west (interior) face of the northbound barrier wall at the Iowa 150. The core samples labeled C1 and C2 were extracted at locations at which the GPR scanning indicated no internal flaws and were used for confirmation of this condition. Subsequently, GPR scanning was performed from the opposite side of the barrier wall to determine whether GPR was an effective method for detecting the small diameter core holes within the barrier wall.

3.1.5.3. Phase B Field Testing Procedures

GPR testing was a primary test method during Phase B field testing on each of the selected barrier walls. GPR scanning was performed as a series of individual horizontal scans collected at various heights on the lateral surfaces and along the top of each barrier. In general, three horizontal scans were collected on the interior face (located approximately 8 inches from top of barrier, 16 inches from top of barrier, and at the center of the chamfer), one horizontal scan was collected at the middle of the top surface, and one horizontal scan was collected on the exterior face of the barrier (located approximately 8 inches from the top of the barrier) at each barrier. The exact position of each horizontal scan was adjusted to avoid scanning directly over the longitudinal bars near the scanned surface in order to provide for better resolution of embedded flaws beyond this reinforcing layer. A summary of the GPR scans collected at each barrier wall, including the scan location and approximate extent of the scan from a reference station on the barrier, is provided in Table 6.

Post-processing of the collected GPR scans consisted of a series of time adjustments, signal filters, and gain adjustments applied similarly to each scan. Subsequent review of each scan was performed to identify signal reflections and disturbances, which indicated the presence of possible voids, concrete defects, or other internal distress within the barrier wall. The approximate cover depth and spacing of the steel reinforcing stirrups oriented perpendicular to the GPR scan direction were determined. To accurately determine reinforcing depth, the data was calibrated through direct measurement of the cover depth to selected reinforcing stirrups at two or more drill locations on each barrier. Plots of the minimum cover depth measured on the interior face of the barrier wall (from all interior surface scans) and the cover depth measured on the exterior surface near the top of the barrier were provided in the appendices of the IDOT report.

3.1.5.4. Testing and Analysis Results: Laboratory and Field Mock-ups

Figure 71 through Figure 74 provide examples of the GPR trial testing performed on the mock-up barrier wall sample. An elevation view of the interior face of the mock-up barrier wall indicating the locations of selected horizontal scans in relation to the embedded flaws is provided in Figure 71. Selected horizontal scans after signal filtering and post-processing are shown along with an indication of the locations of the embedded voids or honeycomb defect panels along the scans.

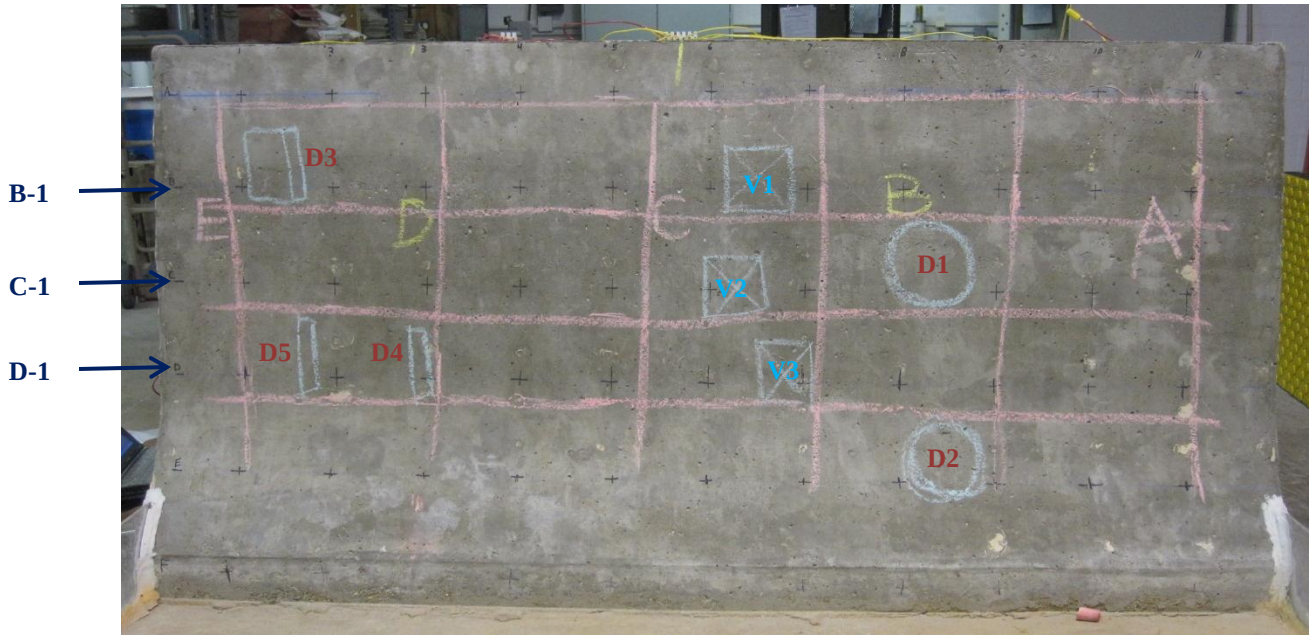

Figure 71. View of interior face of the mock-up barrier wall indicting locations of embedded voids (V1-V3) and honeycomb defects (D1-D5) and locations of selected horizontal GPR scans (B1, C1, D1).

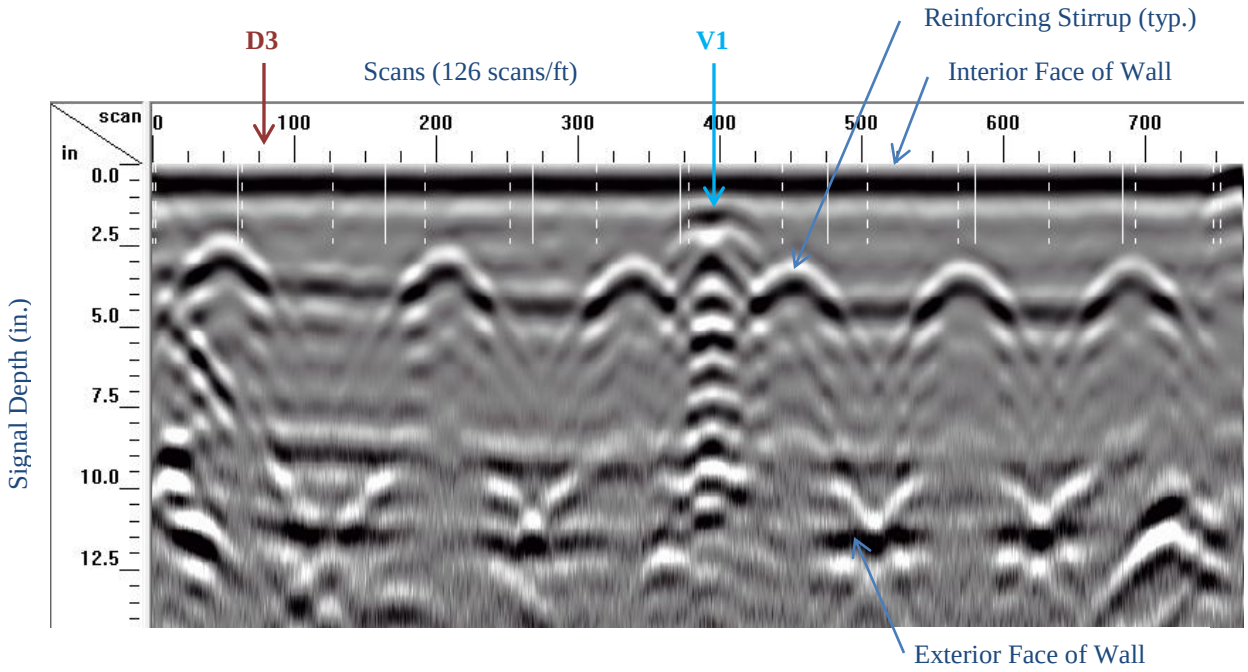

Figure 72. Sample GPR scan B-1 collected horizontally along gridline B of the mock-up barrier wall.

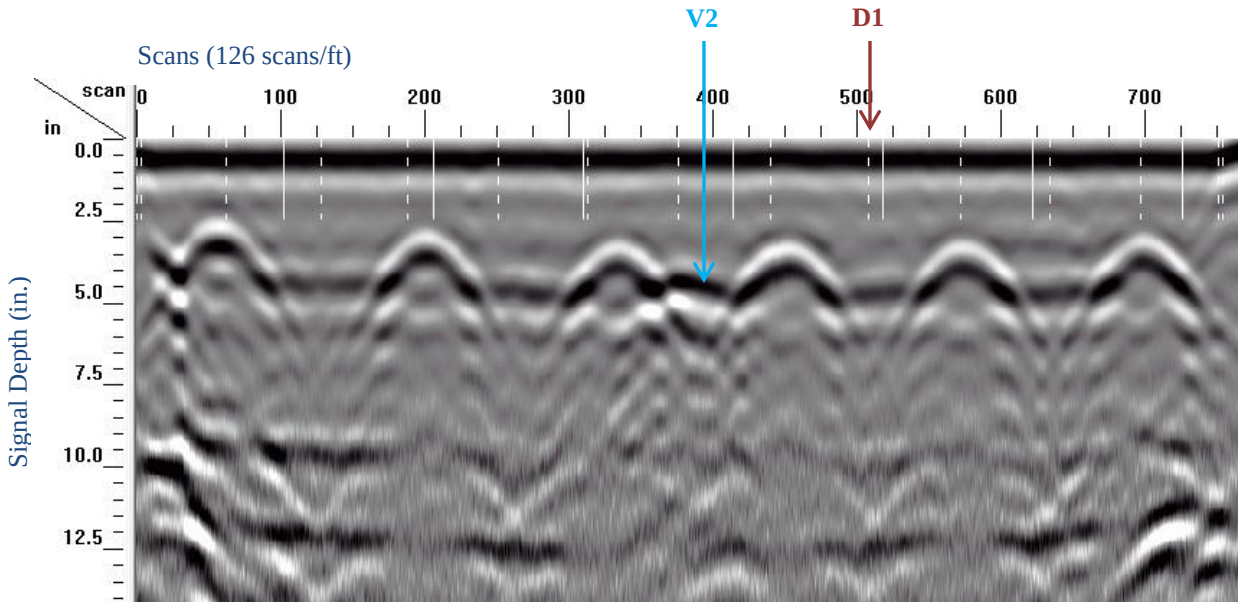

Figure 73. Sample GPR scan C-1 collected horizontally along gridline C of the mock-up barrier wall.

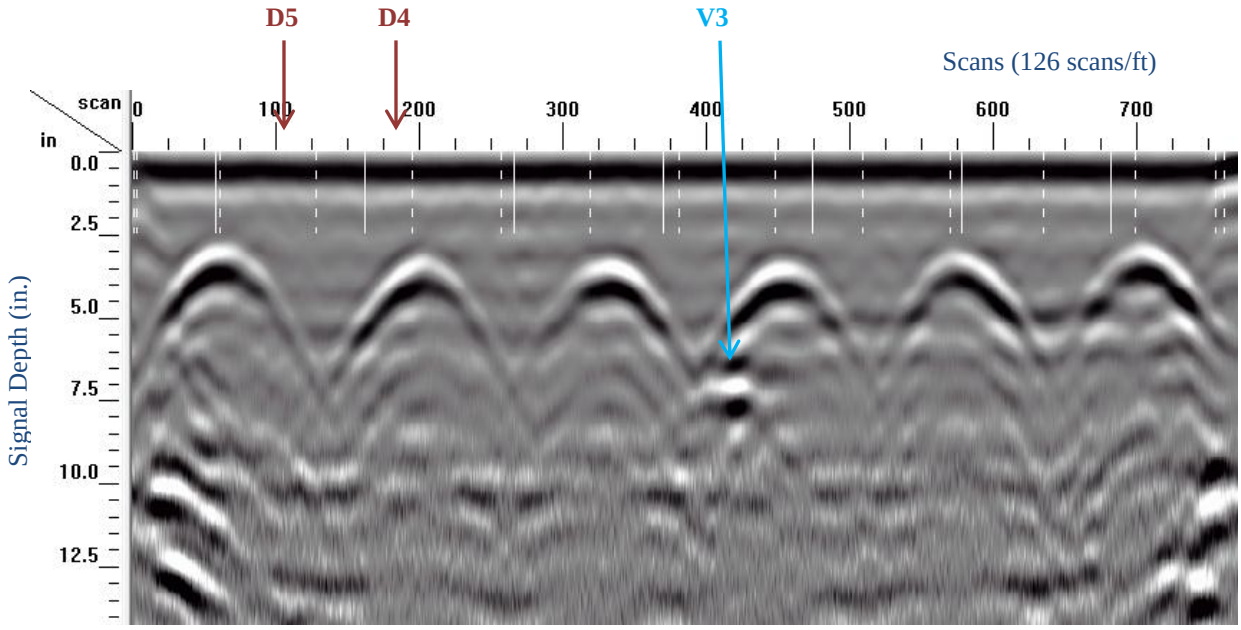

Figure 74. Sample GPR scan D-1 collected horizontally along gridline D of the mock-up barrier wall.

In additional to the laboratory mock-up testing, GPR testing was performed on the Killian trial barrier segments. Results of the testing indicated that GPR testing of early-age slip formed barrier walls (48 hour after construction) was feasible. However signal resolution was adversely affected by the concrete age (Figure 75). Early-age concrete contains higher free moisture levels, resulting in higher signal attenuation through the thickness of the wall. Detection of internal conditions beyond the nearest reinforcing layer was limited in these test samples.

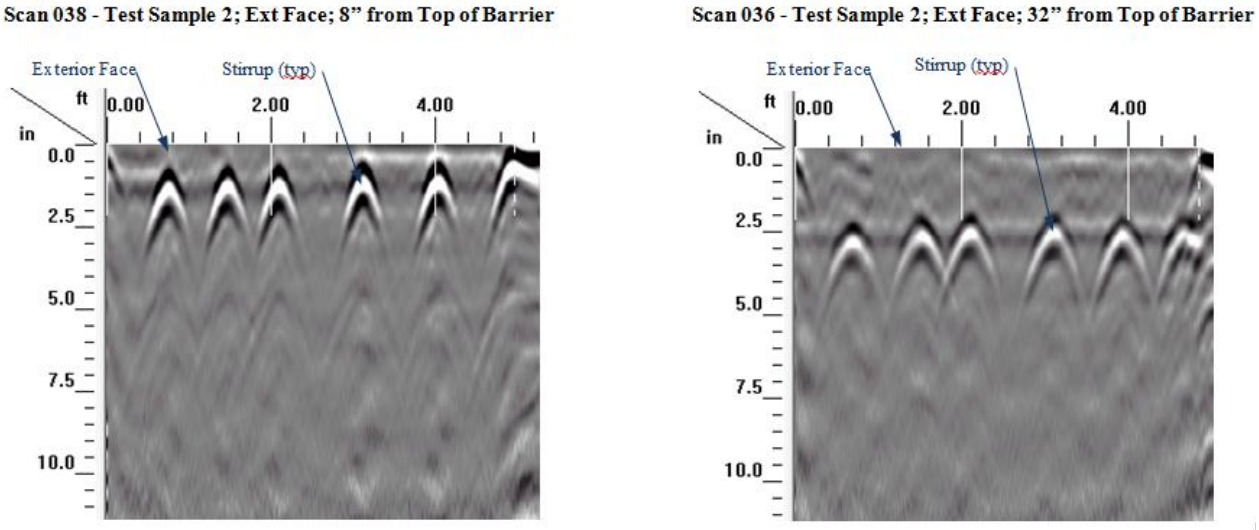

Figure 75. Sample GPR scan s collected horizontally on the exterior face of the Killian Test Sample 2. GPR Result: Signal penetration limited, not able to resolve interior reinforcing from exterior face.

3.1.5.5. Testing and Analysis Results: Phase A Field Testing

Phase A field testing of GPR provided general conclusions about the feasibility and capabilities of using the test method for barrier assessment; more specific flaw detection studies were completed during Phase B field testing. It was determined that the higher frequency 2.6 GHz antenna provided optimum signal resolution through the thickness of the barrier wall. GPR testing at the Iowa 150 bridge did not identify any internal reflections indicating potential internal flaws or voids. Several partial-depth exploratory cores were collected from the exterior face of the barrier at selected locations to confirm the unflawed condition (Figure 76). Subsequently, GPR scanning of the barrier wall on the interior face at each core location confirmed that GPR was capable of detecting the drilled core holes (Figure 77).

Figure 76. Exploratory coring in progress on the exterior face of the northbound barrier of Iowa 150.

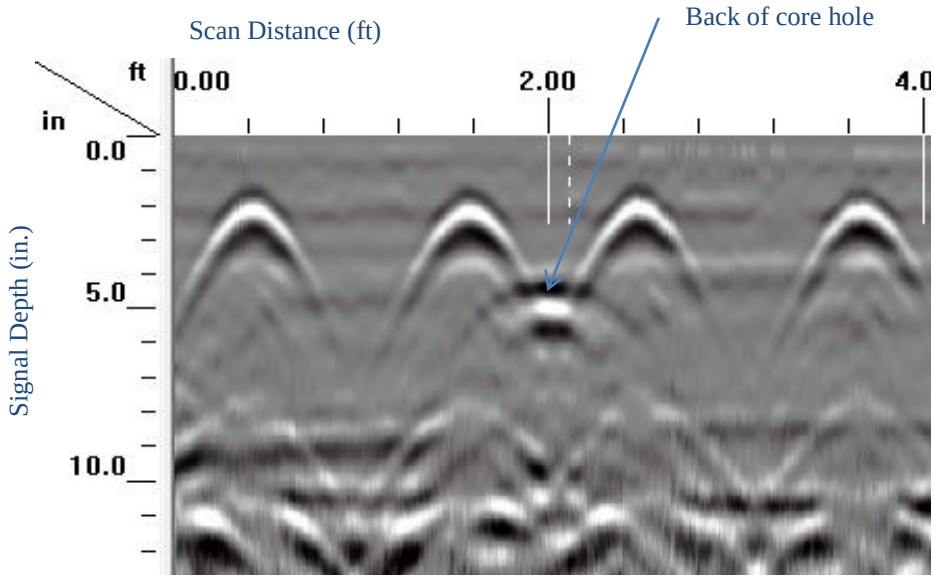

Figure 77. Horizontal GPR collected on the interior face of the barrier at typical exploratory core location at northbound barrier of Iowa 150.

An additional study was performed on the northbound barrier wall of Iowa 150. Concrete cracking and moisture staining was observed along the top surface and extending down each face of the barrier wall at locations coinciding with previously installed light pole or railing bases. Some of these severely affected areas had been previously patched or covered with a parge coat of cementitious material. GPR scans collected at a height corresponding to the occurrence of this observed distress were analyzed to determine if GPR was capable of directly detecting the distress or if additional data analysis was required to detect

the distress. A specific method, analogous to methods used to detect delamination of concrete bridge decks, was explored during which the amplitude of the signal reflection from the vertical reinforcing bars within the barrier was analyzed along with cover depth data. Signal amplitude and cover depth were plotted, and the results were compared with photographs and condition assessment notes along the length of the scans. Figure 78 provides an excerpt of a GPR scan collected on the west face of the southbound barrier at station 2+45 to 2+57 along with selected photographs showing the surface condition of the area. Note the presence of a cracking and moisture staining around a repair patch reduces signal velocity, signal reflection amplitude from the embedded vertical reinforcing bars, and signal reflection amplitude from the back surface of the barrier. Figure 79 shows a plot of signal amplitude and cover depth from a full sample horizontal GPR scan relative to areas that were visibly distressed. Some correlation between the observed distress and signal velocity and reflection amplitude values was observed. However, this correlation requires additional study.

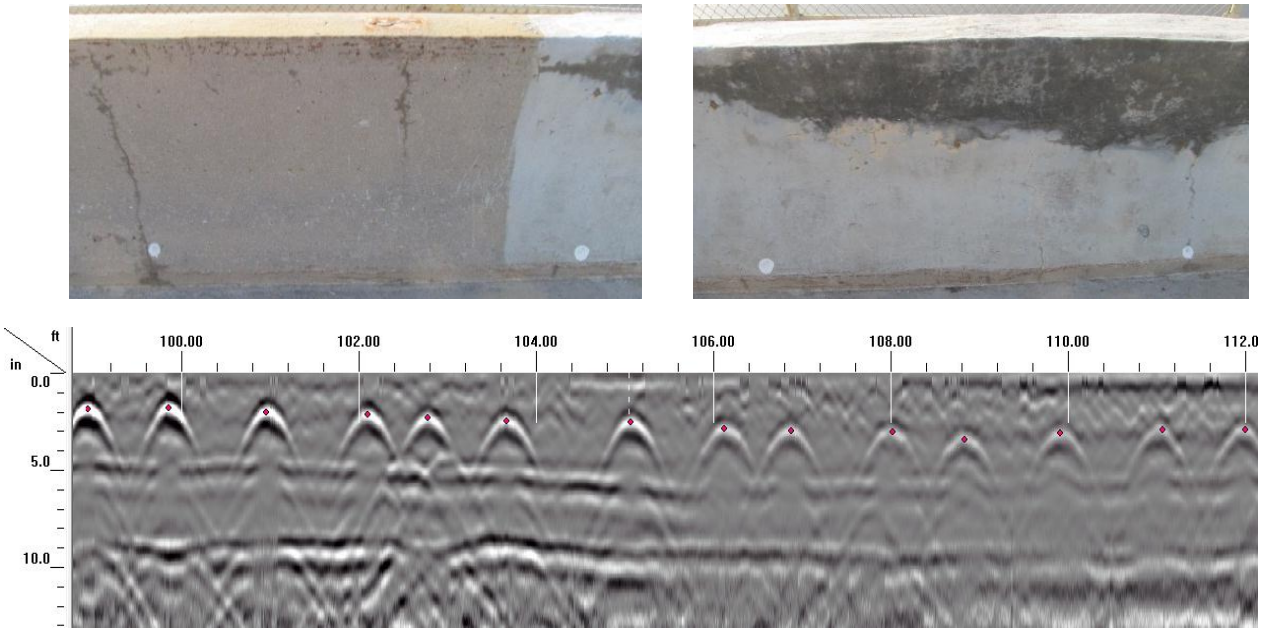

Figure 78. Sample GPR scan D-1 collected horizontally along gridline D of the west face of the southbound barrier at station 2+45 to 2+57 for Iowa 150.

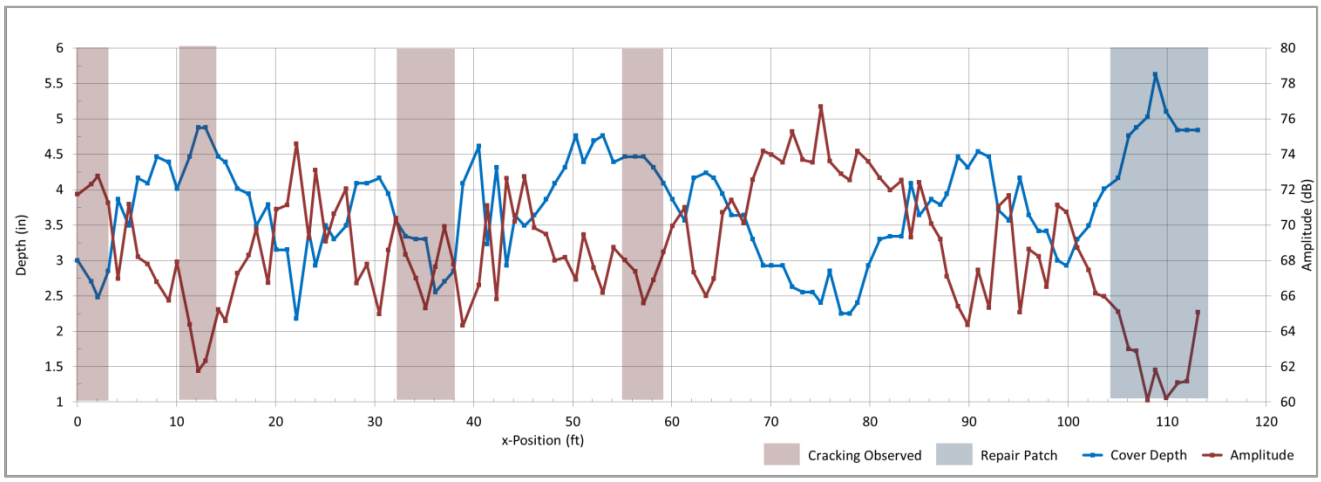

Figure 79. Sample GPR scan D-1 collected horizontally along gridline D of the west face of the southbound barrier at station 2+45 to 2+57 for Iowa 150.

3.1.5.6. Testing and Analysis Results: Phase B Field Testing

Ground-penetrating radar and subsequent exploratory coring during Phase B field testing provided specific conclusions about the method's ability to detect production-related concrete flaws within both slip formed and cast-in-place barriers.

Figure 80 shows the interior face of the west barrier of the Armitage Spur Bridge [IDOT Str. No. 054-0503]. Results of a GPR scan collected on the exterior face approximately 8 inches from the top of the barrier are provided in an excerpt of the processed GPR scan shown in Figure 81. The interior and exterior layer of reinforcing stirrups and the opposing interior surface of the barrier wall are identifiable in the horizontally oriented scan. The scan shows a negative signal reflection indicative of possible internal voiding near the exterior face stirrup at 42 feet-6 inches from north end of barrier. Core F-3, shown in Figure 82, indicated a void measuring 1-1/4 inch diameter located adjacent to the stirrup and longitudinal bar at this location.

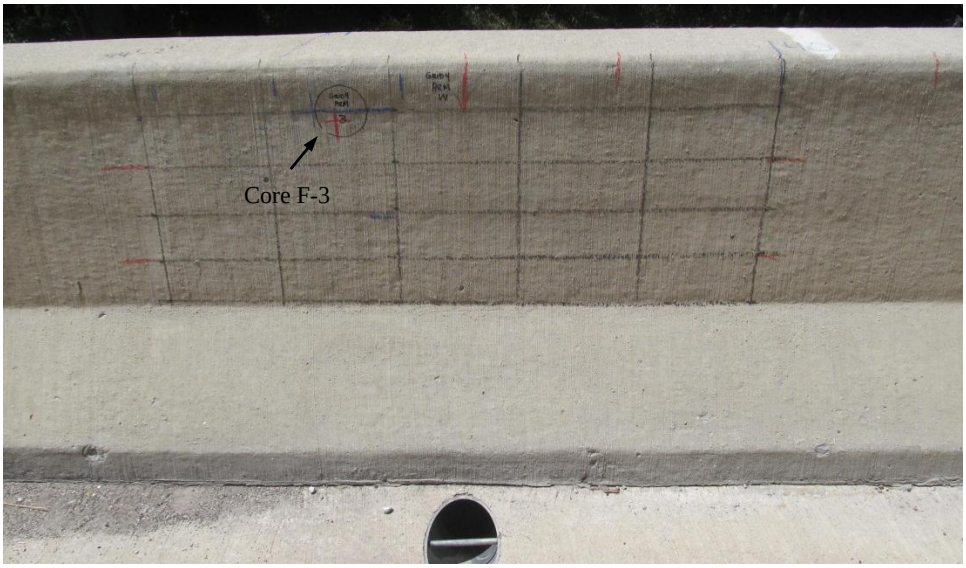

Figure 80. Photograph of interior face of west barrier of Armitage Spur. Core F-3 located 42'-10" from N end.

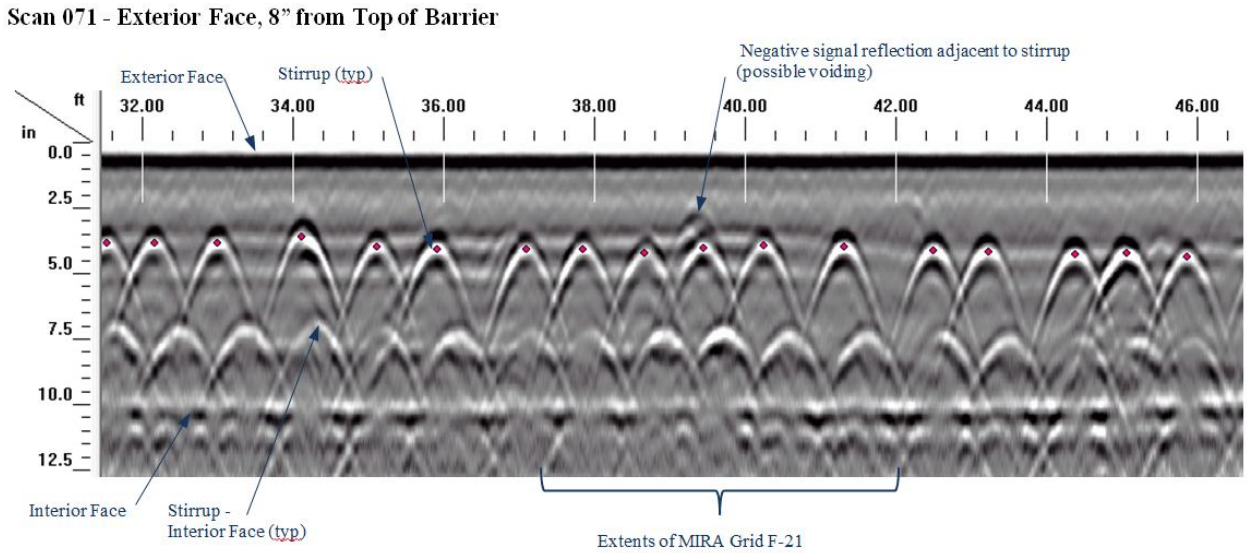

Figure 81. GPR Scan Excerpt: Scan 071 collected on Armitage Spur, west barrier, exterior face , 8" from top of barrier. GPR Analysis Results: Negative signal reflection near exterior face stirrup at 42'-6" from north end of barrier.

Figure 82. Core F-3. Core Location: Armitage Spur, west barrier, 42'-10" from north end, 4" from top of barrier. Observations: Well-consolidated through core, (1) void (1/4 inch diameter) adj. to ext. longitudinal bar

In contrast to ultrasonic testing methods, the GPR test method is capable of penetrating visibly deteriorated areas, including those areas with moderate to severe cracking and freeze-thaw deterioration. An excerpt of the GPR scan collected on the interior face of the south barrier at the Emden Road Bridge [IDOT Str. No. 054-0078] shows that the interior and exterior reinforcing stirrups and the exterior surface of the barrier can be identified in the scan. However, signal wave speed (depth measurement) and signal amplitude are affected by the presence of the deterioration (Figure 83). Additionally, minor negative reflections observed near the longitudinal reinforcing bars in the scan indicated possible voiding along the bar. Note that this test location coincides with the MIRA test location G-2 shown in Figure 58. As noted earlier, Core G-3 indicated moderate voiding (3/8 to 1/2 inch diameter) behind reinforcing and around aggregate (Figure 60).

More severe voiding around the reinforcing bars was identified by GPR at a test location at 150 feet to 170 feet from the north end of the north barrier of the Emden Road Bridge (Figure 84). An excerpt of the GPR scan collected on the exterior face of the barrier identifies severe voiding along the exterior longitudinal bar (Figure 85). Core G-5, shown in Figure 86, indicated severe voiding at the interior and exterior reinforcing. Based on the appearance of the voids, the separation was caused by a vertical shift, or sag, in the concrete during slip forming while the material was still in a plastic state.

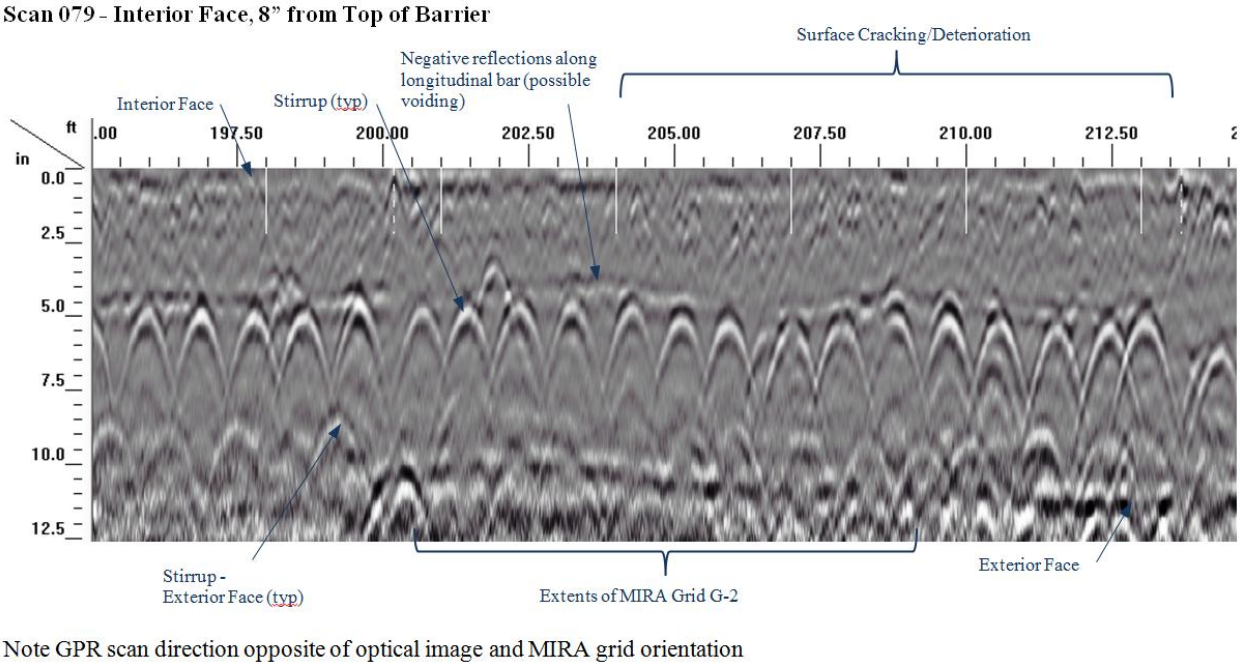

Figure 83. GPR Scan Excerpt: Scan 079 collected on Emden Road, south barrier, interior face , 8" from top of barrier. GPR Analysis Results: Overall signal disturbance near-surface, wave speed affected by deterioration/cracking, negative reflections along longitudinal bar indicates possible voiding along bar

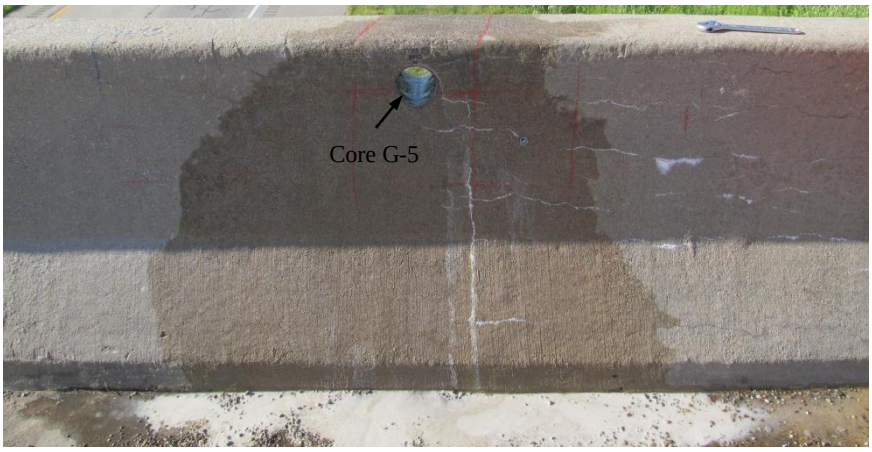

Figure 84. Photograph of interior face of the north barrier of Emden Road. Core F-5 located 162'-7" from N end.

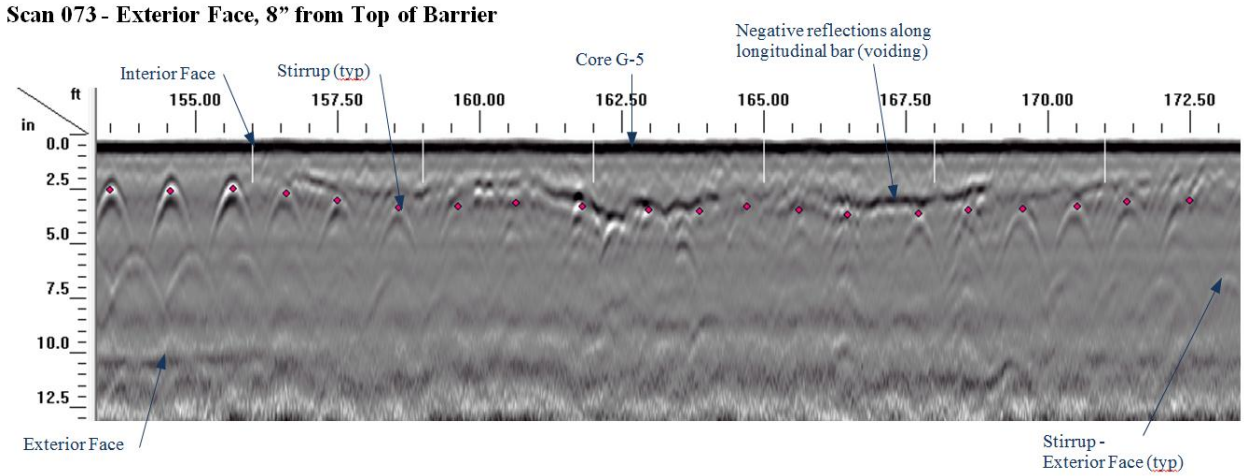

Figure 85. GPR Scan Excerpt: Scan 073 collected on Emden Road, north barrier, exterior face , 8" from top of barrier. GPR Analysis Results: Severe negative reflection along exterior longitudinal bar, wave speed affected by condition, severe voiding identified.

Figure 86. Core G-5. Core Location: Emden Road, north barrier, 162'-7" from north end, 4.5" from top of barrier. Observations: Severe voiding at reinforcing, separation of concrete from reinforcing in plastic state ~1 inch wide

Additionally, signal disturbance observed in the GPR scans collected on the south barrier of MRB Eastbound indicate that GPR may be able to detect smaller, interconnected voids within slip formed barriers. As noted in Figure 63 above, IDOT Core No. 16 showed interconnected voids near the interior reinforcing typical of consolidation problems during slip forming. GPR scans collected on the interior surface of the barrier at Sta. 105+21 to 105+14 (Figure 62) identified minor disturbances coinciding with the voiding detected during ultrasonic (MIRA) testing and conditions observed at IDOT Core No. 16 (Figure 87).

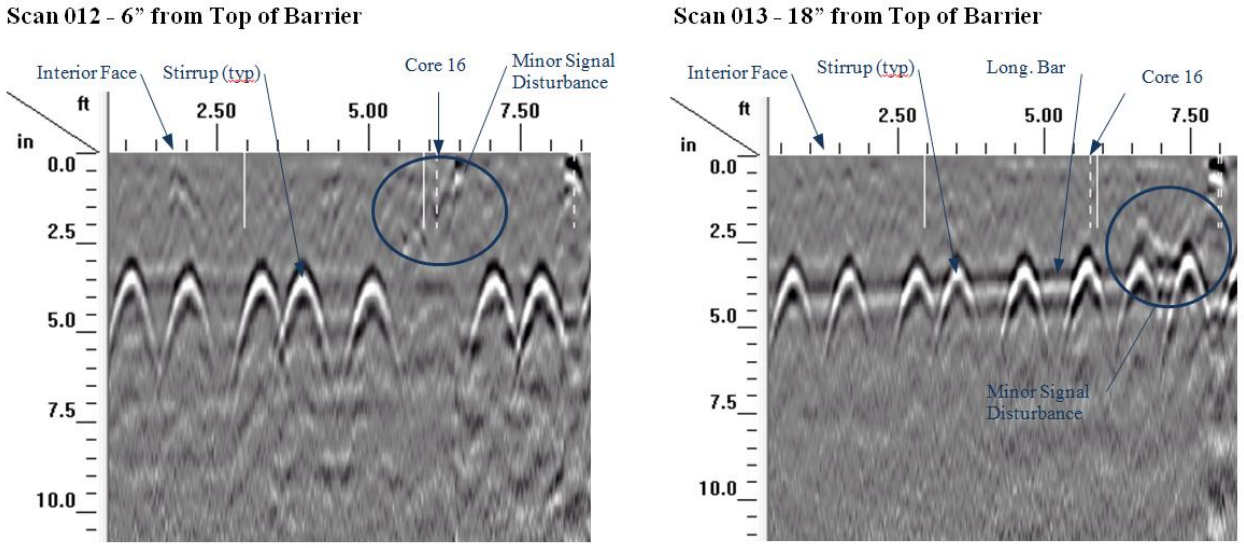

Figure 87. GPR Scan Excerpt: Scan 012, 013 collected on MRB Eastbound, south barrier, north barrier, exterior face , 8" from top of barrier. GPR Analysis Results: Minor internal signal disturbances near IDOT Core No. 16 and east of joint.

3.1.5.7. Advantages and Limitations of Test Method

The following summarizes the results and conclusions of trial-testing of the GPR test method for concrete flaw detection:

Capabilities and Advantages:

- Accurate measurement of the location and approximate depth of reinforcing bars, conduit, and other embedded elements with wave speed calibration and adequate spacing of targets.
- Areas of relative low concrete cover can be identified shortly after production.
- Internal voids measuring 3-inches wide and greater, and situated at depths of up to 8-inches from the lateral surface of the barrier wall can be detected.
- Individual internal voids measuring >1-inch diameter, continuous voids along longitudinal bars measuring ≥1/2-inch wide, and interconnected voids in concrete measuring ≥1/4-inch thick can be detected if these voids are situated near near-surface reinforcing or shallower. Larger internal flaws and voids positioned deeper within the barrier may be detectable depending on flaw type and severity.
- Signal reflections from embedded voids are detected at the approximate depth of the void (measured from the scanned surface) and are characterized by negative signal reflections (signal phase reversal occurs), which can be distinguished from embedded reinforcing. Additionally, reflections from deeper within the barrier are affected or obscured by the presence of voids or other flaws.

- Embedded honeycomb which include low-density material and severe paste-voiding (air-filled or water-filled) can typically be detected. Signal reflections do not appear as defined reflection layers (as compared to embedded voids). However, minor signal reflections are typically apparent and reflections from the back lateral surface of the barrier wall are affected or obscured. Embedded honeycomb that consist of higher density material are undetectable.
- Can be used to assess internal conditions in areas that are visibly deteriorated, including areas of surface scaling, surface cracking, and freeze-thaw deterioration.
- Higher frequency antennas, specifically 2.6 GHz, provide higher resolution and more accurate depth measurement for the detection of both embedded reinforcing and embedded voids.
- Ideal signal post-processing consists of position correction, a series of finite impulse response (FIR) filters (if necessary), and velocity migration.
- Data collection is efficient, continuous scans can be collected at high collection rates depending on required scan resolution.
- Data collection requires access to only one side of the barrier wall; however collection from both sides provides additional information.

Limitations:

- Data is collected along individual scans and standard practice is to assume that flaws and embedded items positioned outside of the scan are not detected. Therefore, detection of flaws throughout the barrier requires multiple scans at various heights or locations or the use of a multiple antenna array.
- Reinforcing bars can mask the detection of flaws positioned behind the reinforcing. Procedures should include collecting longitudinal scans between longitudinal reinforcing bars.
- Small individual voids (less than 1-inch in diameter), voids around reinforcing bars measuring ≤1/2-inches wide, moderate-density honeycomb flaws, minor consolidation issues, and internal cracking generally cannot be detected.
- Planar cracking measuring >1/4-inches wide or which contain moisture may be detected; however, thinner planar cracking and out-of-place cracking generally cannot be detected.
- Signal attenuation is severe in early-age concrete. Testing at 48 hours indicated that flaw detection was limited beyond nearest reinforcing layer.

3.1.6. Infrared Thermography (IR)

3.1.6.1. Mock-up Testing Procedures

Trial testing of the laboratory mock-up barrier wall consisted of capturing digital infrared images and optical images of the interior face of the wall under a variety of ambient conditions. The testing was designed to assess the effect of thermal gradient variation on the testing results. Testing was primarily performed outside under various ambient heating and cooling conditions. However, some additional testing was performed in an indoor environment. Exterior testing included a full day of data collection with the camera set up to capture one infrared image every 30 minutes, including the morning heating cycle (provided by direct sunlight) and the evening cooling cycle. Comprehensive testing was performed in which the barrier surface was monitored over a heating period of one hour with images captured every 15 seconds. Additionally, testing was performed during which the interior surface of the mock-up barrier was actively heated at selected locations using halogen lamps in order to assess whether larger thermal gradients could be useful in identifying embedded flaws.

Trial testing of the IR method for the evaluation of early-age concrete was performed on the Killian test samples 48 hours after construction. The IR testing did not identify any internal flaws within the test

samples. Additional study of early-age IR testing to determine if active heat of hydration can provide for better testing results is necessary.

3.1.6.2. Phase A Field Testing Procedures

Phase A field testing of IR was performed on the eastbound and westbound barrier walls of the Blair Bridge (US30 over Missouri River) and the southbound barrier wall of US Route 218 over Hinkle Creek. Digital infrared thermogram images were collected at various stations along the portions of the barrier walls selected for in-depth testing and under various ambient conditions during the day of testing.

The following trial testing was performed at each field testing location:

US 30, Westbound Barrier.

Infrared thermogram images collected at 15 minute intervals at Sta. 785 during heating cycle

Iowa 150, Northbound Barrier.

Infrared thermogram images collected at 5-foot spacing, Sta. 145 to Sta. 160, during heating cycle

US 218, Southbound Barrier.

Infrared thermogram images of interior face collected at 5-foot spacing, full barrier length, collected after transition from direct sunlight to shade (ambient cooling cycle).

3.1.6.3. Phase B Field Testing Procedures

IR assessment was performed on each of the selected barrier walls during Phase B field testing. Optical photographs and IR images of the interior lateral face of each barrier wall were typically collected at a spacing of 10 feet over the entire length of the barrier. Testing was performed at various times during the day to provide for optimal temperature variation between the ambient and the barrier. A summary of the IR thermography performed at each location is provided in Table 7. The optical images and post-processed IR thermograms were stitched together using photo editing software to provide continuous images of each selected barrier wall. The full images of the barrier walls were provided in the appendices of the IDOT report.

3.1.6.4. Testing and Analysis Results: Laboratory and Field Mock-ups

Optical and thermogram images of the mock-up barrier wall and the barriers tested in the field were analyzed to determine whether known internal defects could be detected using infrared thermography. An optical image of the interior face of the mock-up barrier wall is shown in Figure 88. Figure 89 provides a corresponding infrared thermogram during an ambient heating cycle in an exterior environment. In this example, a wide temperature range was selected and the resultant thermogram clearly indicates the presence of embedded void panel V1, which is positioned approximately 1-1/8 inches from the front face of the barrier. Post-processing of the collected images, including attempts to enhance the images at other areas with known internal defects, showed only near surface defects were detected. Similar testing at various times during the ambient heating cycle and using various temperature range settings had similar results. Embedded void panels positioned at 4 inches and 6-3/16 inches and embedded honeycomb defects D1 through D3 were undetectable using infrared thermography.

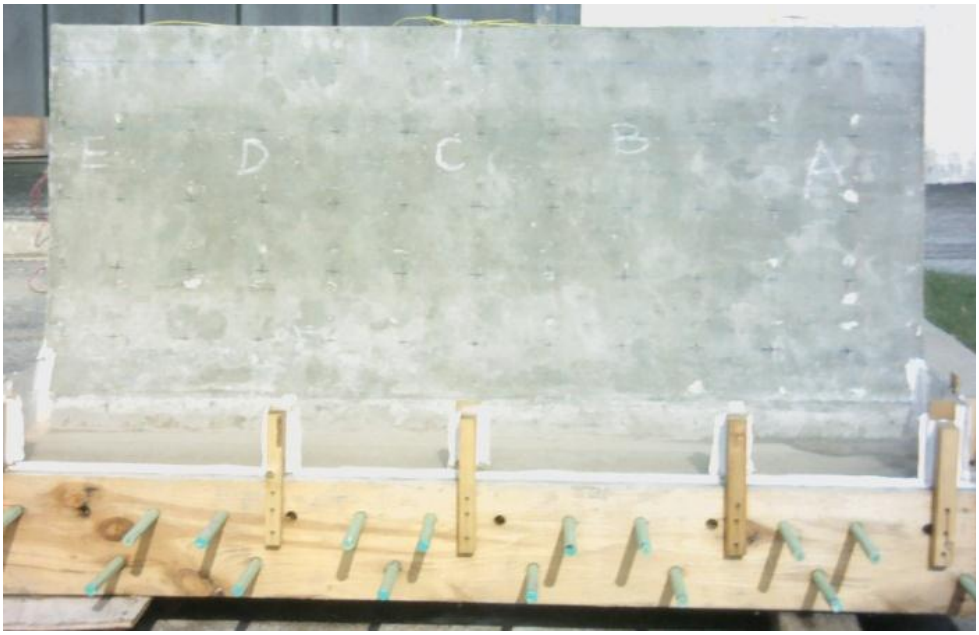

Figure 88. View of interior face of the mock-up barrier wall prior to exterior infrared thermography testing.

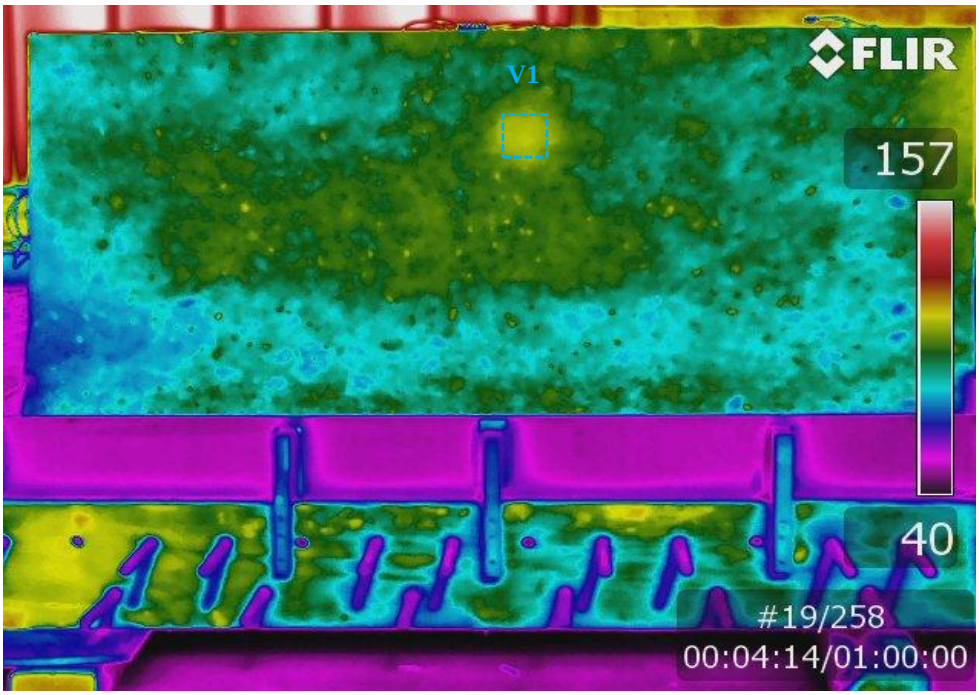

Figure 89. Sample IR thermogram image collected during an ambient heating cycle.

3.1.6.5. Testing and Analysis Results: Phase A Field Testing

Phase A field testing of the IR method performed at each of the three selected bridges provided some information regarding the feasibility of testing in-situ barrier walls. Figure 90 and Figure 91 provide sample thermogram images collected on the eastbound barrier of Blair Bridge (US30 over the Missouri River) and the northbound barrier wall of Iowa 150 over the Cedar River during an ambient heating cycle, respectively. The images indicate that natural variation in the surface temperatures over the height of the wall due to varying exposure to sunlight is significant and must be accounted or adjusted for during data collection and analysis. Vertical cracking in the barrier wall can be identified using the IR method. Although the cracking was apparent on the barrier wall surface, the distress was more easily identified in thermogram images compared with optical images of the barrier walls, especially when moisture was present within the cracks. Areas of moisture staining and repair patches at the barrier surfaces were identifiable in the thermogram images due to differences in surface emissivity, which detracted from the ability to identify internal defects at these locations. Figure 92 provides a close-up thermogram image of cracking and freeze-thaw damage at a selected location along the top of the northbound barrier wall of Iowa 150 over the Cedar River. This distress, observed at locations coinciding with previously installed light pole or railing bases, was found to result in higher thermal gradients during the ambient heating cycles and was therefore identifiable using the IR method.

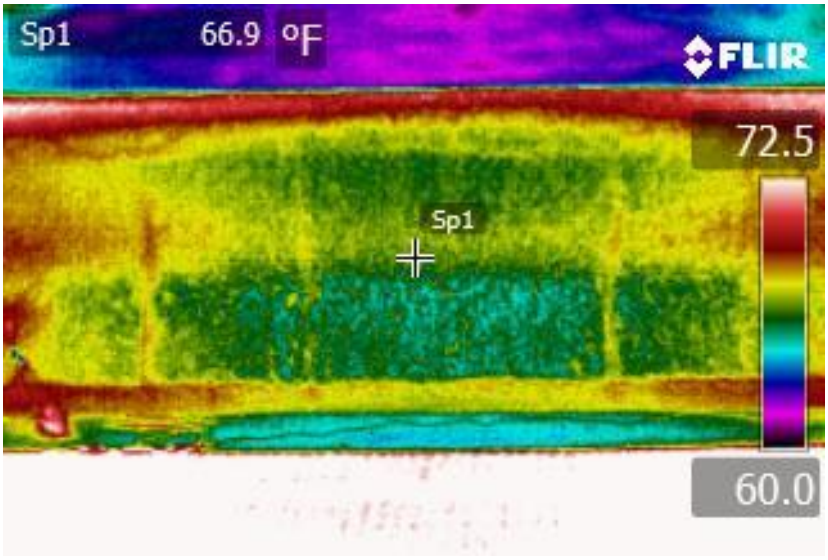

Figure 90. Sample IR thermogram image collected on the eastbound barrier of Blair Bridge (US30 over Missouri River) during an ambient heating cycle.

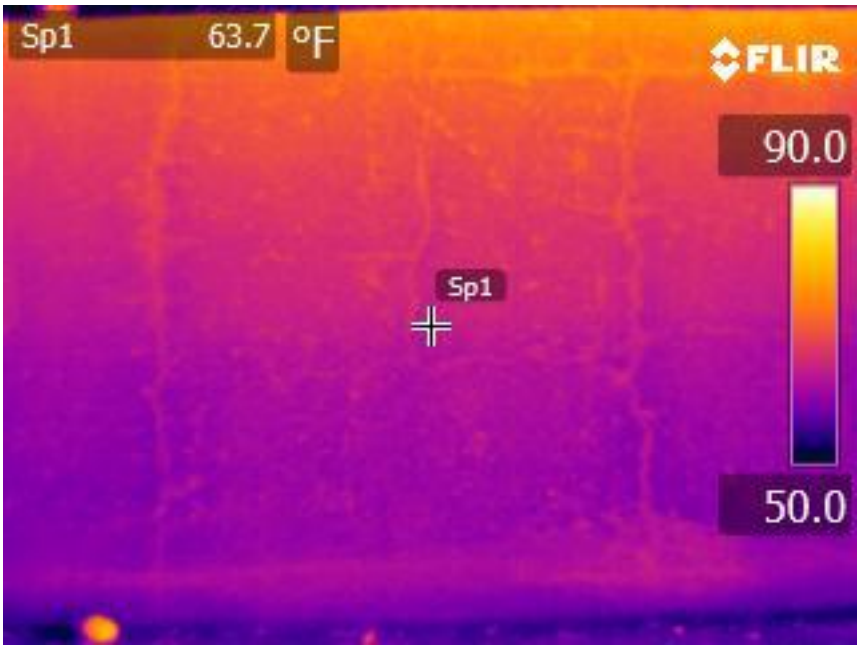

Figure 91. Sample IR thermogram image collected on the northbound barrier of Iowa 150 over the Cedar River during an ambient heating cycle.

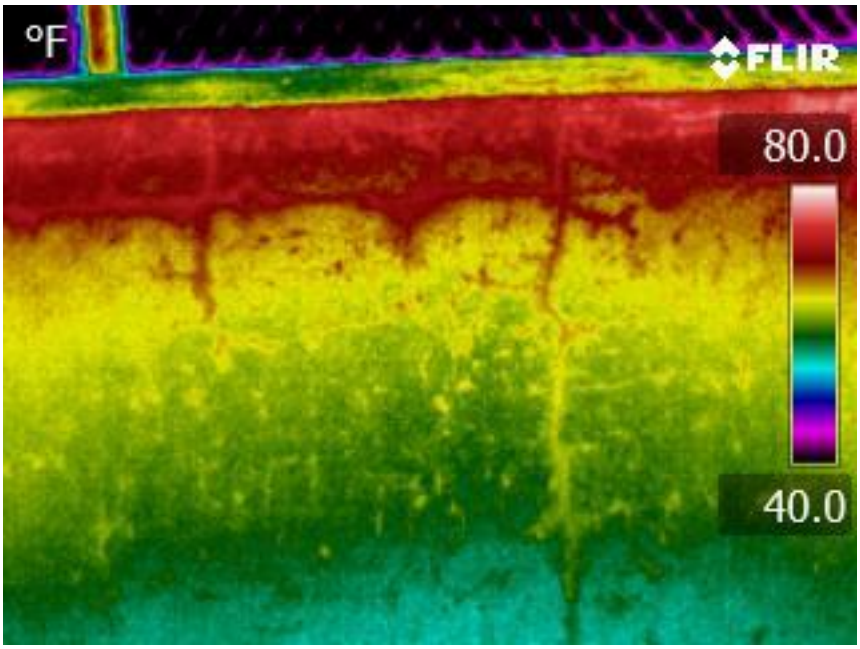

Figure 92. Close-up IR thermogram image of cracking and freeze-thaw distress collected on the northbound barrier of Iowa 150 over the Cedar River during an ambient heating cycle.

3.1.6.6. Testing and Analysis Results: Phase B Field Testing

Results of the Phase B field testing of IR thermography were presented in the appendices of the IDOT report. After careful collection of the IR data during both ambient heating and cooling cycles, all thermograms were processed to provide optimum contrast of the temperature data. Results were provided as stitched thermogram images of the interior face of each tested barrier wall. In general, IR testing did not identify any potential areas of internal concrete distress. Note that both ultrasonic (MIRA) and GPR testing identified internal flaws within each of the tested barriers—flaws, which were confirmed through exploratory coring. Therefore, internal flaws typical of slip formed or cast-in-place production are likely not detectable using the IR test method. Internal flaws may not be large enough or are not positioned close enough to the interior face of the barrier wall to be identified.

3.1.6.7. Advantages and Limitations of Test Method

The following summarizes the results and conclusions of trial-testing of the IR thermography test method for concrete flaw detection:

Capabilities and Advantages:

- Embedded voids measuring 3-inches wide and greater, and situated at depths of up to 1-1/2 inches from the lateral surface of the barrier wall can be detected by IR.
- Near surface and surface cracking can be identified in IR images. The presence of moisture within cracks can improve detection.
- Material degradation resulting in widespread surface cracking or micro-cracking (such as freeze-thaw damage) can be identified in IR images.
- Data collection is efficient. Individual thermogram images of barrier lengths of up to 10 feet, depending on available standoff distances from the barrier wall, can be collected.
- High resolution infrared video cameras can be used to provide data collection at speeds of up to 150 frames per second. Improved resolution may provide for better detection of embedded flaws.
- Testing does not require contact with the surface of the barrier wall and can be performed at considerable distances.
- Data is image-based requiring minimal interpretation. Data may be reviewed in the field. However, post-processing of thermogram images consisting of adjustment to color palettes and image contrast should be performed to provide standardized results for long lengths of barrier.
- Infrared cameras are commercially available with a wide variety of options by a number of suppliers.

Limitations:

- Natural thermal variation due to ambient heating, moisture variation, and connection to the deck results in a large thermal range within the barrier walls during field testing. This affects the ability to identify subtle temperature differences, which may be present due to embedded flaws.
- Flaw detection is limited to near-surface defects affecting surface emissivity.
- Depths of flaws cannot be determined.
- Surface emissivity is affected by color, surface roughness, moisture content, and material differences (such as repair materials) at the surfaces of the barrier wall. Variations in surface emissivity can mask or affect the identification of internal flaws.
- Radiant heating or cooling of the barrier is required for flaw detection. If relying on ambient temperature variation, optimal collection times must be determined.
- Small voids (less than 2-inches in diameter), voids around reinforcing bars, moderate-density honeycomb flaws, minor consolidation issues, and internal cracking generally cannot be detected.

- High resolution infrared cameras and video cameras are relatively expensive.

3.1.7. Radiography (X-ray)

3.1.7.1. Laboratory Mock-up Testing Procedures

Radiographic testing of the laboratory mock-up barrier wall required that the wall sample be moved to an empty parking lot, that the surrounding area be blocked off to prevent accidental exposure of radiation, and that ambient weather conditions were dry. Large vehicles were placed in the direction of the imaging to act as additional shields to further reduce the potential for accidental radiation exposure. To capture the images, access to both sides of the testing specimen was required. Radiation was applied to the interior face of the barrier. The collection screen (film) was correspondingly placed on the exterior face of the barrier wall. Due to the thickness of the barrier wall, exposure of each screen took roughly 45 minutes to set up and capture.

The screen size used measured approximately 1 foot-2 inches by 1 foot-5 inches The film sheets were developed on site in a mobile darkroom and were subsequently reviewed and retained by WJE. The top portion of the barrier wall was tested 2 screens high, which provided test results extending from top of the barrier to the top portions of the 5c1 bars. An attempt to collect radiographic images of the construction joint between the deck and the barrier wall using long exposure times was made. Due to the overall thickness of the barrier wall at the toe, the resulting images were underexposed (light in saturation). And the level of contrast was barely enough to differentiate the reinforcing steel from the concrete.

3.1.7.2. Field Testing Procedures

Due to the expense of the NDE procedure and potential risk of accidental radiation exposure to the public, field testing of radiography was not performed.

3.1.7.3. Testing and Analysis Results: Laboratory Mock-up

The images obtained from the developed radiographic screens, a sample of which is provided in Figure 93, clearly showed the location of reinforcing bars and the void panels within the tested portions of the barrier wall. The darkness of a radiographic image relates directly to the number of photons that are able to pass through the barrier wall and reach the collection screen. Correspondingly, paths that are relatively denser than surrounding paths (i.e. paths that travel through reinforcing bars) appear lighter in comparison. The transmitted intensity received by the collection screen is inversely proportional to the attenuation coefficient. This coefficient is dependent on an object's density, with values of 1 for steel, 0.3 for concrete, and 0 for air.

An image created by stitching the radiograph images of multiple screens along the length of the barrier wall (as seen from the outside face) is shown in Figure 94. It is clear from this figure that the reinforcing steel and void panels are discernible. The embedded honeycomb panels positioned within the tested areas, were not identifiable in the radiographic images. The relative high density of the honeycomb panels likely contributed to the difficulty in identifying them using radiography.

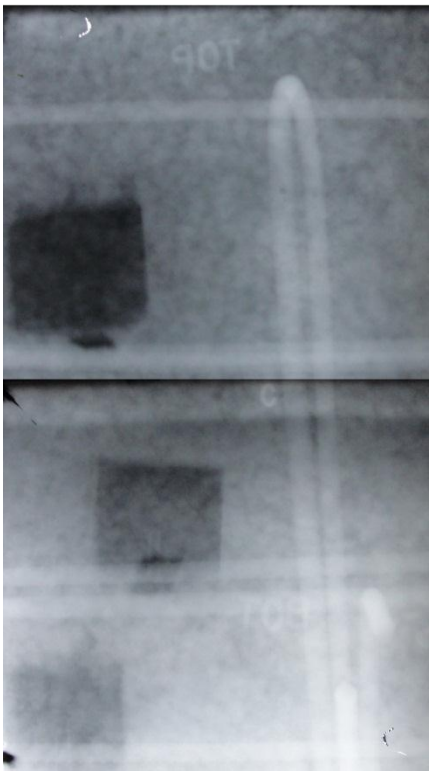

Figure 93. Developed screens from radiographic testing of the mock-up barrier wall showing reinforcing (lightly shaded lines) and void panels (dark areas) in a fairly consistent concrete matrix.

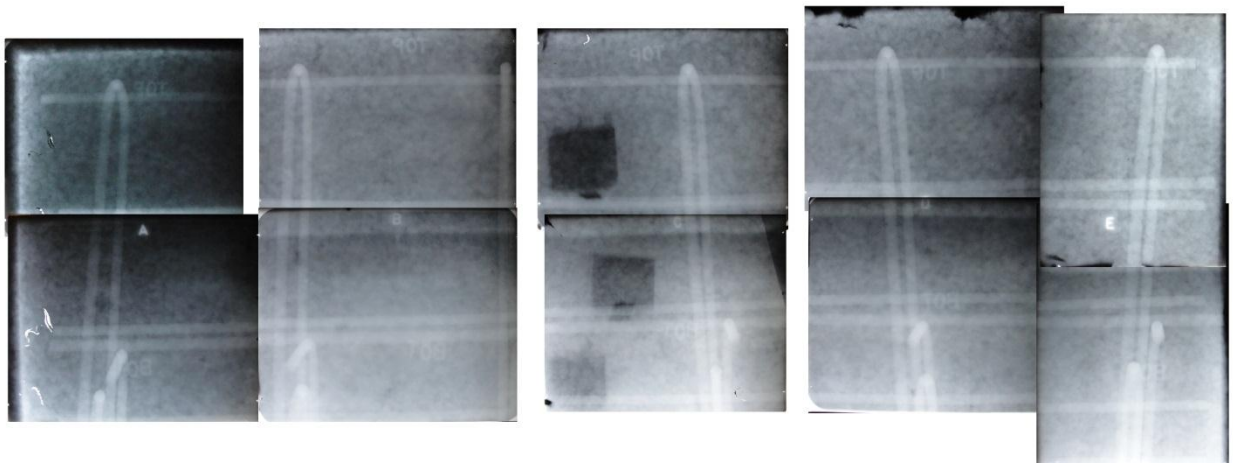

Figure 94. Stitched screens from radiographic testing of the mock-up barrier wall.

3.1.7.4. Advantages and Limitations of Test Method

The following summarizes the results and conclusions of trial-testing of the radiography (X-ray) test method for concrete flaw detection:

Capabilities and Advantages:

- Identification of in-plane locations of reinforcing bars and concrete voids (did not detect internal honeycombing).
- Identification of presence of embedded voids measuring 3-inches wide and greater and positioned at any depth. Smaller voids may be detectible. The ability to identify other flaws depends on differences in the relative density of the flaw compared with the density of the concrete substrate.
- Data is image-based requiring minimal interpretation

Limitations:

- Access to both sides of test specimen required.
- Radiation exposure times increase with thickness of specimen, resulting in relatively long testing times when compared to other test methods.
- Safe practices for handling of equipment and protection of the testing areas are required due to the hazards related to radiation.
- Depth to internal flaws is not measurable unless multiple screens are used to test at varying orientations.
- Multiple setups are required for complete mapping of the barrier wall.
- Images of toe of barrier wall are difficult to obtain due to positioning of radiation source and collection screen.
- Detection of corrosion is limited to large amounts of section loss, although this could not be evaluated by the trial methods due to the barrier geometry.
- Cost of data collection is relatively high (approximately $10,000 for 100 feet of wall, per quote from one contractor).

3.2. Detection of Corrosion-Related Distress

3.2.1. Half-cell Potential Measurement

3.2.1.1. Laboratory Mock-up Testing Procedures - Flat Slab

Half-cell potential (HCP) measurements were collected on the mock-up flat slab sample each week over a 12-week period during which cycling of chlorides through the construction joint was performed. The ends of the 10 transverse bars in the slab sample protruded from the edge of the concrete slab to allow a direct electrical connection to the bars. In addition to the HCP testing with a direct connection to the bars, "relative" HCP testing was performed between various points on the slab surface. Potentials were measured both with the transverse bars electrically connected and independent of each other as actual levels of connectivity of epoxy-coated bars in the field is expected to range between these two conditions. A summary of the HCP testing performed each week is as follows:

- HCP readings with lead connected directly to reinforcing bars and all bars electrically connected
- HCP readings with lead connected to reinforcing bar tested, but other bars not electrically connected
- Relative HCP readings between adjacent bars in the longitudinal direction, all bars connected
- Relative HCP readings in transverse direction across joint, bars not connected together

3.2.1.2. Laboratory Mock-up Testing Procedures - Barrier Wall

Half-cell potential readings were performed on the front and back side of the mock-up barrier wall sample with both single cell and rolling wheel equipment at various ages since casting. Measurement spacing with the single cell equipment was generally 12 inches by 12 inches. Measurement spacing with the rolling wheel equipment was finer, with rows spaced vertically 6 inches apart and readings obtained horizontally at 2 inch spacing.

A summary of the HCP testing performed was as follows:

- HCP readings with lead connected directly to reinforcing bars and all bars electrically connected
- HCP readings with lead connected to reinforcing bar tested, but other bars not electrically connected
- Relative HCP readings with one probe placed near construction joint at bottom of barrier and one placed in-line vertically near the top of the barrier.

3.2.1.3. Field Testing Procedures

Field trial testing was performed on the northbound and southbound walls of US 30, the northbound barrier test section of Iowa 150, and the southbound barrier of US 218. Testing was comprised of the following:

US 30, Westbound Barrier.

Equipment: single reference cell
Measurement spacing: 6 inches vertical, 14 to 18 inches horizontal (centered on vertical bars)

US 218, Southbound Barrier.

Equipment: Rolling wheel with data logger
Measurement spacing: rows 6 and 24 inches above deck, 3-inch horizontal spacing

Iowa 150, Northbound Barrier.

Equipment: Rolling wheel with data logger
Measurement spacing: rows at 8 inches above deck and top of wall, 3-inch horizontal spacing
Measurements performed on both front and back sides of wall

The electrical resistivity of the concrete was also measured along the base of the barriers at US 218 and Iowa 150. The resistivity measurements provided a rapid means to assess where the highest moisture content in the barrier concrete was present. Areas of high moisture content should correlate to areas in which corrosion risk is highest.

3.2.1.1. Testing and Analysis Results: Laboratory Mock-ups

Flat slab sample

Half-cell potential contours for the mock-up flat-slab sample at the initiation and conclusion of the 12-week chloride exposure period are shown in Figure 95. Different results were obtained when all bars were electrically connected compared to when the half-cell was connected to individual bars. In January 2011, corrosion of individual bars was not clearly indicated by HCP testing except for a couple of locations when connections were made to individual bars. In March 2011 after continued cycling with salt water, the half-cells indicated general corrosion along the construction joint, but individual bar corrosion could not be well distinguished. When connected to an individual bar, corrosion of the individual bars could be better assessed as shown in the 3-18-2011 Single Bar Connected plot. These results indicate that it may be difficult to test barriers having epoxy-coated reinforcing since the results are affected by the electrical

continuity to the bar being tested. Testing using two half-cells placed on two different areas of the slab and without making an electrical ground to the bars was inconclusive. Little variation was noted between test areas.

The mock-up slab sample was stored in the laboratory and periodically wetted over a period of 2-1/2 years. Additional half-cell potential testing and corrosion rate testing remained inconclusive in identifying individually corroding bars. Half-cell potential measurements were not able to clearly differentiate corrosion magnitudes of adjacent epoxy-coated bars; however, values did indicate that corrosion was occurring at the joint location. Potentials near the joint became more negative and ranged between -100 mV and -400 mV CSE (June 2013) and -200 mV to -440 mV CSE (October 2013). Measurements directly over bars having active corrosion did not always have more negative potentials than non-corroding bars.

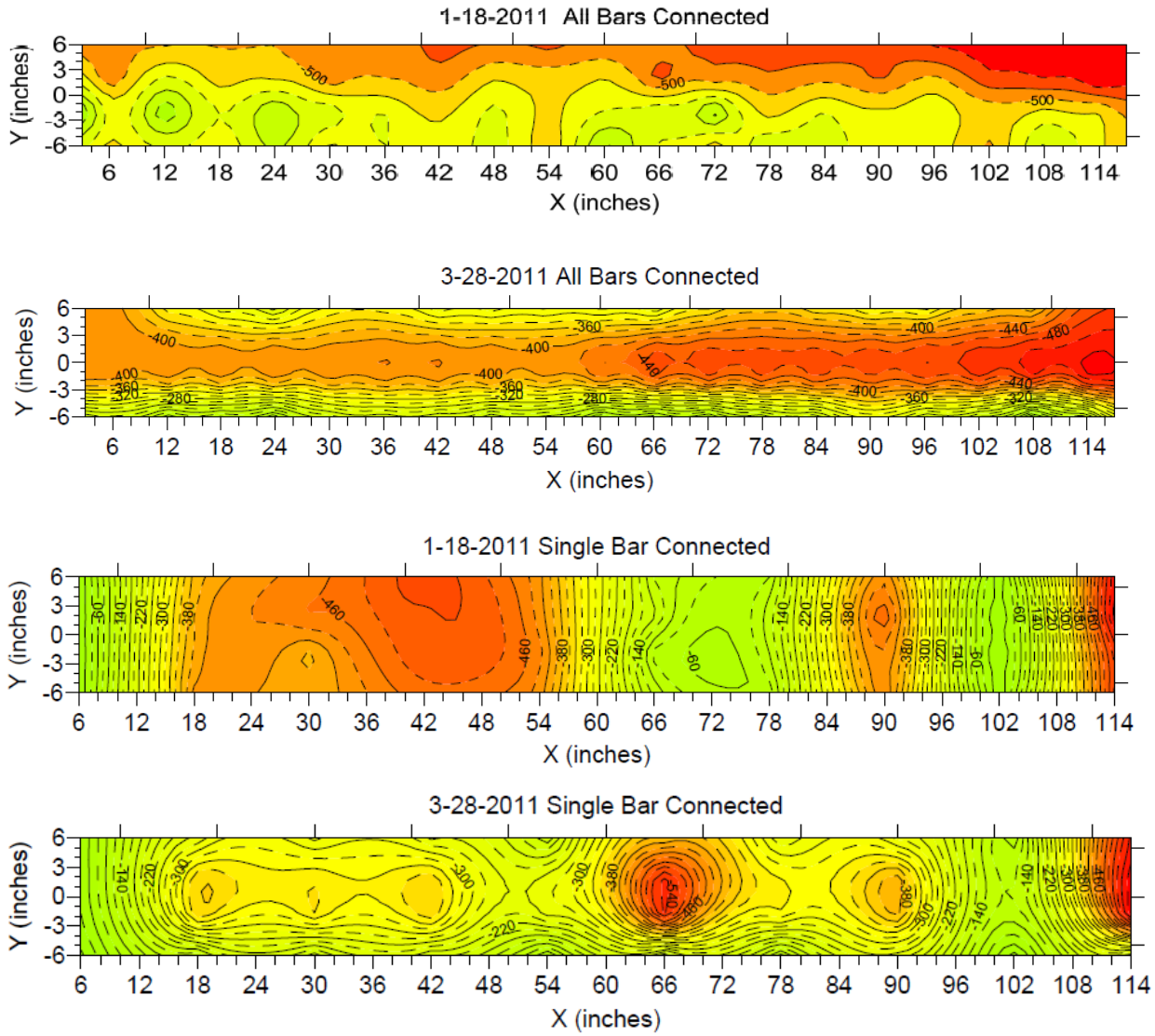

Figure 95. Half-cell potential plots of the flat slab mock-up, at the initiation and conclusion of 12 weeks of ponding.

Autopsies of the dowel bars crossing the joint were performed. The three ECR bars (1, 1', and 1") that were installed without damage showed no signs of corrosion after over 2-1/2 years of exposure and the adhesion of the epoxy coating to the bars was excellent. This indicates that ECR can be effective in preventing corrosion if it is installed without damage to the coating.

Bar 2 had the epoxy removed from a 2-inch section of the bar at the joint. It showed minor-to-moderate corrosion staining at the joint; however, some areas of the exposed bare steel were un-corroded, indicating passivation from the concrete contact. Coating adhesion next to the bare area was good and corrosion was limited to only some of the intentionally bare area.

Epoxy coated bars that had the epoxy removed at the joint and were pre-corroded for 6 weeks (Bar 3) or 8 weeks (Bars 4 and 4') showed active corrosion and heavy rust scale. Corrosion undercut the exposed edges of the epoxy film and pitting beneath the coating occurred. Corrosion stains were present along the bar imprint in the concrete surrounding the bare area. While some undercutting and corrosion occurred beneath the coating immediately adjacent to the intentionally bare area, away from the edge the coating adhesion was good.

The bars that had the epoxy removed at the joint area, were milled and pre-corroded for 8 weeks (Bars 5, 6 and 6') showed minor-to-moderate rust staining adjacent to the bare area. For Bar 5, the bond of the coating on either side of the bare area was good with only minor undercutting. Bars 6 and 6' had corrosion of the bare area and areas adjacent to the bare area beneath the coating. The coating had some loss of adhesion next to the bare area, but away from the bare area coating adhesion remained good.

In summary, the ECR bars installed without intentional damage had no corrosion and retained excellent coating adhesion. Bars with coating removed exhibited corrosion of the bar, but the adjacent areas retained good adhesion and little underfilm corrosion. Removing the coating and pre-corroding the bars prior to placing them in the concrete caused more aggressive underfilm corrosion adjacent to the intentionally bare area and some underfilm pitting corrosion.

Barrier mock-up

For the mock-up barrier wall sample, half-cell potentials contours of the front and back sides are shown in Figure 96 with all bars being electrically connected to the half-cell. At the time measurements were taken, the concrete had been allowed to dry in ambient indoor conditions for a number of months. Overall, the plots show electronegative areas near the base of the wall (along the construction joint) where saltwater was ponded. These negative potentials may be indicative of corrosion occurring in the bars along that zone. No distinction could be identified between the different types of damage of the bars in the contour maps.

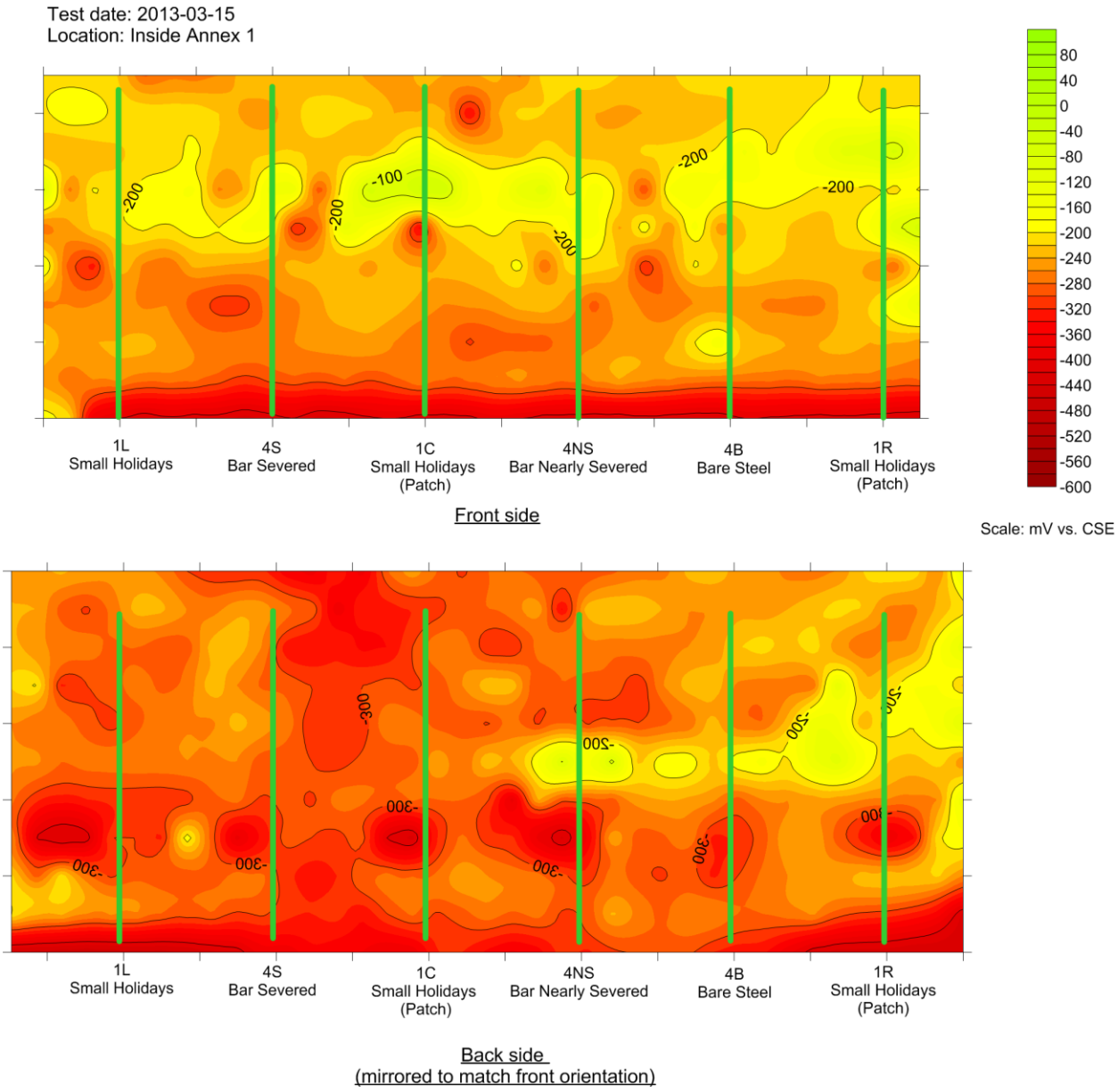

Figure 96. Half-cell potential contours of the barrier wall mock-up. Locations of embedded bars and their intentional defects are overlaid on the plots.

3.2.1.1. Testing and Analysis Results: Field Testing

Field trials indicated that the half-cell potential technique was effective at identifying corrosion locations in uncoated barrier reinforcing (dowels). For epoxy-coated reinforced dowel assessment, laboratory and field testing indicated half-cell potential measurements may indicate if general corrosion is occurring, but may not be able to locate individual bars having corrosion.

Results of the field testing, as shown in Figure 97, varied widely between the three bridges. For US 30, the epoxy-coating on the bars appeared to result in more negative potentials. This may reflect that the bars in the barrier wall were not well electrically connected. For the two bridges with uncoated bars (US 218 and Iowa 150), the contour plots show both anodic (more negative) and cathodic (more positive) zones along the length of the wall. The concrete electrical resistivity varied along the length of the barriers and ranged from about 45 k-ohms to 445 k-ohms. Areas of low resistivity are indicative of water or deicer saturated areas that would be more prone to corrosive conditions. As indicated in the figure, an inspection opening performed on US 218 located a corroding bar at one of the anodic zones on the plot. The half-cell survey results shown for Iowa 150 were collected at the same location as the shear wave tomography scan shown in Figure 54. The location of internal flaws identified by shear wave tomography correlated with an anodic region. This may indicate that the internal flaws have resulted in faster penetration of chloride and subsequent reinforcing steel corrosion. The half-cell potential technique was able to identify active corrosion of dowel bars in barriers having black reinforcing steel. However, barriers having epoxy-coated reinforcing did not show significant distinctions in corrosion activity.

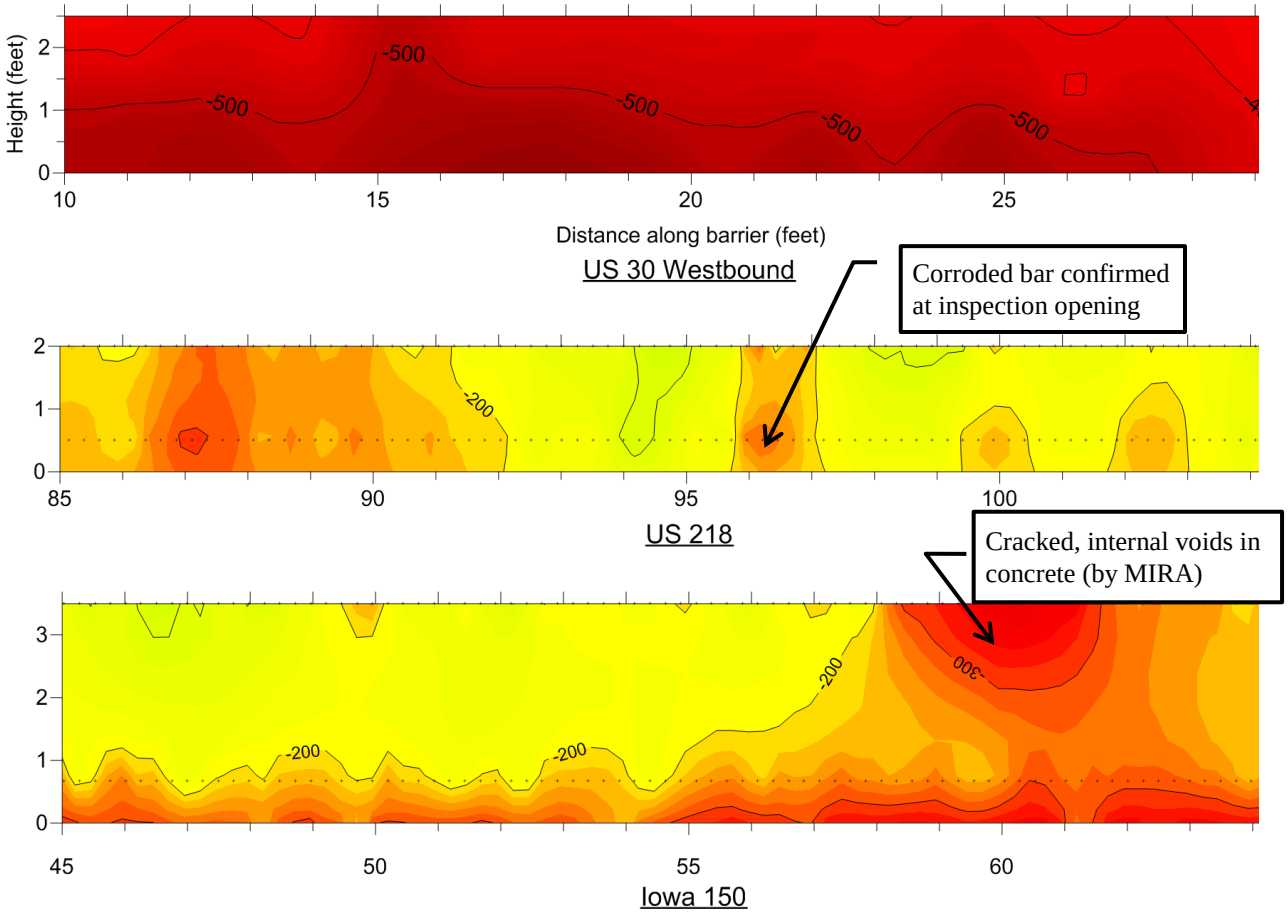

Figure 97. Selected portions of half-cell potential contour plots from field trials at three bridge barrier walls. All plots are from the front side of the barriers. Note that US 30 had epoxy-coated bars, but US 218 and Iowa 150 had uncoated bars. All maps are plotted with the same scale. The location selected for Iowa 150 is the same section shown for the MIRA results in Figure 54.

3.2.1.2. Advantages and Limitations of Test Method

The following summarizes the results and conclusions of trial-testing of the half-cell potential measurement test method for dowel corrosion assessment:

Advantages:

- Rapid technique that can evaluate long lengths of barrier quickly.
- Requires access to only one side of the barrier wall.
- Provides the location of black bars undergoing active corrosion.
- Automated data collection can be done using rolling half-cell units.

Limitations:

- Does not provide information on the extent of corrosion or bar section loss.
- Requires an electrical ground to a bar in each independent barrier section.
- Was not effective on barriers with epoxy-coated reinforcing.
- Cannot be used in freezing weather.
- May not be able to distinguish corrosion of individual bars if ponded water is against barrier surface.

3.2.2. Corrosion Rate Measurement

3.2.2.1. Laboratory Mock-up Testing Procedures

Corrosion rate measurement is an extension of the half-cell potential technique and provides additional information on the condition of the reinforcing steel. Corrosion rate values provide a snap-shot of the corrosion condition of a section of reinforcing bar at the time of measurement. Like half-cell readings, corrosion rate measurement does not provide an indication of the amount of bar section loss that has occurred. It is a point by point measurement, and testing must be done directly over the reinforcing bar being measured. Like half-cell measurements, an electrical ground to the reinforcing steel bar is needed.

Linear polarization testing was done on the laboratory samples but was not used on the field barriers. A custom probe would be needed to make this technique practical for field use. The GalvaPulse© unit from Germann Instruments, based on the galvanostatic pulse technique, was used. Due to the general dry condition of the test barriers, a pulse duration of 10 seconds and a current of 400 microamps were used. Each measurement took approximately 60 to 90 seconds to perform, not including steel ground connection and set-up.

3.2.2.2. Field Testing Procedures

Corrosion rate testing was not performed on the field barriers since a custom probe would need to be constructed and the time required for data collection makes the technique ill-suited for widespread application at this time.

3.2.2.3. Findings and Analysis Results

Corrosion rate measurement on the laboratory test slabs was able to measure differences between individual bar samples. However, dry concrete conditions made measurements less steady and often data did not converge. When concrete was mostly saturated, readings were typically obtained.

In the flat slab sample, the measured corrosion rates varied significantly. However, similar corrosion rates were measured on the epoxy bars installed intact (11.5 to 34.5 microamps per sq. cm) and the pre-

damaged and corroded bars (10 to 42 microamps per sq. cm). Stable readings were often not obtained during the measurements. The readings varied somewhat depending on if the bars were all connected together or if just an individual bar was connected to the probe.

Corrosion rate testing of the barrier mockup was not successful when the probe was placed directly on the vertical face of the barrier. This may be due to the high electrical resistivity of the concrete and epoxy coated reinforcing. Readings could be obtained when the probe was place on the deck in front of the barrier within the ponding well. However, test results were unexpected as the bars with small holiday damage had the highest corrosion rates (2, 5, and 11 microamps per sq. cm) compared with the pre-damaged and corroded bars (1 to 2 microamps per sq. cm).

3.2.2.4. Advantages and Limitations of Test Method

The following summarizes the results and conclusions of trial-testing of the corrosion rate measurement test method for dowel corrosion assessment:

Advantages:

- Should provide an indication of the corrosion rate at a particular bar location at the time of measurement.
- Requires access to only one side of the barrier wall.

Limitations:

- Does not provide information on the extent of corrosion or bar section loss in the past.
- Requires a bar electrical ground to each independent barrier section.
- Test time is several minutes at each test location.
- Barrier geometry makes it difficult to take measurements. A custom probe is necessary for routine field barrier assessment.
- Results were not considered accurate on the laboratory slab and barrier containing epoxy-coated reinforcing. Testing on barriers with black bars may improve results.
- Cannot be used in freezing weather.
- May not be accurate if ponded water is against barrier surface.
- Testing is performed at individual test locations, requiring each test bar to be located prior to testing.
- Amount of data collection is limited and is affected by ambient conditions at the time of testing as well as concrete moisture and carbonation.

3.2.3. Impulse-Response Structural Mobility Testing

3.2.3.1. Laboratory Mock-up Testing

Laboratory testing comprised of the collection of impulse-response measurements at selected test spacing along the length of the mock-up barrier near the base of the front face of the wall. Due to the limited size of the mock-up wall segment, testing was performed at a 6-inch test spacing. However, field testing would likely not require this tight of a spacing. Testing was generally performed along the middle of the angled face of the wall. Results were plotted and analyzed to determine the effectiveness of the test method in identifying the varying dowel conditions.

3.2.3.2. Field Testing Procedures

Field testing of impulse-response was performed on the southbound barrier wall of Route 218 over Hinkle Creek. Testing comprised of the collection of impulse-response measurements at a test spacing of 1 foot on center along the length of the barrier wall. Testing was performed on the vertical interior face of the wall at the center of the thickened section near the base of the barrier.

The following trial testing was performed at each field testing location:

US 218, Southbound Barrier.

Equipment: s'MASH Impulse-Response system (Germann Instruments)
Measurement spacing: 1 row of 131 measurements, 1-foot horizontal spacing

3.2.3.3. Findings and Analysis Results

Results of impulse-response trial testing performed on the mock-up barrier wall highlighted several limitations of the test method in the assessment of short lengths and test samples of the barrier wall. Impulse-response is foremost a test of structural mobility and therefore is highly influenced by the natural variation in stiffness of the tested element. Element size and support conditions have a more influential effect on test results relative to internal conditions. Relatively small or short test samples will therefore yield significantly different test results compared with full-scale elements regardless of the similarities in the internal flaws present. This was evident in the results of the testing of the mock-up barrier wall, which showed high mobility results at either end of the test sample compared to the interior portion of the wall. Additionally, no significant increase in mobility was detected at the locations of the intentionally severed dowels or those at which the cross section was reduced.

Impulse-response testing performed on the southbound barrier of US 218 provided a more useful assessment of the testing method. Testing was performed laterally at 131 test locations along the base of the barrier wall. Although testing requires individual tests to be performed at each location, data collection was relatively fast and the entire length of the barrier was evaluated in less than 1 hour. Average mobility was found to be the most appropriate component calculation for evaluation of corrosion-related dowel deterioration. A plot of average mobility along the length of the barrier wall is shown in Figure 99. There were several locations where average mobility readings were elevated, indicating that the lateral response of the barrier wall from the imparted impact was higher and may indicate damaged or severed dowels. An inspection opening was made at the peak measured response at test location 75. The dowel exposed at this location was moderately corroded with some section loss observed. Note that surface conditions at the joint were not visible, and additional inspection openings were difficult at this barrier due to the recessed joint design and presence of a deck overlay. More testing and correlation is required to determine the extent and severity of corrosion-related damage in the dowels necessary to be detectable by the impulse-response method for various barrier wall designs.

Figure 98. View of the interior face of the southbound barrier wall of US 218, the s'MASH impulse response system, and the approximate impulse-response test locations.

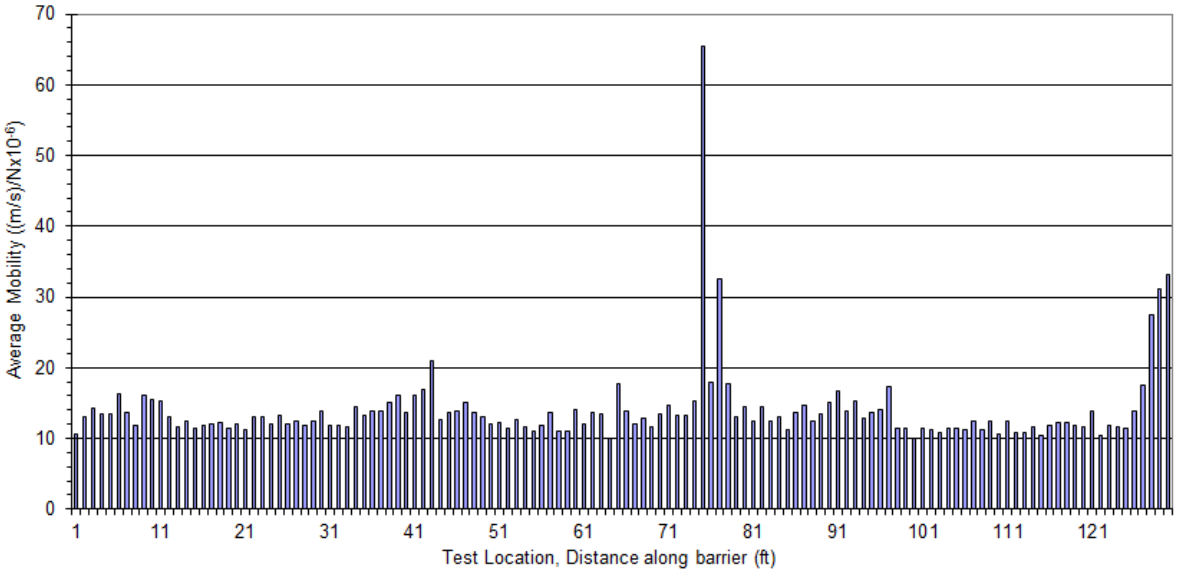

Figure 99. Plot of average mobility obtained from impulse-response testing along the length of the southbound barrier wall of US 218.

3.2.3.4. Advantages and Limitations of Test Method

The following summarizes the results and conclusions of trial-testing of the impulse-response test method for dowel corrosion assessment:

Advantages:

- Possible identification of large areas where multiple dowels have been severed by corrosion.
- Possible identification of internal planar cracking delamination and debonding of patch repairs
- Requires access to one side of the barrier wall
- Multiple tests performed at each test location ensured repeatability of data
- Mobility assessment may be useful in evaluating connection of barrier wall to slab, integrity of dowels (may be limited to location of severed dowels)

Limitations:

- Will not detect a mobility change until several dowels are severed by corrosion. Cannot identify bar section loss.
- Depth to internal defects cannot be determined.
- Dowel loss or flaw size needs to be large enough to affect overall mobility of barrier and may not be suitable for detecting typical production-related concrete flaws.
- Testing is performed at individual test locations, requiring setup of testing grids on the exterior face of the barriers.
- Experienced equipment operators are needed.

4. DISCUSSION

4.1. Internal Flaw Detection

The ability of NDE testing to identify internal, production-related flaws in slip formed barriers depends on a number of variables, including ambient conditions, the type and severity of internal flaws present, the presence and severity of visible distress, and the specific advantages and limitations of each testing method. Of the NDE methods used during this assessment, GPR proved to be the most effective and versatile testing method. A summary of the flaws observed during this assessment and the NDE methods that are effective in detecting each is provided in Table 9.

Deterioration observed during visual assessment of the barriers, namely cracking, freeze-thaw deterioration, and corrosion staining, indicates the presence of possible internal defects. Ultrasonic-based testing methods, which rely on the propagation and reflection of stress waves, are typically ineffective at evaluating internal conditions in visibly distressed areas, especially if widespread surface cracking is present. Conversely, although affected by the presence of surface cracking and moisture, GPR testing can be effective at identifying internal conditions even in visibly distressed areas.

Testing of the mockup barrier sample showed infrared thermography to be effective at identifying relatively large internal voids or delamination situated near the tested surface. However, field testing indicated that the IR test method was ineffective at identifying the small-scale internal flaws typical of slip formed construction method. Internal flaws were typically positioned too deep within the existing barriers or were too small to detect. Additionally, use of the IR method requires ideal ambient conditions and requires that the barrier be experiencing an active heating or cooling cycle, inhibiting testing times. It is possible that the heat of hydration present shortly after production would provide ideal conditions for near-surface flaw detection using IR; however, this condition was not evaluated during this assessment.

The GPR testing method was found to be an effective and efficient method for evaluating reinforcing placement and for the detection of some slip formed production-related flaws. GPR scans can be collected and analyzed relatively quickly and testing can be performed shortly after production to identify areas of low cover or other variations in reinforcing placement. Individual internal voids measuring >1-inch diameter, continuous voids along longitudinal bars measuring ≥1/2-inch wide, moderate-to-severe consolidation issues can be detected by GPR if flaws are situated near near-surface reinforcing or shallower. Larger internal flaws and voids positioned deeper within the barrier may be detectable depending on flaw type and severity. GPR signal reflections from internal voids are detected at the approximate depth of the void (measured from the scanned surface) and are characterized by negative signal reflections, which can be distinguished from embedded reinforcing.

Ultrasonic testing method, specifically impact echo (IE), ultrasonic pulse velocity (UPV), and shear wave ultrasonic tomography (MIRA) were all found to be effective at identifying large voids within barriers. IE and UPV are point-based ultrasonic testing methods, and therefore data collection is time-consuming. Typically, only larger defects coincident with an individual test point are detectable. MIRA shear wave tomography is also a point-based testing method. However larger local areas are measured simultaneously, and the method provides for full coverage of the test area through use of a testing grid and the 3-D tomographic imaging capability. MIRA was found to be an effective method for identifying moderate-to-severe consolidation issues situated near near-surface reinforcing or shallower, planar cracking at or within the reinforcing cage, and larger internal concrete voids (>3-inch diameter).

Additionally, MIRA can detect embedded ducts and conduit and provide a measurement of cage placement. MIRA testing was not an effective method for the detection of internal flaws typical of slip formed production methods, including small internal voids and continuous voids around reinforcing bars. Signal reflections from embedded reinforcing are typically indistinguishable from internal flaws and assessment of internal conditions adjacent to and behind reinforcing is limited. Improvements in signal resolution and signal processing capabilities may provide for more effective ultrasonic testing in the future.

Radiography (X-ray) was found to be an effective method for identifying internal flaws through most of the full thickness of the barrier. However, X-ray is likely too expensive, time consuming, and environmentally sensitive to be practically applied for routine barrier assessment.

A combination of techniques may be best suited for barrier evaluation. Visual condition surveys can identify cracking or consolidation issues resulting from slip formed production problems or identify the extent of freeze-thaw or material deterioration present in existing barriers. Longitudinal GPR scans can be collected quickly on the lateral surfaces or top surface of a barrier and can provide useful information on reinforcing location and freeze-thaw and other degradation cracking. Additionally, GPR surveying was determined to be the most efficient and accurate approach for identifying a range of internal production-related flaws, including interconnected voids within the concrete, voiding around reinforcing resulting from consolidation issues or cage displacement during production, and wide internal cracking. Despite some of the limitations identified, MIRA tomography testing remains a viable testing approach to investigate limited areas at suspect locations in order to better identify the extent and severity of voided areas. Regardless of the nondestructive testing approach used, exploratory coring remains the most effective method for classifying the specific internal defect present at suspect locations.

4.2. Detecting Dowel Bar Corrosion

The study indicated that half-cell potential measurements provide the most accurate identification of corrosion-related distress. Identification of corroded dowel bars at barrier construction joints is practical using a rolling half-cell unit when the barrier is built using black reinforcing steel. A simple ground should be made to the barrier section and the rolling half-cell can be used to quickly traverse the bottom edge of the barrier. Corroding black bar dowels can be quickly identified through field analysis of the testing results. Field and laboratory tests of epoxy-coated dowels were inconclusive, and further testing is required. Measuring the concrete electrical resistivity on the barrier surface in the black bar barriers showed a wide range of values and can provide useful information for locating areas of possible corrosion. Low resistivity measurements are indicative of water or deicer saturated areas that would be more prone to corrosive conditions. Visual inspection of the backside of the barrier can sometimes show corrosion staining at dowel locations, providing further evidence of corrosion related distress. None of the techniques were able to identify the amount of section loss of the reinforcing. However, Impulse-Response structural mobility testing may be able to identify sections of barrier having a series of multiple severed dowels. Visual inspection and rolling half-cell testing is a reasonable procedure for assessment of dowel bar corrosion in barriers with uncoated reinforcing steel.

5. CONCLUSIONS AND RECOMMENDED NDE METHODS

An evaluation of available NDE techniques was carried out to assess each technique's capability to identify, characterize, and locate internal flaws and dowel bar corrosion in concrete barrier walls. Laboratory mock-ups were used to establish testing procedures and examine the effectiveness of the technology. Concrete barriers on three bridges identified by IaDOT were examined using a range of techniques. Additional field testing for the assessment of internal concrete flaws using the most promising NDE techniques was completed on four bridges identified by IDOT. Based on the laboratory and field testing, each NDE technique was judged on its capabilities, Table 9 and Table 10 provide a summary of each NDE technique's capabilities with respect to internal flaw detection and dowel bar corrosion, respectively.

5.1. Nondestructive Evaluation Guidelines

The following guidelines have been developed for the preliminary assessment of barrier walls:

GUIDELINES FOR PRELIMINARY BARRIER WALL ASSESSMENT

The following provides guidelines for preliminary assessment of cast-in-place barrier walls for internal defects and reinforcing corrosion. The purpose of these guidelines is to assist bridge owners in the selection of suitable NDE methods for detecting and evaluating specific conditions related to concrete distress and dowel bar corrosion distress of in-place barriers. These guidelines were developed based on laboratory and trial field testing of barrier walls constructed per the standard designs of the IaDOT and IDOT.

The following methods may be useful in identifying barrier distress and reinforcing corrosion. The recommended procedures begin with overall scanning and inspection, followed by more in-depth NDE, and finally verification by inspection openings or coring.

Detection of Slip Formed Concrete Distress

Complete the following steps:

1. ***Visual Assessment***
   Applicable Reference Standards/Guidelines: ACI 201.1R, ACI 228.2R, SEI/ASCE 11-99
   Coverage: All accessible surfaces
   Perform and document visible condition of accessible surface of the barrier wall. Specific visible distress noted should include horizontal and vertical cracking, material deterioration (most notably freeze-thaw damage), incomplete consolidation, shadowing of internal reinforcing steel, and near-surface irregularities (voids, bugholes, streaking), and moisture staining and efflorescence. Also note previous repair areas and repair conditions.

2. ***Infrared Thermography (IR) Survey***
   Applicable Reference Standards/Guidelines: ACI 228.2R, ASTM D4788
   Coverage: All accessible vertical surfaces
   Perform an infrared thermography survey of accessible vertical surfaces of the barrier wall by collecting thermogram images at individual stations or as continuous video. IR surveys provide a rapid means to quickly assess the overall barrier condition. If large voids are present near the

barrier face, temperature differences can be noted. Barriers with severe honeycombing that were covered over by the contractor by surface sacking should be apparent. Note that ambient conditions must be ideal to provide adequate testing results. Detectable distress includes horizontal and vertical cracking, material deterioration, near-surface internal voids, shallow delamination, near-surface honeycomb, and debonding of repair patches. This technique will not be successful at identifying voids or delaminations deep within the barrier.

3. Hammer Acoustic Sounding

Applicable Reference Standards/Guidelines: ACI 228.2R, ASTM D4580
Coverage: All accessible surfaces
Perform hammer sounding of barrier surfaces to identify any delaminations or large voids that will result in hollow sounds when impacted with a hammer. Hammer sounding will identify moderate-to-large areas of voids or honeycomb that are within several inches of the surface. This may find large voids or delaminations somewhat deeper than IR thermography, but sounding is more labor intensive and time consuming. Perform and document a targeted acoustic impact survey to assess bond quality of patch repairs. Traffic noise can interfere with sounding.

4. Ground-Penetrating Radar (GPR) Survey

Applicable Reference Standards/Guidelines: ACI 228.2R, ASTM 6432
Coverage: Targeted horizontal scans
Perform ground-penetrating radar survey of accessible surface of the barrier wall by collecting continuous, longitudinal GPR scans at various heights using a high-frequency (2.0-2.6 GHz) surface-coupled antenna. Detectable distress includes material deterioration, internal voids at all depths, corrosion-based delamination at reinforcing layers. Note that distress will be detected along individual scan locations only. GPR will also provide for evaluation of reinforcing placement, reinforcing cover depth, and barrier wall thickness measurement, if desired. Note that cover depth and thickness measurements require proper calibration for radar wavespeed.

5. Ultrasonic Testing: Shear Wave Tomography (MIRA) or Scanning Impact-Echo Testing

Applicable Reference Standards/Guidelines: ACI 228.2R, ASTM C1383
Coverage: Targeted areas
Perform targeted ultrasonic testing at areas of probable internal defects using the shear wave tomography (MIRA) of the scanning impact-echo testing method. Detectable distress includes material deterioration, internal voids at all depths, internal delamination and planar cracking, severe internal honeycomb, and debonding of patch repairs. Shear wave tomography can provide the most accurate and comprehensive assessment of internal defects. However, it must be performed at limited survey areas selected based on the results of other testing. Alternatively, scanning impact-echo testing may provide for larger areas of the barrier to be scanned during field testing, but will require significantly more data processing and analysis.

6. Inspection Openings or Cores

Applicable Reference Standards/Guidelines: None.
Coverage: local areas identified with defects to confirm NDE results.
Chip concrete cover or take core samples to confirm the presence of internal defects at several locations where NDE techniques indicate defects.

Detection of Dowel Bar Corrosion Distress

Inspection for corroded dowel bars should focus along the construction joint between the deck and barrier at the curb. Complete the following steps:

1. ***Visual Assessment***
   Applicable Reference Standards/Guidelines: ACI 201.1R, ACI 228.2R, SEI/ASCE 11-99
   Coverage: All accessible surfaces of barrier and adjacent deck, including joint
   Perform and document visible condition of accessible surface of the barrier wall and adjacent portions of the deck, including the condition on the front and back side of the barrier at the joint. Specific visible distress noted should include cracking, spalling, moisture staining and efflorescent, and corrosion staining. Special attention should be given to the inspection of the back side of the barrier where corrosion staining may be present that has not been washed or abraded away. Also note previous repair areas and repair conditions.

2. ***Half-cell Potential (HCP) Survey***
   Applicable Reference Standards/Guidelines: ASTM C876
   Coverage: Full length of barrier wall near construction joint.
   Perform half-cell potential survey of accessible vertical surfaces of the barrier wall by collecting half-cell potential scans using a rolling HCP setup. Prior to half-cell potential surveying, an electrical connection to the dowel reinforcing and verification of electrical connectivity between dowels is necessary. It is recommended that the rolling HCP setup provide for individual half-cell potential readings at a maximum spacing of 6 inches. A minimum of two longitudinal scans should be collected on the vertical face of the barrier, one of which is positioned directly above the deck joint. Results of the surveying should be plotted and analyzed to identify areas at which active corrosion is likely occurring. Note that half-cell potential measurements have been shown to be useful for barriers constructed using uncoated, black reinforcing bars. Additional studies are necessary to determine the effectiveness of the half-cell potential method for barriers constructed with epoxy-coated reinforcing.

3. ***Impulse-Response Testing***
   Applicable Reference Standards/Guidelines: ACI 228.2R
   Coverage: Full length of barrier wall
   Perform impulse-response structural mobility testing along the bottom of the accessible vertical face of the barrier wall. Impulse-response mobility measurements can identify portions of the barrier wall at which several dowels have been severed, affecting the overall lateral support and structural stiffness of the barrier. Test spacing can be adjusted based on the length of the barrier. However, a maximum test spacing of 5 feet is recommended.

4. ***Concrete Resistivity***
   Applicable Reference Standards/Guidelines: AASHTO standard (under development) for "Surface Resistivity Indication of Concrete's Ability to Resist Chloride Ion Penetration".
   Coverage: Spot checks on the face of barrier at joint along the full length of barrier wall
   Concrete resistivity is an indirect measure of the moisture and salt content in the concrete. Spot tests along the joint can be performed quickly and provide information on where the highest

relative corrosion conditions exist. Testing should be done near the joint elevation and at an interval of 1 to 5 feet along the length of barrier.

5. Inspection Openings or Cores

Applicable Reference Standards/Guidelines: None.
Coverage: local areas identified with defects to confirm NDE results.
Chip concrete cover or take core samples to confirm the presence of internal defects at several locations where NDE techniques indicate defects.

BIBLIOGRAPHY

ASTM Standards

ASTM C876-09	Test Method for Half-Cell Potentials of Uncoated Reinforcing Steel in Concrete
ASTM C1383-04 (2010)	Test Method for Measuring P-Wave Speed and the Thickness of Concrete Plates Using the Impact-Echo Method
ASTM D4748-10	Test Method for Determining the Thickness of Bound Pavement Layers Using Short-Pulse Radar
ASTM D4788-03 (2007)	Test Method for Deflecting Delaminations in Bridge Decks Using Infrared Thermography
ASTM D6432-11	Standard Guide for Using the Surface Ground Penetrating Radar Method for Subsurface Investigation

British Standards

BS 1881 Part 205	Recommendations for Radiography of Concrete

The above publications may be obtained from the following organizations:
American Society for Testing and Materials (ASTM)
100 Barr Harbor Drive
West Conshohocken, Pa. 19428-2959

British Standards Institution (BS)
2 Park Street
London W1A 2BS
England

Works Cited

ACI Commitee 311. *Manual of Concrete Inspection (ACI 311.1R-07).* Farmington Hills, MI: American Concrete Institute, 2007.

ACI Committee 228. *Nondestructive Test Methods for Evaluation of Concrete in Structures (ACI 228.2-98) (reapproved 2004).* Farmington Hills, MI: American Concrete Institute, 1998.

Bertram, C. L., R. M. Morey, and S. S. Sander. *Feasibility Study for Rapid Evaluation of Airfield Pavements, Report No. AFWL-TR-71-178.* U.S. Air Force Weapons Laboratory, 1974.

Clark, M.R, D.M McCann, and M.C Forde. "Application of infrared thermography to the non-destructive testing of caoncrete and masonry bridges." *NDT&E International*, 2003: 265-275.

Clemeña, G. G., and R. E. Steele. *Inspection of the Thickness of In-Place Concrete with Microwave, Rep. VTRC-88-R16.* Charlottesville, VA: Virginia Tansportation Research Council, 1988.

Cui, Fushuang, John S. Lawler, and Paul D. Krauss. "Corrosion Performance of Epoxy-Coated Reinforcing Bars in a Marine Bridge Substructure." *CORROSION 2007.* Houston, TX: NACE International, 2007.

Gucunski, N., R. Feldmann, F. Romero, S. Kruschwitz, A. Abu-Hawah, and M. Dunn. "Multimodal Condition Assessment of Bridge Decks by NDE and Its Validation." *Proceedings of the 2009 Mid-Continent Transportation Research Symposium.* Ames, IA: Iowa State University, 2009.

Hoegh, K., L. Khazanovich, and H. T. Yu. "Ultrasonic Tomography Technique for Evaluation of Concrete Pavements." *Journal of the Transportation Research Board, No. 2232.* Transportation Research Record, 2011. 85-94.

Malhotra, V. M., and N. J. Carino, . "Handbook on Nondestructive Testing of Concrete, Second Edition." CRC Press, 2003.

Malhotra, V.M. *Testing Hardened Concrete: Nondestructive Methods, ACI Monograph; No. 9.* Detroit: American Concrete Institute, 1976.

Maser, K. R., and M. Roddis. "Principles of Thermography and Radar for Bridge Deck Assessment." *Journal of Transportation Engineering*, 1990: 583-590.

Parrillo, R., R. Roberts, and A. Haggan. "Bridge Deck Condition Assessment Using Ground Penetrating Radar." *European Federation for Non-Destructive Testing (ECNDT).* Berlin, Germany: German Society for Non-Destructive Testing, 2006.

Pla-rucki, G. F., and M. O. Eberhard. "Imaging of Reinforced Concrete: State-of-the-Art Review." *Journal of Infrastructure Systems* Vol. 1, no. 2 (June 1995): 134-141.

Sansalone, M. "Detecting Delaminations in Concrete Bridge Decks With and Without Asphalt Overlays Using an Automated Impact-Echo Field System." *NDT in Civil Engineering.* Liverpool: British Institute of Non-Destructive Testing, 1993. 807-820.

Sansalone, M. J., and W. B. Streett. *Impact-Echo Nondestructive Evaluation of Concrete and Masonry.* Ithica, NY: Bullbrier Press, 1997.

Sansalone, M., and N. J. Carino. "Impact-Echo Method: Detecting Honeycombing, the Depth of Surface-Opening Cracks, and Ungrouted Ducts." *Concrete International, V. 10, No. 4*, Apr. 1988: 38-46.

Sansalone, M., and N. J. Carino. *Impact-Echo: A Method for Flaw Detection in Concrete Using Transient Stress Waves.* NBSIR 86-3452, National Bureau of Standards, 1986, 222 pp.

Scott, M., et al. "A Comparison of Nondestructive Evaluation Methods for Bridge Deck Assessment." *NDT&E International 36*, 2003: 245-255.

TABLES

Table 1. Half-Cell Potential Corrosion Risk (ASTM C876)

Half-Cell Potential vs. CSE	Corrosion Risk
> -200 mV	low - 10% probability of corrosion
-200 to -350 mV	moderate - increasing probability of corrosion
< -350 mV	high - 90% probability of corrosion

Table 2. Bridges Selected for Phase A Field Testing

Bridge	US 30 over Missouri River		US Route 218 over Hinkle Creek	Iowa 150 over Cedar River
Structure No. (IA)	4300.0S030		0648.4S218	0601.5S150
County (IA)	Harrison		Benton	Benton
Barriers tested	North	South	West	East
Length of wall tested	40 ft	40 ft	130 ft.	120 ft.
Production method	CIP		CIP	CIP
Reinforcement	Epoxy-coated		Uncoated	Uncoated
Barrier wall description	Jersey Type		Curb and overlay	Jersey Type
Access	Front		Front	Front & Back

Table 3. Bridges Selected for Phase B Field Testing

Bridge	Armington Spur over Middle Fork Sugar Creek		Emden Rd over I-155		Old 121 over Kickapoo Creek		Mississippi River Bridge (MRB)		
Structure No. (IL)	054-0503		054-0078		054-0505		-		
County (IL)	Logan		Logan		Logan		St. Clair		
Barriers tested	East	West	North	South	East	West	WB North	WB South	EB South
Length of wall tested	217 ft.	217 ft.	291 ft.	291 ft.	223 ft.	223 ft.	244 ft.	244 ft.	10 ft.
Production method	CIP	Slip Formed	Slip Formed		Slip Formed		Slip Formed	CIP	Slip Formed
Reinforcement	Epoxy-coated		Epoxy-coated		Epoxy-coated		Epoxy-coated		
Barrier description	Jersey Type		Jersey Type		Jersey Type		Jersey Type		
Access	Front		Front		Front		Front		

Table 4. NDE Methods Used

NDE Method	Mock-up Evaluation (Laboratory & Field)			Phase A Field Testing (Iowa)			Phase B Field Testing (Illinois)			
	Laboratory: Flat Slab	**Laboratory: Barrier Wall**	**Field: Killian Barrier**	**US 30**	**US 218**	**Iowa 150**	**Armington**	**Emden**	**Kickapoo**	**MRB**
Internal Concrete Flaw Detection										
Impact Echo	No	Yes	No	Yes	Yes	Yes	No	No	No	No
Shear Wave Ultrasonic	No	Yes	Yes	Yes	Yes	Yes	Yes	Yes	Yes	Yes
Ultrasonic Pulse Velocity	No	Yes	No	No	No	No	No	No	No	No
Ground-Penetrating Radar	No	Yes	Yes	Yes	Yes	Yes	Yes	Yes	Yes	Yes
Infrared Thermography	No	Yes	Yes	Yes	Yes	Yes	Yes	Yes	Yes	Yes
Digital Radiography (X-ray)	No	Yes	No	No	No	No	No	No	No	No
Corrosion-Related Distress										
Half-cell Potential	Yes	Yes	No	Yes	Yes	Yes	No	No	No	No
Corrosion Rate	Yes	Yes	No	No	No	No	No	No	No	No
Impulse Response	No	Yes*	No	No	Yes	No	No	No	No	No

*Barrier wall mock-up too short for adequate response.

Table 5. Phase B Field Testing: Summary of MIRA Ultrasonic Shear Wave Test Locations

Bridge	Barrier	Test Grid Designation	Testing Orientation, Grid Size	Extent of Scans
Armington [Str. No. 054-0503]	East	Grid F-15	Horizontal: 50” w x 24” h	72’-4”-76’-6” from N end
		Grid F-16	Vertical: 48” w x 20” h	72’-4”-76’-4” from N end
		Grid F-17	Horizontal: 50” w x 24” h	36’-11”-41’-1” from N end
		Grid F-19	Vertical: 48” w x 20” h	36’-11”-40’-11” from N end
		Grid F-20	Horizontal: 50” w x 24” h	27’-4”-31’-6” from N end
Armington [Str. No. 054-0503]	West	Grid F-21	Horizontal: 50” w x 24” h	44’-2”-40’-0” from N end
		Grid F-22	Horizontal: 50” w x 24” h	125’-2”-121’-0” from N end
		Grid F-25	Vertical: 48” w x 20” h	125’-2”-121’-2” from N end
		Grid F-23	Horizontal: 50” w x 24” h	152’-0”-148’-8” from N end
		Grid F-24	Vertical: 48” w x 20” h	152’-0”-148’-10” from N end
Emden [Str. No. 054-0078]	South	Grid G-1	Horizontal: 100” w x 20” h	171’-7”-163’-3” from W end
		Grid G-2	Horizontal: 90” w x 20” h	210’-6”-203’-0” from W end
Kickapoo [Str. No. 054-0505]	East	Grid H-1	Horizontal: 70” w x 18” h	74’-2”-80’-0” from N end
		Grid H-2	Vertical: 70” w x 24” h	74’-2”-80’-0” from N end
		Grid H-3	Horizontal: 70” w x 18” h	214’-0”-220’-0” from N end
MRB WB [Illinois Approach]	North	Grid A-1	Horizontal: 60” w x 32” h	Sta. 126+93 - 126+87
		Grid A-2	Horizontal: 60” w x 36” h	Sta. 126+47 - 126+41
MRB WB [Illinois Approach]	South	Grid B-1	Horizontal: 70” w x 36” h	Sta. 126+78 - 126+72
		Grid B-2	Horizontal: 70” w x 36” h	Sta. 125+64 - 125+58
MRB EB [Illinois Approach]	South	Grid C-1	Horizontal: 90” w x 40” h	Sta. 105+21 - 105+14

Table 6. Phase B Field Testing: Summary of GPR Assessment

Bridge	Barrier	Scan No.	Horizontal Scan Location: Face - Height (from top of barrier)	Extent of Scans
Armington [Str. No. 054-0503]	East	063	West (Interior) - 8”	4’ - 217’ (0’ at N end)
		064,065	West (Interior) - 16”	4’ - 217’ (0’ at N end)
		066	West (Interior) - Middle of chamfer	3’ - 217’ (0’ at N end)
		061	Top - Center	1’ - 217’ (0’ at N end)
		062	East (Exterior) - 8”	5’ - 217’ (0’ at N end)
Armington [Str. No. 054-0503]	West	068	East (Interior) - 8”	4’ - 217’ (0’ at N end)
		069	East (Interior) - 16”	4’ - 217’ (0’ at N end)
		070	East (Interior) - Middle of chamfer	3’ - 217’ (0’ at N end)
		067	Top - Center	1’ - 217’ (0’ at N end)
		071	West (Exterior) - 8”	3’ - 217’ (0’ at N end)
Emden [Str. No. 054-0078]	North	074	South (Interior) - 8”	0’ - 291’ (0’ at W end)
		075	South (Interior) - 14	0’ - 291’ (0’ at W end)
		076	South (Interior) - Middle of chamfer	0’ - 291’ (0’ at W end)
		072	Top - Center	0’ - 291’ (0’ at W end)
		073	North (Exterior) - 8”	0’ - 291’ (0’ at W end)
Emden [Str. No. 054-0078]	South	079	North (Interior) - 8”	0’ - 291’ (0’ at W end)
		080	North (Interior) - 14	0’ - 291’ (0’ at W end)
		081	North (Interior) - Middle of chamfer	0’ - 291’ (0’ at W end)
		078	Top - Center	0’ - 291’ (0’ at W end)
		077	South (Exterior) - 8”	0’ - 291’ (0’ at W end)
Kickapoo [Str. No. 054-0505]	West	083	East (Interior) - 9”	3’ - 222’ (0’ at N end)
		084	East (Interior) - 17”	4’ - 222’ (0’ at N end)
		085	East (Interior) - Middle of chamfer	4’ - 222’ (0’ at N end)
		082	Top - Center	0’ - 223’ (0’ at N end)
		086	West (Exterior) - 8”	4’ - 222’ (0’ at N end)
Kickapoo [Str. No. 054-0505]	East	088	West (Interior) - 11”	3’ - 220’ (0’ at N end)
		089	West (Interior) - 18”	3’ - 222’ (0’ at N end)
		090	West (Interior) - Middle of chamfer	3’ - 222’ (0’ at N end)
		087	Top - Center	0’ - 223’ (0’ at N end)
		091	East (Exterior) - 10”	0’ - 223’ (0’ at N end)
MRB - WB [Illinois Approach]	North	002	South (Interior) - 6”	Sta. 127+44 - 125+00
		004	South (Interior) - 20”	Sta. 127+44 - 125+00
		007	South (Interior) - 30” (Chamfer)	Sta. 127+44 - 125+00
		006	North (Exterior) - 6”	Sta. 127+44 - 125+00
		005	Top - Center	Sta. 127+44 - 125+00
MRB - WB [Illinois Approach]	South	009	North (Interior) - 6”	Sta. 127+44 - 125+00
		010	North (Interior) - 21”	Sta. 127+44 - 125+00
		011	North (Interior) - 30” (Chamfer)	Sta. 127+44 - 125+00
		008	Top - Center	Sta. 127+44 - 125+00
MRB - EB [Illinois Approach]	South	012	North (Interior) - 6”	Sta. 105+21 - 105+14
		013	North (Interior) - 18”	Sta. 105+21 - 105+14
		014	North (Interior) - 30” (Chamfer)	Sta. 105+21 - 105+14
		020	South (Exterior) - 9”	Sta. 105+21 - 105+14
		015	Top - Center	Sta. 105+21 - 105+14

Table 7. Phase B Field Testing: Summary of IR Thermography Locations

Bridge	Barrier	Extent of Assessment
Armington [Str. No. 054-0503]	East	0’ - 217’ (0’ at N end)
Armington [Str. No. 054-0503]	West	0’ - 217’ (0’ at N end)
Emden [Str. No. 054-0078]	North	0’ - 291’ (0’ at W end)
Emden [Str. No. 054-0078]	South	0’ - 291’ (0’ at W end)
Kickapoo [Str. No. 054-0505]	West	0’ - 223’ (0’ at N end)
Kickapoo [Str. No. 054-0505]	East	0’ - 223’ (0’ at N end)
MRB Westbound [Illinois Approach]	North	IDOT Sta. 127+44 - 125+00
MRB Westbound [Illinois Approach]	South	IDOT Sta. 127+44 - 125+00
MRB Eastbound [Illinois Approach]	South	IDOT Sta. 105+21 - 105+14

Table 8. Phase B Field Testing: Summary of Exploratory Core Locations

Bridge	Barrier	Core No.	Core Location (Station, Height)	Average Core Length (in.)	Reinforcing (Bar, Cover (in.))	Observations
Armington [Str. No. 054-0503]	East	F-1	74'-2", 9" from top of barrier	11	None	Minor bugholes (<3/8-in. diameter), (1) void (3/4-in. diameter)
		F-2	30'-1", 14.5" from top of barrier	12 1/4	Int. long.: 1 1/2 Ext. long.: 4	Crack extends full length, mineral buildup in crack, (1) void (1-in. diameter) adj. to ext. longitudinal bar
Armington [Str. No. 054-0503]	West	F-3	42'-10", 4" from top of barrier	10 3/8	Int. long.: 2 1/8 Ext. long.: 3 1/4	(1) void (1 1/4-in. diameter) adj. to ext. longitudinal bar
Emden [Str. No. 054-0078]	South	G-1	164'-2", 9" from top of barrier	11	Ext. stirrup: 2 1/4	Planar cracking at int. and ext. reinforcing locations, minor voiding (<1/4-in. diameter) around aggregate
		G-2	164'-2", top of barrier (vert. core), center	~9	None	Crack extends full length, mineral buildup in crack, moderate voiding (1/4-3/8-in. diameter) around aggregate
		G-3	206'-6", 5" from top of barrier	10 1/8	Int. long.: 4 Ext. long.: 5/8	Moderate voiding (3/8-1/2-in. diameter) behind reinforcing and around aggregate
Emden [Str. No. 054-0078]	North	G-4	207'-10", 9" from top of barrier	10 7/8	None	Minor voiding (1/4-3/8-in. diameter) around aggregate near ext. face
		G-5	162'-7", 4.5" from top of barrier	10 3/8	Int. long.: 2 3/8 Ext. long.: 2 3/8	Severe voiding at reinforcing, separation of concrete from reinforcing in plastic state ~1-in.
Kickapoo [Str. No. 054-0505]	West	H-1	144'-5", 6" from top of barrier	12 3/8	Int. long.: 3 1/8 Ext. long.: 2 7/8	No voiding
Kickapoo [Str. No. 054-0505]	East	H-2	76'-11", 8.5" from top of barrier	12 1/2	Int. long.: 4 Ext. long.: 2 1/8	(1) void (~1/2-in. diameter) near ext. face
MRB WB [Illinois Approach]	North	IDOT 9	Sta. 126+98	10 5/8	Int. stirrup: 3 7/8 Int. long.: 4 5/8 Ext. stirrup: 5/8 Ext. long.: 1 3/8	Minor voids adjacent to ext. stirrup
MRB EB [Illinois Approach]	South	IDOT 16	Sta. 105+16, 8" from top of barrier	10	Int. stirrup: 3 3/4 Int. long.: 4 7/8 Ext. stirrup: 1 1/4 Ext. long.: 1 7/8	Moderate voiding at interior reinforcing and around aggregate

Table 9. NDE Methods for Detection of Internal Flaws and Other Conditions

Condition\NDE Method	Ground-Penetrating Radar (GPR)	Infrared Thermography (X-ray)	Impact-Echo Ultrasonic Testing (IE)	Shear Wave Ultrasonic Testing (MIRA)	Ultrasonic Pulse Velocity Testing (UPV)	Radiography (X-ray)
One-Sided Testing	x	x	x	x		
Thickness Measurements	R[1]		R	x		
Void Detection - 3 x 3 inch within 1 1/2 inches of surface	R	R	x	x		x
Void Detection - 3 x 3 inch within 6 inches of surface	R		x	x		x
Void Detection - 3 x 3 inch within 8 inches of surface	R			x		x
Void Detection - 3 x 3 inch at any depth	x			x	x	x
Void Detection - Individual voids, >1 inch wide, located near near-surface reinforcing or shallower	x			x		
Void Detection - Interconnected voids, $>^1/_4$ inch wide, located near near-surface reinforcing or shallower	x			R		
Void Detection - Continuous voids along longitudinal reinforcing, $>^1/_2$ inch wide, at near-surface reinforcing	x					
Crack Detection - Near-surface cracking		x	x	x		
Crack Detection - Surface micro-cracking		x				
Crack Detection - Internal planar cracking	x[2]		x	R		
Depth-to-Crack Determination	x[2]			x		
Patch Repair Delamination and Debonding Detection		R	x	x	x	
Depth to Delamination and Debonding			x	x		
Honeycombing Detection - 3 x 3 inches within 5 inches of surface	x		x	x	x	
Honeycombing Detection - Any depth	x		x	x	x	
Depth to Honeycombing Determination				x		
Concrete Compressive Strength Correlation					R	
Locate Reinforcement (or other embedded elements)	R[1]			x		x

x indicates ability

R indicates ability and recommended

[1] Capable of detecting condition through surface deterioration/freeze-thaw damage

[1] Capable of detecting internal, planar cracking that is $>^1/_4$ inch wide or contains moisture

Table 10. NDE Methods for Detection of Corrosion-Related Distress

Condition\NDE Method	Half-Cell Potential Surveying	Corrosion Rate Measurement	Impulse-Response Structural Mobility Testing	Inspection Opening/Coring
Active Corrosion Detection - Black Bars	R	x		
Corrosion Rate		x		
Extent of Corrosion				R
Change in Stiffness			R	
Internal Crack Detection			x	
Path Repair Delamination and Disbonding Detection			x	
One-sided Testing	x	x	x	

x indicates ability
R indicates ability and recommended